A SYSTEMATIC STUDY OF PHOSPHORESCENT PROBES IN CRYOSOLVENTS,

AMORPHOUS SOLIDS AND PROTEINS

by

ANDREW R DRAGANSKI

A dissertation submitted to the

Graduate School-New Brunswick

Rutgers, The State University of New Jersey

in partial fulfillment of the requirements

for the degree of

Doctor of Philosophy

Graduate Program in Food Science

Written under the direction of

Dr. Richard D. Ludescher

And approved by

_____

_____

_____

_____

New Brunswick, New Jersey

May, 2014

ABSTRACT OF THE DISSERTATION

A Systematic Study of Phosphorescent Probes in Cryosolvents, Amorphous Solids, and Proteins

by

ANDREW R DRAGANSKI

Dissertation Director: Dr. Richard D. Ludescher

A systematic comparison was made of four different phosphorescent probes: erythrosine, tryptophan, tyrosine, and vanillin. Over a large temperature range, phosphorescence decays were collected for each in a 3:1 glycerol-water (v/v) mixture, a well characterized glass-forming solvent. The molecular mobility results were compared to fluctuations in the solvent as determined by dielectric relaxation spectroscopy. The rate of non-radiative decay of each probe followed the solvent fluctuations at different temperature ranges and with differing degrees of efficiency.

Phosphorescence of two single-tryptophan proteins, human serum albumin (HSA) and a 20-amino acid tryptophan cage mini-protein, was collected in glycerol-water solvent. The results are consistent with the solvent slaving model in that the activation energy for the observed rate of non-radiative transition for the tryptophan residue matches that of specific solvent motions. In the glassy state, Arrhenius-like behavior reveals that the probe mobility is dominated by a low-energy vibrational process. As temperature is raised above T_g, the probe motions become increasingly driven first by β-fluctuations of the protein hydration shell, and eventually by α fluctuations of the bulk solvent.

The effect on protein dynamics of an amorphous solid matrix was investigated. Free tryptophan and HSA were embedded in glucose, sucrose, maltose, and trehalose glasses. Tryptophan phosphorescence decays were collected over a wide temperature range. Temperature correlations

between protein mobility and bulk mobility were generated. In the glassy state, despite a significantly faster process in the protein than in the bulk, Arrhenius-like behavior revealed similar energetics. Both values climb in similar fashion until the T_g of the bulk matrix is approached, where there is a decoupling of matrix and protein dynamics. The fluorescence of pyranine bound to HSA probes the water in the protein's hydration shell. The sugars are seen to dehydrate the hydration shell to different degrees.

TABLE OF CONTENTS

LIST OF TABLES

LIST OF FIGURES

albumin embedded in glassy sucrose matrix at 0°C.

CHAPTER I:

<u>Introduction</u>

Phosphorescent probes: When an aromatic organic molecule absorbs the energy of a photon of UV/Visible light, it quickly ($\sim 10^{-15}$ s) jumps to an excited singlet electronic state, finding itself out of equilibrium with its neighbors. Inevitably—and quickly—its newly acquired excess energy must be lost to the surroundings, re-establishing equilibrium. But sometimes a low probability *forbidden* event occurs: during its excited state lifetime a high energy electron flips its spin to create an unpaired electronic orbital configuration. This configuration is called a *triplet state*, since unpaired electrons split into three quantized states in the presence of a magnetic field[1].

A molecule in an excited triplet state is unique. Though it is out of equilibrium with its surroundings, it cannot return to the ground state without again undergoing a low probability spin forbidden process. This has the effect of prolonging the high-energy state. Where an excited singlet state may have a lifetime of a few nanoseconds, an excited triplet state may persist for several seconds. If a photon is emitted from a molecule in the excited triplet state it is called *phosphorescence*. The time-resolved collection of photons from an ensemble of phosphorescent molecules allows for the triplet state lifetime to be determined.

Importantly, the triplet state lifetime can be shortened by a radiationless process. In the non-radiative de-excitation process the electronic energy of the excited state is lost to the surroundings as heat in the form of vibrational energy. In the case of aromatic molecules, its rate is directly dependent on the various bending and twisting motions of the atoms that make up the conjugated ring[1]. More specifically, there are three necessary conditions for radiationless transition, all of which are dependent on molecular mobility: (1) the nuclear geometry of the excited triplet state must closely match that of the ground singlet state; (2) some fluctuation must create a vibronic force to promote spin flip; and (3) the excess electronic energy must be able to be dissipated to the surroundings through coupled vibrations. The rate of this non-radiative process—k_{NR}—is of central importance. In the absence of other quenchers of the triplet state, k_{NR} provides a measure of molecular mobility local to the site of a phosphorescent molecule.

Ludescher and colleagues have exploited the fact that many *generally recognized as safe* (GRAS) molecules, often naturally occurring organic compounds, display strong phosphorescence emission in rigid environments. Such molecules have been used as phosphorescent probes to characterize a large variety of glassy/viscous systems of relevance to problems in food storage, stability, and packaging. Works have focused on dry saccharide matrixes[2-4], amorphous solid proteins[5], and edible polymeric films[6]. Probes that have been utilized include erythrosine[7], vanillin[8, 9], and tryptophan. Because they are GRAS, these and other compounds show great potential as phosphorescent sensors of on-the-shelf food quality.

While understanding the principles behind the preservation of foods and food ingredients are important problems, glassy biological systems are relevant in a larger biophysical framework. Slowing down or halting naturally occurring processes is not a challenge solely faced by the food scientist.   The pharmaceutical scientist strives to stabilize and maximize the effectiveness of biological therapeutic agents[10]. The protein biophysicist slows down biomolecules to facilitate observation of their mechanisms[11, 12]. Many organisms are faced with the task of preserving themselves when subjected to desiccation stress, in which event they overproduce saccharides and go into a state of anhydrobiosis[13-15]. In these cases and others, various polyols or small saccharides are frequently introduced in massive quantities to the system to help form a stabilizing matrix. These molecules or their mixtures may be known as excipients, cryosolvents, or glass-forming liquids.

Phosphorescence, almost exclusively that of tryptophan, has been used to a limited degree to probe protein mobility[16-21]. As an intrinsic amino acid it can provide site-specific information at any conceivable protein locale: e.g. at a protein surface, buried deep in a hydrophobic core, or at a flexible binding site.

On the whole, the typically low quantum efficiency of the formation of the triplet state has caused phosphorescent probes to be severely underutilized. One of the unfortunate results is that not many efforts

have been made to attain a deeper understanding of how a probe responds to its environment, or for that matter to systematically explore the response in a number of well-characterized solvents or matrixes. The combination of this lack of information and the great potential shown by phosphorescent probes has driven the research outlined in this dissertation.

A 3:1 glycerol-water (v/v) mixture was chosen as solvent for most of this work. It is a model glass-former, often used in protein dynamics studies, that has been well characterized by a myriad of experimental techniques[22-26]. First, four different phosphorescent probes, erythrosine, tryptophan, tyrosine, and vanillin, were dispersed in the solvent and monitored as a function of temperature. By extending the range down to well below the glass transition temperature, each probe's response was collected from the rigid glassy state up through the solid-liquid transition. In the next piece of work two single tryptophan proteins, human serum albumin (HSA) and a 20 amino acid trp-cage mini-protein, were dissolved into glycerol-water solvent and subjected to the same experimental procedure. Finally HSA was embedded in dry glassy sugar matrixes (glucose, sucrose, maltose, and trehalose).

References:

1. Turro, N.J., V. Ramamurthy, and J.C. Scaiano, *Principles of molecular photochemistry : an introduction*2009, Sausalito, Calif.: University Science Books. xxi, 495 p.

2. You, Y.M. and R.D. Ludescher, *The effect of glycerol on molecular mobility in amorphous sucrose detected by phosphorescence of erythrosin B.* Food Biophysics, 2007. **2**(4): p. 133-145.

3. You, Y.M. and R.D. Ludescher, *The effect of sodium chloride on molecular mobility in amorphous sucrose detected by phosphorescence from the triplet probe erythrosin B.* Carbohydrate Research, 2008. **343**(2): p. 350-363.

4. You, Y.M. and R.D. Ludescher, *Effect of Xanthan on the Molecular Mobility of Amorphous Sucrose Detected by Erythrosin B Phosphorescence.* Journal of Agricultural and Food Chemistry, 2009. **57**(2): p. 709-716.

5. Draganski, A.R., et al., *Photophysical Probes of the Amorphous Solid State of Proteins.* Food Biophysics, 2010. **5**(4): p. 337-345.

6. Lukasik, K.V. and R.D. Ludescher, *Phosphorescence of erythrosin and fusin as a probe of dynamic heterogeneity in amorphous gelatin films.* Biophysical Journal, 2004. **86**(1): p. 159a-159a.

7. Ludescher, R.D., et al., *Beyond Tg: optical luminescence measurements of molecular mobility in amorphous solid foods.* Food Hydrocolloids, 2001. **15**(4-6): p. 331-339.

8. Tiwari, R.S. and R.D. Ludescher, *Vanillin Phosphorescence as a Probe of Molecular Mobility in Amorphous Sucrose.* Journal of Fluorescence, 2010. **20**(1): p. 125-133.

9. Tiwari, R. and R.D. Ludescher, *Molecular mobility in a homologous series of amorphous solid glucose oligomers.* Food Chemistry, 2012. **132**(4): p. 1814-1821.

10. Yoshioka, S. and Y. Aso, *Correlations between molecular mobility and chemical stability during storage of amorphous pharmaceuticals.* Journal of Pharmaceutical Sciences, 2007. **96**(5): p. 960-981.

11. Doster, W., *The protein-solvent glass transition.* Biochimica Et Biophysica Acta-Proteins and Proteomics, 2010. **1804**(1): p. 3-14.

12. Austin, R.H., et al., *Dynamics of ligand binding to myoglobin.* Biochemistry, 1975. **14**(24): p. 5355-73.

13. Blackman, S.A., R.L. Obendorf, and A.C. Leopold, *Maturation Proteins and Sugars in Desiccation Tolerance of Developing Soybean Seeds.* Plant Physiology, 1992. **100**(1): p. 225-230.

14. Leslie, S.B., et al., *Trehalose and Sucrose Protect Both Membranes and Proteins in Intact Bacteria during Drying.* Applied and Environmental Microbiology, 1995. **61**(10): p. 3592-3597.

15. Sun, W.Q., P. Davidson, and H.S.O. Chan, *Protein stability in the amorphous carbohydrate matrix: relevance to anhydrobiosis.* Biochimica Et Biophysica Acta-General Subjects, 1998. **1425**(1): p. 245-254.

16. Gonnelli, M. and G.B. Strambini, *Phosphorescence Lifetime of Tryptophan in Proteins.* Biochemistry, 1995. **34**(42): p. 13847-13857.

17. Gottfried, D.S., et al., *Evidence for damped hemoglobin dynamics in a room temperature trehalose glass.* Journal of Physical Chemistry, 1996. **100**(29): p. 12034-12042.

18. Fidy, J., B. Ullrich, and F. Tolgyesi, *Room temperature phosphorescence of tryptophan to study protein dynamics.* Biophysical Journal, 2000. **78**(1): p. 29a-29a.

19. Strambini, E.G. and G.B. Strambini, *Tryptophan phosphorescence as a monitor of protein conformation in molecular films.* Biosensors & Bioelectronics, 2000. **15**(9-10): p. 483-490.

20. Udgaonkar, J.B., et al., *Exploration of the Correlation between Solvation Dynamics and Internal Dynamics of a Protein.* Biochemistry, 2011. **50**(3): p. 397-408.

21. Schay, G., et al., *Millisecond Time-Scale Protein Dynamics Exists Prior to the Activation of the Bulk Solvent Matrix.* Journal of Physical Chemistry B, 2011. **115**(19): p. 5707-5715.

22. Swenson, J., et al., *Properties of hydration water and its role in protein dynamics.* Journal of Physics-Condensed Matter, 2007. **19**(20): p. -.

23. Sudo, S., et al., *Broadband dielectric study of alpha-beta separation for supercooled glycerol-water mixtures.* Journal of Non-Crystalline Solids, 2002. **307**: p. 356-363.

24. Sokolov, A.P., et al., *Dynamics of Strong and Fragile Glass Formers - Differences and Correlation with Low-Temperature Properties.* Physical Review Letters, 1993. **71**(13): p. 2062-2065.

25.   Dashnau, J.L., B. Zelent, and J.M. Vanderkooi, *Tryptophan interactions with glycerol/water and trehalose/sucrose cryosolvents: infrared and fluorescence spectroscopy and ab initio calculations.* Biophysical Chemistry, 2005. **114**(1): p. 71-83.

26.   Dashnau, J.L., et al., *Hydrogen bonding and the cryoprotective properties of glycerol/water mixtures.* Journal of Physical Chemistry B, 2006. **110**(27): p. 13670-13677.

CHAPTER II: Characterization of phosphorescence decay from tryptophan, tyrosine, vanillin and erythrosine B in glycerol/water.

<u>Introduction</u>

The goal of this work is to characterize the triplet-state photophysical response of four *generally recognized as safe* (GRAS) molecules—erythrosine, tyrosine, tryptophan, and vanillin—dispersed in a 3:1 (v/v) glycerol-water solvent. The glycerol-water mixture was chosen because it is a versatile glass-forming cryosolvent that has been well characterized by other experimental techniques, in particular dielectric relaxation spectroscopy [1-5]. In biomolecule dynamics studies, it is a great benefit to drastically slow down the rates of conformational transitions. Large amounts of glycerol are often added to the system because it interrupts the crystallization of water that will occur at low temperature. Water and glycerol at this ratio are completely miscible, with no water- or glycerol-rich regions appearing across a broad temperature range[6, 7]. The glass transition temperature (T_g) is -103°C (170K), as defined by the point where the solvent α relaxation occurs at rate of 0.01 s^{-1}[7].

Erythrosine is a cherry-pink die that has a large absorption and strong phosphorescent signal. It is composed of a fluorescein molecule substituted with four iodine atoms on the main xanthene ring (Fig. 1A). The presence of iodine produces the heavy atom effect, a facilitation of electron spin flip, which increases the phosphorescence quantum yield[8]. Erythrosine displays absorption maximum of 535 nm, fluorescence maximum of 560 nm, and phosphorescence maximum of 682 nm. The quantum yield of phosphorescence (Φ_P) is 0.0264[9]. Erythrosine has been extensively used as a probe of rotational diffusion in solution[10-12], and of molecular mobility[9, 11-14] and oxygen diffusion[15-17] in glassy systems. Tryptophan and tyrosine (Figs. 1B,C) are especially important as they are the two significantly luminescent aromatic amino acids[18]. Numerous protein dynamics studies have utilized tryptophan phosphorescence[19-23]. However, there has been considerably less interest in the photophysics of tyrosine than in that of trp because UV light absorbed by proteins is preferentially absorbed by trp residues, or is transferred from tyr to trp[24]. Tyrosine's extinction coefficient at 290 nm is approximately 45 times less than that of tryptophan, though the ionized form of tyrosine is much higher than the neutral form[24].

Tyrosine has been scarcely utilized as a phosphorescent probe, and as such has not been well characterized. Despite its shortcomings it may be a valuable source of information for future dynamics studies—especially for proteins lacking tryptophan[25]. Vanillin (Fig. 1D) is a flavoring compound that has a moderate signal and long lifetime. Its phosphorescence is not well characterized, though it shows promise as a probe of amorphous solids[26, 27], and the liquid state[28].

After dispersing probe into cryosolvent, experiments were conducted by first cooling to liquid nitrogen temperature to form a rigid, glassy matrix. With increasing temperature, the sample passed from the glassy state, through the glass-liquid transition, and into the melt. Through each of these regions, the phosphorescence decay of the probe ensemble reports on the degree and heterogeneity of molecular mobility. The systematic study of four different molecules in a well characterized glass-forming solvent allows for side-by-side comparison. Detailed understanding of the phosphorescence sensitivity of these molecules in glassy or viscous environments is lacking.

Materials and Methods

Materials: Water was distilled and deionized. High purity (>99%) vanillin (3-methoxy-4-hydroxy benzaldehyde), L(-)-tryptophan, and Erythrosin B (2,4,5,7-tetraiodofluorescein disodium salt) were obtained from Acros organics (New Jersey, USA). Ultrapure, spectrophotometric grade glycerol was obtained from Alfa Aesar (Ward Hill, MA). L(-)-Tyrosine (>99% purity) was obtained from Sigma Chemical Co. (St. Louis, MO). At 77K glycerol emitted phosphorescence that was deemed to be due to trace impurities. Attempts at further purification with activated charcoal proved fruitless, though in all cases the signal was less than 1% therefore glycerol was used without further purification.

Preparation of samples: Aqueous stock solutions of probes were prepared: 50 mM vanillin, 50 mM tryptophan, 10 mM erythrosine.   The appropriate amount of stock solution was added to glycerol and water to yield a final ratio of probe:solvent of 1:1000 (weight), and water:glycerol of 1:3 (volume). This ratio of probe to solvent has been determined to be sufficiently small to preclude probe-probe phosphorescence quenching (REF). Because of its low solubility in water, tyrosine was added directly to glycerol/water mixture at 1mg/mL. The final mixture was heated in a water bath to 60°C for 30 mins. The heat served two purposes: to ease mixing, and to facilitate the removal of oxygen from the solution. After heating, the solution was placed under vacuum pump until bubbling stopped.

Luminescence measurements: A small copper apparatus was fabricated to fit into a small dewar with a quartz coldfinger to allow cooling of the sample. About 8 µL of solution was pipetted into the recessed area; the high viscosity, surface tension, and adhesion to the copper wall were sufficient to hold the solution in place. After sliding into the dewar, where the sample was optically accessible, liquid nitrogen was poured into the above reservoir, and conduction along the copper stem quickly brought the sample temperature to 77K. Enough space between the copper apparatus and dewar remained for a thin thermocouple wire; the thermocouple touched the copper stem at a point directly behind the sample reservoir. It was assumed that due to the small sample volume (8 µL) in contact with large surface area of copper (2 mm diameter x ½ mm depth) that thermostat and sample were at all times near thermal

equilibrium. The entire apparatus was positioned with the sample along the emission light path with front face geometry. As the sample slowly warmed, phosphorescence decays were collected on a Cary Eclipse fluorescence spectrophotometer (Varian Instruments, Walnut Creek, CA, USA). The instrument contains a high-intensity pulsed lamp and collects in analog mode; excitation / emission wavelengths for the probes were: erythrosine, 525 / 690 nm; tryptophan, 280 / 450 nm; tyrosine 270 / 430 nm; and vanillin 320 / 490 nm. In all cases both monochromator slit widths were set at a maximum of 20nm to maximize signal. A delay time of at least 1 ms avoided the collection of scattering and prompt fluorescence.

For tyrosine a sequence of 5 lamp flashes were used to increase signal intensity. With increasing temperature, once phosphorescence decay times were below 5 seconds, excitation was limited to a single lamp flash. In this case the signal to noise ratio was improved by taking an average of increasingly more cycles with increasingly shorter decay times. Gate time (channel width) varied from 40 ms for the longest decays to 0.5 ms for the shortest decays. Gate time was also adjusted according to overall decay length for tryptophan (60 - 0.5 ms) and vanillin (3 – 0.5 ms). Erythrosine phosphorescence does not display the temporal range of the other three molecules; gate time was 0.06 ms at all temperatures. Decays were collected over the temperature range of -200°C to -50°C; as the solvent glass transition temperature is -103°C this temperature range allowed for observation of behavior both in the glassy state and through the glass transition.

The spectrophotometer is also equipped with automatic polarizer accessories for both the excitation and emission that allowed for the collection of steady state phosphorescence anisotropy for erythrosine as a function of temperature. For all temperatures, the gate time for collection was 3.7 ms, and photomultiplier voltage set to high. Excitation / emission wavelengths and slit widths were the same as for collection of erythrosine phosphorescence decays. The G factor (I_{HH} / I_{HV}) was measured at 77K for each sample.

Analysis of phosphorescence decays: To eliminate the tendency of over-fitting the long tail of phosphorescence intensity decays, a simple code was written in Mathematica to remove data points from the tail. Based on random number generation, data points were selectively dropped yielding a thinned

decay with points equally spaced on a log-time scale. Typically a decay of 1000 points was reduced to ≈100.

A discrete lifetime model is inappropriate to describe phosphorescence decays in heterogeneous environments[16, 29, 30]. The collected decay is an ensemble measurement of many chromophores, each located in a similar but unique environment[16]. Two fitting models that allow for a heterogeneous decay were used: the stretched exponential function and maximum entropy method (MEM) distribution of lifetimes[31, 32]. The stretched exponential, or Kohlrausch-Williams-Watts (KWW) function:

$$I(t) = I_0 \times \exp(-time/\tau_{KWW})^{\beta} \hspace{3cm} \textbf{[1]}$$

has often been successfully used to describe relaxation processes in glassy or glass-like systems[16, 33-35]. The simplicity of this function, where the single variable β describes the degree of heterogeneity, holds great appeal and was proved suitable for fitting all erythrosine and the majority of tryptophan, tyrosine, and vanillin decays. Beta can vary from 0 to 1; when β is 1, there is no spread and the decay is described by a single exponential. The smaller the value, the greater the spread in the decay. The average lifetime was determined by the relation:

$$<\tau> = (\tau_{KWW}/\beta) \times \Gamma(1/\beta) \hspace{3cm} \textbf{[2]}$$

where Γ is the gamma function.

Lifetime distributions of tryptophan, tyrosine, and vanillin phosphorescence decays were also determined by the hybrid maximum-entropy / nonlinear-least-squares software MemExp version 3.0[31, 32], which is freely available through the NIH center for molecular modeling site (http://cmm.cit.nih.gov/memexp/). The algorithm utilizes a maximum entropy function and maximum likelihood fitting to analyze time dependent data in terms of distributed lifetimes. The obtained lifetime distributions frequently spread across two decades of time due to more quickly decaying phosphorescent impurities (verified by analysis of probe-free solvent); due to its long lifetime, the component of the distribution due to tryptophan was easily distinguished from impurities. Fits were judged to be adequate when the modified residual (Poisson noise) was seen to vary randomly about zero.

Photophysical rate constants: According to basic photophysical principles, the inverse of the observed phosphorescence lifetime can be expressed as a sum of rates, each of which is a potential route for the return from the excited triplet state to the ground singlet state[8]:

$$\tau_P^{-1} = k_P = k_{RP} + k_{NR} + \sum_i (k_{Q,i}[Q_i]), \qquad\qquad \textbf{[3]}$$

k_{RP} is the intrinsic radiative rate of the triplet state, known from measurements in low-temperature glass to be roughly 0.167 s^{-1} for tryptophan [36, 37]; 0.35 s^{-1} for tyrosine[38]; 40 s^{-1} for erythrosine[8]; and 2.63 s^{-1} for vanillin[27]. Each product $k_Q[Q]$ gives the rate due to collision with a quenching molecule of concentration [Q]. There are two potential quenchers: oxygen, which has been purged from the system, and other probe molecules, which are at sufficiently low concentration. Therefore, $k_Q[Q] = 0$ for all molecular quenchers. The value k_{NR} may thus be calculated directly from the phosphorescence lifetime:

$$k_{NR} = <\tau>^{-1} - k_{RP}. \qquad\qquad \textbf{[4]}$$

Analysis of anisotropy: The phosphorescence anisotropy (r) of a molecule provides a measure of the extent of polarization of emission; it is determined by the following relation[18]:

$$r = (I_{VV} - G \times I_{VH}) / (I_{VV} + 2G \times I_{VH}), \qquad\qquad \textbf{[5]}$$

where I is emission intensity, and V/H are vertical/horizontal polarization. The first subscript describes the orientation of the excitation light and the second describes the orientation of the emission light; the G factor is I_{HH} / I_{HV}. Because of its transition dipole moment orientation, erythrosine emits polarized phosphorescent light[10]. The steady state phosphorescence anisotropy (r_P), has been measured in solid PMMA ($r_P = 0.25$) and arabinose glass ($r_P = 0.22$). Depolarization of anisotropy occurs when rotational diffusion is faster than the emission process. The rate of rotational diffusion is dependent on the size of the molecule and the viscosity of the solution. As the viscosity of the solution decreases, r_P will decrease to zero. Erythrosine lends itself to phosphorescence polarization experiments because of its high quantum yield and large transition dipole moment.

Results and Discussion

PART 1: Erythrosine B

Phosphorescence lifetimes: Phosphorescence intensity decays of erythrosine in glycerol/water solvent (3:1 vol/vol) were collected from 77K to 220K and fit to a stretched exponential function (Eq. 1). Figure 2 shows the phosphorescence intensity decay at 77K, as well as the stretched exponential fit and fit parameters. All decays were well fit ($R^2 > 0.999$). The average phosphorescence lifetime, as determined from the fits to the decays ($<\tau>$; Eq. 2), is plotted against temperature in Fig. 3A. In the absence of quenching molecules, the phosphorescence lifetime provides a measure of molecular mobility of the probe's local environment[16]. At 77K, $\tau = 0.95$ ms—an expected long lifetime for erythrosine in a glassy environment at low temperature—and slowly decreases with increasing temperature, until the solvent T_g of -103°C is surpassed. The effect of the glass transition is not detected immediately though, as it is not until -90°C is reached that the lifetime begins to rapidly decrease. The decrease in τ is an indication that the probe has become sensitive to decreasing solvent viscosity. At -70°C the trend unexpectedly stops and a second plateau is reached, similar to the behavior below T_g , and τ once again decreases slowly with increasing temperature.

Heterogeneity: In Fig. 3B the value of the stretching exponent β, an indicator of site heterogeneity, is plotted against temperature. The value of β follows a similar trend as τ with increasing temperature from -100° to -70°C: it slowly increases in the glass and then sharply increases above T_g. This is likely a reflection of increasing averaging as the matrix softens around the probe. In the glassy state the ensemble of probes occupy a large number of different conformations that are "frozen" in place with respect to the phosphorescence lifetime; in this case each probe has a unique decay time, based on differences from site to site, and the ensemble emission gives rise to a non-exponential decay[29, 30]. As the probe sites become more mobile, each probe will begin to explore multiple conformations during the lifetime. This conformational averaging at a suitable rate will yield a decay that is well described by a single exponential

function[39, 40]. This is the case for erythrosine at ≈-75°C, where β >0.98. However as temperature is further increased β begins to fall in a complicated pattern with no immediately apparent explanation.

Anisotropy: To find further insight into the unusual pattern followed by τ and β with increasing temperature, the steady state phosphorescence anisotropy (r) of erythrosine was collected; r is plotted alongside τ and β in Fig. 3C. The value of r = 0.19 was consistent for T < T_g, indicating that when the solvent was in the glassy state the probe was fixed in a rigid environment and unable to diffuse rotationally within the phosphorescence lifetime. At -70°C, r began to decrease rapidly, reaching a plateau of 0.03 at -50°C. The depolarization indicated that the solvent became mobile enough to allow the erythrosine molecule to begin rotating. Possibly the residual r = 0.03 is a result of rotation being solely due to rotation in the plane of the ring, and only goes to 0.0 when isotropic rotation becomes sufficiently fast. It is interesting to note that the commencement of the decrease in r at -70°C roughly coincides with the end of the rapid decrease in τ.

Arrhenius analysis: In Figure 4, the logarithm of the rate of non-radiative decay (k_{NR}; Eq. 4) has been plotted against inverse temperature. The slope of the Arrhenius plot reveals the activation energy (E_a) of the non-radiative process which provides a measure of the molecular mobility in the solvent matrix. The dashed line in the plot is the straight line fit of the data at T < T_g (= 170K), yielding E_a = 0.18 kJ/mol. This small activation energy indicates there is little motion in the glass, and suggests that the slight increase in k_{NR} is due to normal mode vibrations of the erythrosine molecule. The increase in slope above T_g indicates that k_{NR} undergoes a transition from a low E_a vibration process to a higher E_a β process. Since normal-mode vibrations and β fluctuations are independent motions[6], their contributions to k_{NR} are separable; thus k_{NR} consists of a vibrational and a non-vibrational component:

$$k_{NR} = k_{vib} + k_{nonvib}, \qquad\qquad [6]$$

At T << T_g, the matrix is "frozen" with respect to α motions while β fluctuations are too weak to compete with vibrations, i.e. $k_{nonvib} \rightarrow 0$ and $k_{vib} = k_{NR}$. Since k_{vib} is an Arrhenius process it can be extrapolated to higher temperatures and subtracted from k_{NR} to yield k_{nonvib} (Fig. 5). The filled circles in the plot are the original k_{NR} data and the open circles are k_{nonvib}. With the vibrational component of k_{NR} subtracted out, a

clear Arrhenius process is revealed in the plot from 180 to 200K with an E_a of 46.66 kJ/mol, a typical

energy for β relaxation in a glassy system[41, 42].

The turndown of the plot in Fig. 5 at 200K is unusual; it does not imply that the 46 kJ/mol process suddenly

ceases, but rather that the process ceases to have an effect on k_{NR}. The second plateau indicates that the

temperature dependence of the non-radiative process of erythrosine is once again, over a small temperature

range, being controlled by small E_a vibrational motions. The probe has, for unclear reason, temporarily lost

its sensitivity to changes in the softening matrix. A low E_a process of 8.33 kJ/mol is observed before the

upturn seen in the plot.

At 250K there is a second upturn in the Arrhenius plot. At this warmer temperature, now 80K above T_g, it

is presumed that erythrosine begins to be affected by the primary relaxation (α) of the solvent. This is

supported by the fact that the phosphorescence lifetime of many molecules has been observed to closely

follow solvent viscosity[43-45]. The gradually increasing slope at 250K indicates the rate may again be

separated into two contributions. Thus, the 8.33 kJ/mol vibrational process is subtracted from k_{nonvib} and

plotted in Fig. 6. The dashed line is the VFT fit to the solvent α relaxation as determined by dielectric

relaxation (k_{diel})[7] shifted down 5.5 log units. The matching slopes strongly suggests that at T_g + 100K,

k_{NR} is under control of the primary relaxation of the bulk solvent. The solvent relaxation is $10^{5.5} \approx 320,000$

times faster than k_{NR}, meaning that it takes a large number of solvent fluctuations to bring about the

erythrosine non-radiative transition. The large degree of inefficiency is a reflection of the forbidden nature

of the spin flip. Despite the difference in magnitude, both rates have the same temperature dependence.

Is it possible that the ≈46 kJ/mol process from 180K to 200K facilitates the rotational diffusion of

erythrosine? Figure 7a shows the original Arrhenius plot of k_{NR}; underneath it, Figure 7b is a plot of

anisotropy, but now against inverse temperature to allow side-by-side evaluation. Because the erythrosine

phosphorescence does not begin to depolarize until T > 200K, it is doubtful that the 46.66 kJ/mol β process

is allowing rotation of the whole molecule. Instead it is much more likely that what is happening to

erythrosine from 180K to 200K is that the benzoic acid moiety begins to obtain freedom of rotation about

the C-C bond that links it to the central 3 ring fluorone. Ample evidence exists linking various photophysical rates of fluorescein to the value of the dihedral angle formed by the benzoic acid residue[46, 47]. Furthermore, molecular orbital analysis on the T_1 to S_0 transition of erythrosine has shown the optimal geometry is when the benzoic acid is at 90° to the fluorone ring system. What is likely happening is that once $T_g = 170K$ is reached, there is enough mobility in the matrix to allow the benzoic acid to slowly begin to explore a greater angle of orientation. Because of the size of the moiety—the aromatic carboxylic acid is bulky—it requires some participatory movement of the local solvent molecules to allow its rotation. The participation of the highly viscous solvent is why the E_a of the process is so high. When the temperature reaches ≈200K, two things simultaneously occur. First, the rotation of the benzoic acid moiety is no longer inhibited by the viscous solvent but instead its freedom of motion is checked by the bulky carboxylic acid. The benzoate moiety cannot rotate a full 360° about the C-C bond. This may explain the plateau in k_{NR} at ≈210K: the non-radiative mechanism of benzoic acid rotation has been exhausted. The second thing that happens at 200K is the entire erythrosine molecule begins to rotate within the timescale of the phosphorescence lifetime, as evidenced by the anisotropy beginning to decrease. The overall progression with increasing temperature makes sense: at $T < T_g$ nothing is able to move, at $T = 180K$ the smaller benzoic acid moiety begins to rotate, and at $T = 200K$ the entire molecule begins to rotate. Finally at 250K there is enough thermal energy in the system to support translational motion, and collisional quenching by solvent α fluctuations ultimately drives the k_{NR} process.

PART II: Tryptophan

Phosphorescence lifetimes: Phosphorescence intensity decays of tryptophan in glycerol/water (3:1 vol/vol) were collected from 77K to 230K. A log plot of the data at 77K (Fig. 8a) demonstrates the decay is nearly single exponential. Most of the decays were able to be well fit ($R^2 > 0.999$) to a stretched exponential function (Eq. 1). However, improved fits to the decays were achieved using the maximum entropy method distribution of lifetimes (MEM; for details on fitting see *Methods*). Various small, short lifetime peaks

were seen in the MEM fits; these coincided closely with peaks seen in glycerol/water blanks and have been

determined to be due to scant quantities of unidentified phosphorescent impurities in the solution (this was

not an issue for erythrosine both because of its high phosphorescence quantum yield and low absorption

energy). Fitting the decays with an MEM-based lifetime distribution function thus allowed for

identification and isolation of the component of the signal due to tryptophan; this was impossible with

previously utilized fit procedures (sum of exponentials and stretched exponential). Once the tryptophan

peak was determined, the rest of the lifetime distribution was discarded. The log (τ) MEM distribution for

the data of Fig. 8a is plotted in Fig. 8b, showing that the decay is best represented by a spread in lifetimes

centered at $10^{3.8} = 6300$ ms. In Fig. 9 the MEM fits are plotted against temperature (a number of

temperature points have been excluded to ease viewing). As expected, the lifetime distribution moves to

shorter times with increasing temperature. The average lifetime (τ) was calculated from the assigned

tryptophan peak in the MEM distribution by calculating the center of gravity (after converting from log (τ)

to τ). The average lifetime was also calculated from the stretch fit parameters (Eq. 2). Both calculated

values of τ are plotted against temperature in Fig. 10a, demonstrating close agreement between both

methods of data analysis. In the absence of quenching molecules, the phosphorescence lifetime provides a

measure of molecular mobility of the probe's local environment[16]. At 77K $\tau \approx 6300$ ms, an expected

long lifetime in a rigid glass at low temperature—in fact one of the longest reported in the literature[38].

Tau very slightly decreases with increasing temperature, until the solvent T_g of -103°C is surpassed, where

the lifetime begins to rapidly decrease. The decrease in τ is an indication that the probe has become

sensitive to decreasing solvent viscosity.

Beneath Fig. 10a the stretching exponent (β) from the stretched exponential fits is plotted against

temperature (Fig. 10b). Beta, a measure of site heterogeneity, remains stable at ≈ 0.95 in the glass until the

T_g of -103°C is reached. The rise of β and approach to a value close to 1 at -78°C is indicative of

conformational averaging (as discussed above for erythrosine). As temperature is further increased above -

78°C β begins to quickly fall with no immediately apparent explanation.

Arrhenius analysis: In Fig. 11, the logarithm of the rate of non-radiative decay (k_{NR}; Eq. 4) has been plotted against inverse temperature. The slope of the Arrhenius plot reveals the activation energy (E_a) of the non-radiative process which provides a measure of the molecular mobility in the solvent matrix[16]. There are two apparent Arrhenius processes, indicated by the dashed lines in the plot. The fit of the data at $T < T_g$ (170K), yields $E_a = 2.02$ kJ/mol. This small activation energy indicates there is little motion in the glass, and suggests that the slight increase in k_{NR} is due to normal mode vibrations of the tryptophan molecule. From 170 to 200K the increase in slope indicates that k_{NR} undergoes a transition from a low E_a vibration process to a β process with E_a of 43.4 kJ/mol. The inverse phosphorescence lifetime of tryptophan has been observed to follow the trend of the solution viscosity[43]. Thus it is expected that at some $T > T_g$ the α relaxation of the solvent will become fast and strong enough to be the primary driver of $k_{NR.}$ In Fig. 12 the rate of the primary solvent relaxation as measured by dielectric relaxation spectroscopy (k_{diel})[7] has been plotted in Arrhenius fashion alongside k_{NR} of tryptophan. It is clear from the comparison of the two plots that k_{NR} does not begin to follow the 95 kJ/mol E_a of the solvent until ≈ 220K, at which point it is at least 4 orders of magnitude slower than k_{diel}. Because the 43.4 kJ/mol Arrhenius process of Fig. 11 does not follow the main fluctuation of the solvent the two process are considered to be statistically independent. Thus k_{NR} may be divided into two components, k_α and k_β, such that $k_{NR} = k_\alpha + k_\beta$. Extrapolation of the β process and subtraction from k_{NR} yields k_α, which has been plotted in Fig. 13 alongside the VFT fit of the solvent dielectric subtracted by 4.4 log units. This demonstrates that the solvent α relaxation begins to have an effect on k_{NR} at 200K and the transition from β dominated to α dominated is completed at 215K. The downward shift of the VFT fit implies that it takes on average $10^{4.4} ≈$ 25,000 α fluctuations of the solvent to bring about the non-radiative transition of the tryptophan triplet state.

PART III: Tyrosine

Phosphorescence lifetimes: Phosphorescence intensity decays of tyrosine in glycerol/water (3:1 vol/vol) were collected from 77K to 200K. The curved log plot of the data at 77K (Fig. 14a) demonstrates the

decay is non-exponential. Most of the decays were able to be well fit ($R^2 > 0.999$) to a stretched

exponential function (Eq. 1). However, improved fits to the decays were achieved using the maximum

entropy method distribution of lifetimes (MEM; for details on fitting see *Methods*). The log (τ) MEM

distribution for the data of Fig. 14a is plotted in Fig. 14b, showing that the decay is best represented by a

spread in lifetimes centered at $10^{3.4} \approx 2500$ ms. In Fig. 15a the MEM fits for $T < T_g$ are plotted against

temperature. With increasing temperature, the distribution spreads wider while maintaining a longest

lifetime anchor point of $\log(\tau) = 3.7$. This indicates a large increase in heterogeneity of probe dynamics in

the glassy matrix. With increasing temperature above T_g, the MEM distribution maintains its wide shape

and moves to shorter lifetimes (Fig. 15b). The average lifetime (τ) was calculated from the tyrosine MEM

distribution by calculating the center of gravity (after converting from log (τ) to τ). Tau was also calculated

from the stretch fit parameters (Eq. 2). Both calculated values of τ are plotted against temperature in Fig.

16a, demonstrating close agreement between both methods of data analysis. In the absence of quenching

molecules, the phosphorescence lifetime provides a measure of molecular mobility of the probe's local

environment[16]. At 77K the lifetime of 2500 ms is in the range of lifetimes reported in the literature in

glassy matrix at 77K[24, 38]. From -200°C up to the glass transition temperature -103°C, the lifetime

significantly decreases with increasing temperature, which is unusual for a phosphorescent probe in a

glassy matrix. When T_g is surpassed, the lifetime begins to decrease at a steeper slope, likely as a response

to the decreasing viscosity of the solvent.

Beneath Fig. 16a the stretching exponent (β) from the stretched exponential fit is plotted against

temperature (Fig. 16b); the plot shows β to steadily decrease from a value of 0.87 at -200°C to a minimum

of 0.63 at T just over T_g. The large decrease was unexpected, and indicates increasing probe heterogeneity

despite the "frozen" nature of the glass (also demonstrated by the widening of the MEM distribution in Fig.

15a). The slight rise of β from -100 to -80°C is likely indicative of conformational averaging (as discussed

above for erythrosine). Useful data was unable to be collected for $T > -80$°C as the phosphorescence

decays became too short and weak to resolve with the phosphorimeter.

Arrhenius analysis: In Fig. 17, the logarithm of the rate of non-radiative decay (k_{NR}; Eq. 4) has been plotted against inverse temperature. The slope of the Arrhenius plot reveals the activation energy (E_a) of the non-radiative process which provides an average measure of the local molecular mobility experienced by the probe ensemble. At $T < T_g$ the Arrhenius plot of tyrosine is unique in that the slope of k_{NR} is steadily increasing with temperature. It is thus impossible to assign a single activation energy to k_{NR} in the glass. The dashed lines in the plot are fits to several adjacent data points to drawn to demonstrate the steadily increasing E_a of k_{NR} in the glass. At 77K the small E_a of 0.74 kJ/mol indicates there is little motion in the glass and k_{NR} of the probe is activated by small amplitude normal vibrations. The E_a slowly increases up to 2.95 kJ/mol at 170K; this gradual increase is not indicative of a transition to a different and distinct process, but rather is likely a result of heterogeneous dynamics experienced by the probe ensemble. This theory is supported by the high degree of non-exponentiality seen in the intensity decays shown by the unusually low value of the stretching exponent β.

Above 170K the slope rapidly increases as k_{NR} undergoes a transition from a low E_a vibration process to a higher E_a process. The transition is sharp and closely coincides with the glass transition temperature, suggesting the probe is responding to the α relaxation of the bulk solvent in a highly sensitive fashion. In Fig. 18 the rate of the primary solvent relaxation as measured by dielectric relaxation spectroscopy (k_{diel})[7] has been plotted in Arrhenius fashion alongside k_{NR} of tyrosine. It is readily apparent that k_{NR} closely follows the 95 kJ/mol k_{diel} process. Not only is the slope of the plot nearly identical, but the rates themselves are very similar, as log (k_{diel}/k_{NR}) = 0.4; thus it takes on average $10^{0.4} = 2.5$ solvent fluctuations to bring about the non-radiative transition of tyrosine. This is an efficient process considering the forbidden nature of the radiationless process. The phosphorescence of tyrosine is closely coupled to solvent fluctuations.

PART IV: Vanillin

Phosphorescence lifetimes: Phosphorescence intensity decays of vanillin in glycerol/water (3:1 vol/vol) were collected from 77K to 190K. The slightly curved log plot of the data at 77K (Fig. 19a) demonstrates

the decay is nearly single exponential. At lower temperatures, the decays were able to be well fit ($R^2 >$

0.999) to a stretched exponential function (Eq. 1). As temperature increased, vanillin phosphorescence

intensity decreased while background impurity phosphorescence did not decrease as much, giving the

effect of a shorter lifetime when analyzed with the stretch function. Greatly improved fits to the decays

were achieved using the maximum entropy method distribution of lifetimes (MEM; for details on fitting see

Methods). Phosphorescent impurities were easily identified and subsequently subtracted by comparing the

vanillin MEM distribution with that of blank solvent. The log (τ) MEM distribution for the data of Fig. 19a

is plotted in Fig. 19b, showing that the decay is best represented by a spread in lifetimes centered at $10^{2.5} \approx$

316 ms. In Fig. 20a the MEM fits for T < T_g are plotted against temperature. With increasing temperature,

the distribution changes shape very little, while gradually shifting to slightly shorter lifetime. Once T_g is

surpassed at -102°C the distribution is seen to immediately widen, indicating the onset of an increase in

heterogeneity of probe dynamics in the melt. With increasing temperature above T_g , the MEM

distribution maintains becomes increasingly wide while rapidly moving to shorter lifetimes (Fig. 20b).

The average lifetime (τ) was calculated from the vanillin peak in the MEM distribution by calculating the

center of gravity (after converting from log (τ) to τ). Tau was also calculated from the stretch fit

parameters (Eq. 2). Both values of τ are plotted against temperature in Fig. 21a, and it can be seen that τ

determined by the stretch function becomes significantly smaller than the MEM determined value at T >

T_g. In the absence of quenching molecules, the phosphorescence lifetime provides a measure of molecular

mobility of the probe's local environment[16]. From -190°C up to the glass transition temperature -103°C,

the lifetime slowly decreases with increasing temperature. When T_g is surpassed, the lifetime sharply

decrease at a steep slope, likely as a response to the decreasing viscosity once the solvent has left the glassy

state and entered the melt.

Beneath Fig. 21a the stretching exponent (β) from the stretched exponential fit is plotted against

temperature (Fig. 21b); the plot shows β to be steady at a value of 0.93 in the glass, and then sharply

decrease with increasing temperature above T_g in similar fashion as the decrease in lifetime. In this case

the value of β is not to be trusted above T_g, as the stretched exponential function was deemed unsuitable for

$T > T_g$. Useful data was unable to be collected soon after T_g was surpassed; at -90°C the phosphorescence decays became too fast and weak to resolve with the phosphorimeter.

Arrhenius analysis: In Fig. 22, the logarithm of the rate of non-radiative decay (k_{NR}; Eq. 4) has been plotted against inverse temperature. The slope of the Arrhenius plot reveals the activation energy (E_a) of the non-radiative process which provides an average measure of the local molecular mobility experienced by the probe ensemble. From 77K up to 140K the slope of k_{NR} is almost flat, indicating the probe is "frozen" into the matrix with little temperature dependence. The E_a of 0.26 kJ/mol indicates there is little motion in the glass and k_{NR} of the probe is activated by small amplitude normal vibrations. Above 140K the E_a slowly increases up to 2.9 kJ/mol at 160K; this gradual increase is likely a result of a heterogeneous environment experienced by the probe ensemble as temperature nears T_g.

At the T_g of 170K the slope rapidly increases; it is apparent that k_{NR} undergoes a quick transition to a high E_a process. The transition is sharp and closely coincides with the glass transition temperature, suggesting the probe is directly responding to the α relaxation of the bulk solvent. In Fig. 23 the rate of the primary solvent relaxation as measured by dielectric relaxation spectroscopy (k_{diel})[7] has been plotted in Arrhenius fashion alongside k_{NR} of vanillin. Inspection of the plot shows not only that k_{NR} closely follows the energy of the 95 kJ/mol solvent process, but the rate is actually *faster* than k_{diel}. It is possible that residual amounts of O_2 in the solution provide an additional quenching route that makes up the excess in the rate.

Conclusions

In Fig. 24 the average τ as determined by the MEM fits of all four probes (erythrosine, tryptophan, tyrosine, and vanillin) has been plotted versus temperature. The overall dynamic range, as judged by the magnitude of τ in the glass, is largest in tryptophan, followed by tyrosine, vanillin, and erythrosine. The short lifetime of erythrosine, even in the glassy state, is due to the heavy atom effect of the four iodine atoms substituted to the fluorone ring. However, erythrosine has a large phosphorescence signal which allows for use as a probe at much smaller concentration, makes it highly amenable to polarization studies, and use in low viscosity environments. Erythrosine also offers potential to attach different groups to the benzoic acid group[46].

In Fig. 25 the lifetimes have been normalized and again plotted against temperature to show the relative dynamic range of the probes in the glass. It is largest in tyrosine, as demonstrated by the large drop in τ from -200 to -100°C. After tyrosine follows vanillin, tryptophan, and then erythrosine. Tyrosine, and to a lesser extent vanillin, is extraordinarily active in the glass; likely it can be utilized to offer insight into glassy dynamics as an excellent probe of weaker secondary relaxations. For the other three probes there is an onset temperature where τ begins to significantly drop, erythrosine (-100°C), tryptophan (-110°C), and vanillin (-140°C). The onset temperature of tyrosine has not been reached in this study and is clearly < -200°C. Presumably further insight into the glassy state of glycerol/water solvent can be achieved with tyrosine simply by extending the scope to lower temperature (current equipment limits T to 77K) as well as collecting more data points in the glassy range.

Fig. 25 also enables a comparison of the effective temperature range of each of the probes. The useful range can be defined from the onset temperature, where τ begins to decrease, to the temperature where τ approaches zero. Both tyrosine and erythrosine are sensitive over a large temperature range, though with almost no overlap: while tyrosine is useful from -200°C (or colder) to -80°C, erythrosine is useful from -90°C to about 20°C. Tyrosine seems to be very sensitive to the subtlest of motion making it especially useful in the glass. The probe is so sensitive to motion that its phosphorescence was quickly quenched

even in the highly viscous melt at -80°C. Erythrosine displays the opposite characteristic, it is relatively

insensitive to solvent motions and thus may act as an effective mobility probe in low-viscosity

environments. Tryptophan and vanillin similarly display a narrow effective temperature range. Vanillin

appears to be primary useful at monitoring changes in the solvent in the glass to liquid transition at -103°C.

Tryptophan is especially important as a phosphorescent probe of protein dynamics, as an amino acid with

high quantum yield and long lifetime. It does not become active until slightly above T_g, and is

considerably more useful in lower viscosity environments than vanillin and tyrosine.

In Fig. 26 the stretching exponent β has been plotted against temperature to show the changing

heterogeneity as seen by the four different probes. One apparent commonality between all 4 probes is the

presence of a transition at T_g where the stretch exponent begins to rise due to conformational averaging

(except for vanillin, where the stretch fit at T > -150°C became less and less adequate). Beta reached a

peak at ≈-75°C, and then began to decline, especially with erythrosine and tryptophan, with further

increasing temperature. Increasing heterogeneity at warmer temperatures is contrary to the expectation that

conformational averaging would become more efficient and produce a single-exponential decay. The

decline in β with increasing temperature in the glassy state for tyrosine is also unexpected, whereas β for

erythrosine and tryptophan remained flat or slowly climbed until T_g was reached. The increasing

heterogeneity as measured by tyrosine is taken as a reflection of the sensitivity of tyrosine in the glass, and

more exploration is needed to get deeper insight.

In Fig. 27 k_{NR} for all probes as well as k_{diel} for the solvent primary relaxation are plotted in Arrhenius

fashion. The dashed lines are vertically shifted plots of k_{diel}., demonstrating each probes' response to

solvent fluctuations. In all cases the E_a of k_{NR} follows that of k_{diel} for the data points at the end part of the

probe temperature range.   There are two important and related differences among the four probes: the

efficiency of the effect (k_{diel}/k_{NR}), and the onset temperature (T_{onset}); the values are summarized in Table 1.

The most efficient/earliest onset is found with vanillin, followed by tyrosine, tryptophan, and then

erythrosine. A possible mechanism responsible for the behavior of vanillin, tyrosine, and tryptophan is

apparent upon consideration that the trend follows the number of H-bonding partners found on the probe

aromatic ring structure (Fig. 1). Complex aromatic ring vibrations have been shown to couple to solvent fluctuations via hydrogen bonding[48]. The solvent driven motions affect the phosphorescence lifetime (as well as fluorescence, IR, and ab initio calculations) of the different molecules studied—which included tyrosine. The indole group of tryptophan has no –OH groups on the bicyclic ring. The solvent is not able to form strong H-bonds to the indole ring thus $\log(k_{diel}/k_{NR}) = 4.3$ and it takes over 20,000 solvent fluctuations to cause the non-radiative transition of the tryptophan triplet state. Furthermore, because of the lack of H-bonding partners on the indole ring, the α relaxation of the solvent is not fully sensed until 200K, roughly 30K above T_g. Contrast this to the phenol group of tyrosine, which consists of a single –OH group covalently bonded to its aromatic ring. The –OH allows for a fluctuating solvent molecule to form with it a strong hydrogen bond that drives the bending and twisting of the chromophore that ultimately determines the rate of the non-radiative transition. This explains why $\log(k_{diel}/k_{NR}) = 0.4$ for tyrosine, and the T_{onset} of 185K is very close to the solvent T_g. Finally for the case of vanillin there is a –OCH_3 in addition to an –OH group bonded to its aromatic ring, offering a second H-bonding partner to the fluctuating solvent molecules. This likely explains the highly efficient response of vanillin to the solvent fluctuations, as well as the near T_g onset temperature of the probe's sensitivity.

A comparison of the other 3 probes with erythrosine is less straightforward. The larger 3 ring fluorone group produces a considerably lower phosphorescence emission energy while the benzoic acid group and four iodine molecules have a complicated effect on probe photophysics[46]. However, a comparison of different fluorescein dyes, systematically substituting the heavy atoms as well as the benzoate moiety would doubtlessly be helpful in drawing inferences regarding specific solvent-erythrosine interactions. The unconfirmed hypothesis that the erythrosine is sensitive to rotation of the benzoic acid moiety in the high viscosity regime may ultimately prove useful as a probe of a highly specific motion. Finally it is observed that the tryptophan Arrhenius process with E_a of 43.4 kJ/mol from 180 to 200K is nearly identical to that tentatively ascribed to erythrosine benzoate rotation (46.7 kJ/mol with identical temperature range). The coincidence suggests the possibility that the indole group, of similar size to benzoate, is beginning to rotate about the tryptophan alpha carbon linkage.

Figure II-1

A)

B)

C)

D)
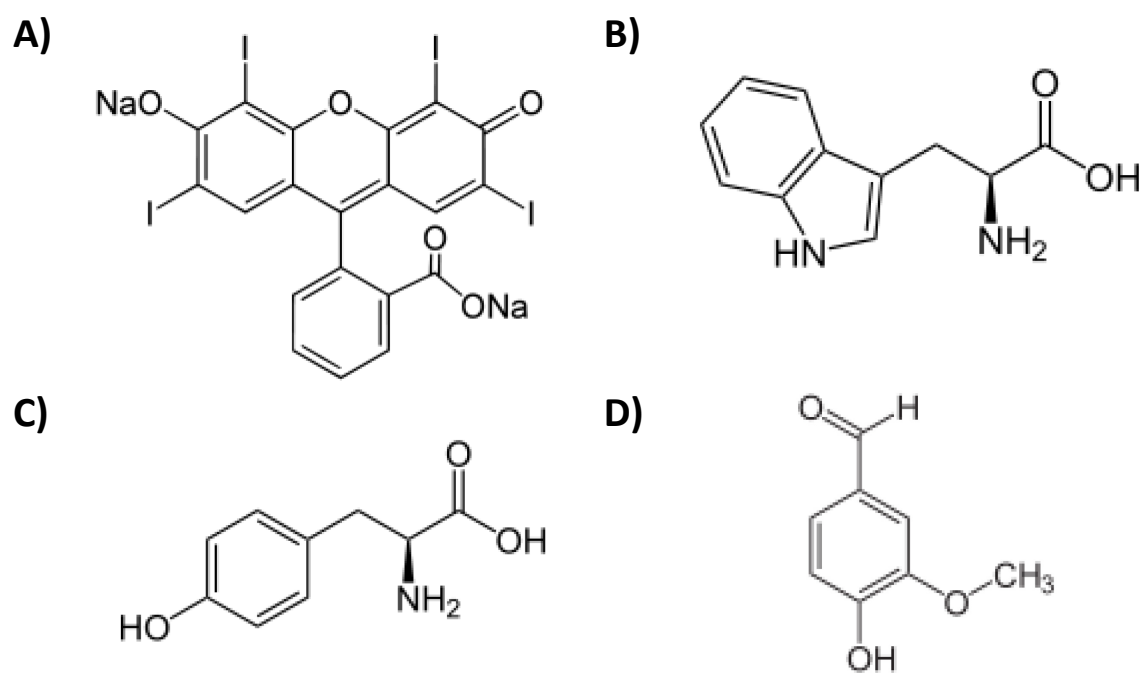
Figure II-1: Structure of (A) erythrosine (2,4,5,7-tetraiodofluorescein), (B) tryptophan, (C) tyrosine, and (D) vanillin (4-Hydroxy-3-methoxybenzaldehyde).

Figure II-2

$\{a \rightarrow 190.087, \text{tau} \rightarrow 0.87898, \text{beta} \rightarrow 0.859435\}$

$R^2 = 0.999943$

$\tau_{kww} = 0.95$

--- Fit

• Intensity

Intensity

Log (time / ms)
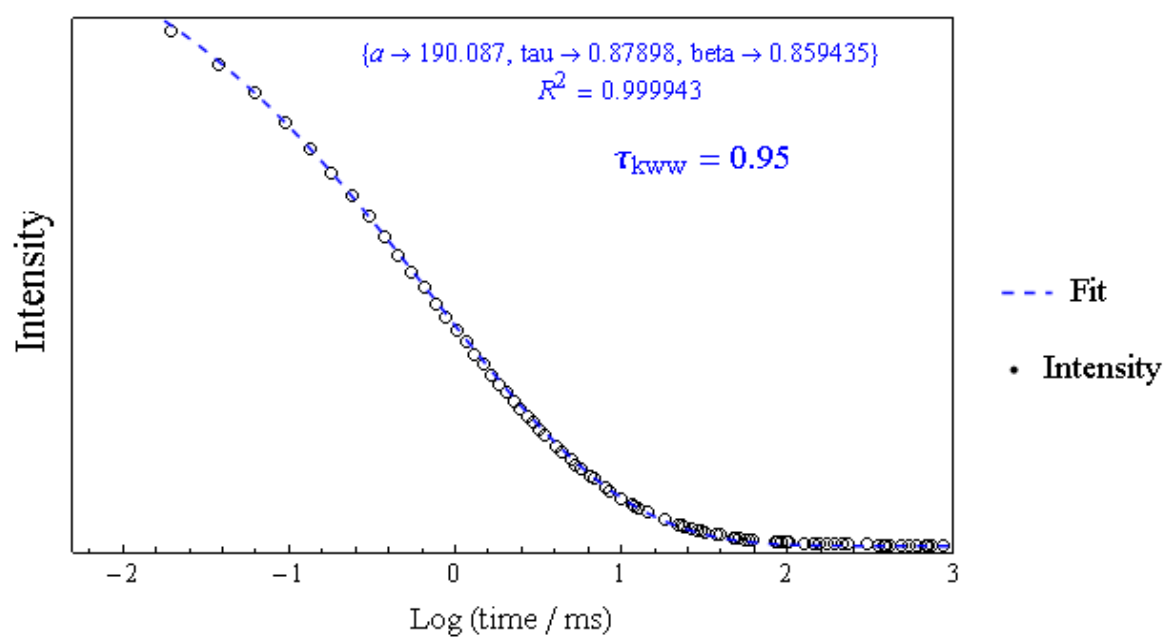
Figure II-2: Phosphorescence intensity decay of erythrosine dispersed in 3:1 glycerol-water (v/v) at 77K. The dashed line is the stretched exponential fit to the data.

Figure II-3
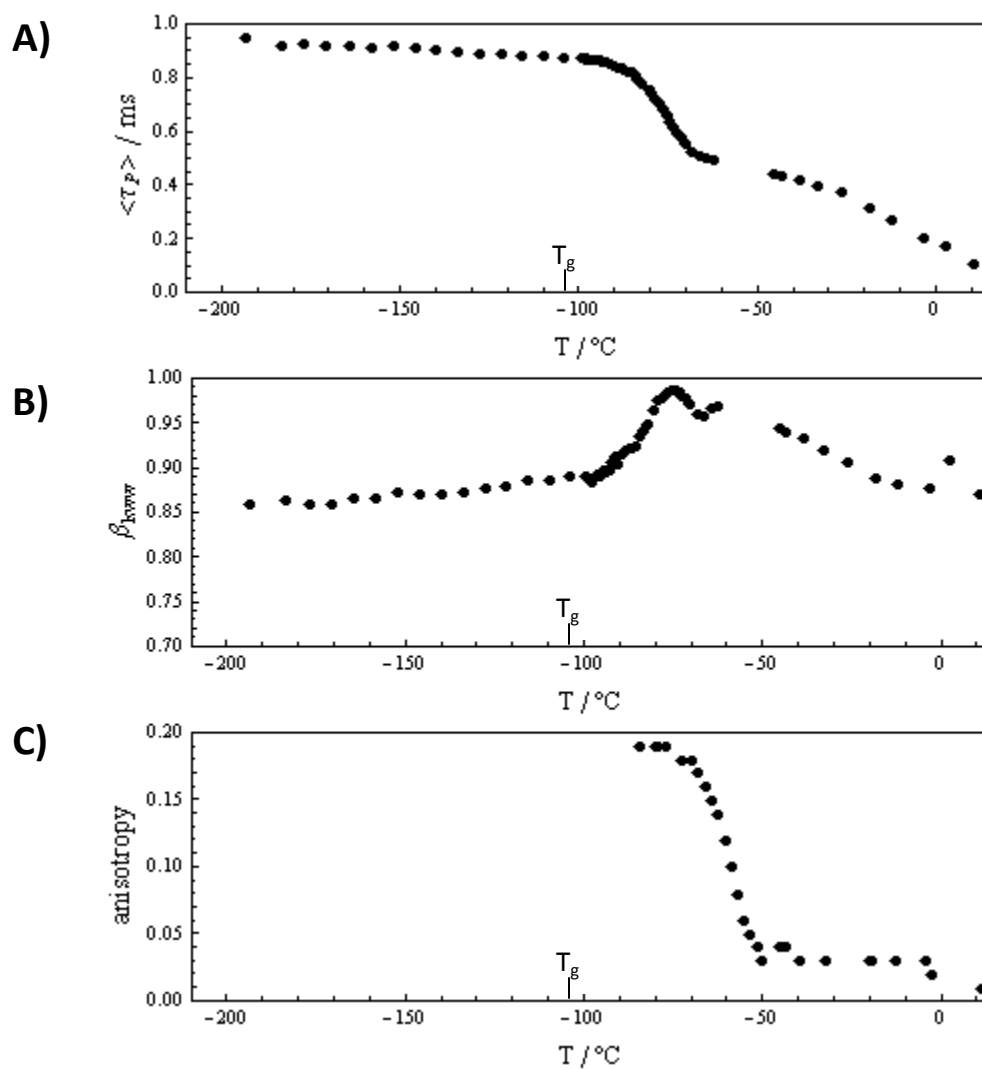
Figure II-3: Data obtained from phosphorescence of erythrosine in 3:1 glycerol-water (v/v) versus temperature. (A) Average phosphorescence lifetime of intensity decays as determined by fits to a stretched exponential function; (B) the stretching exponent (β) of the fits. (C) Steady state phosphorescence anisotropy.

Figure II-4
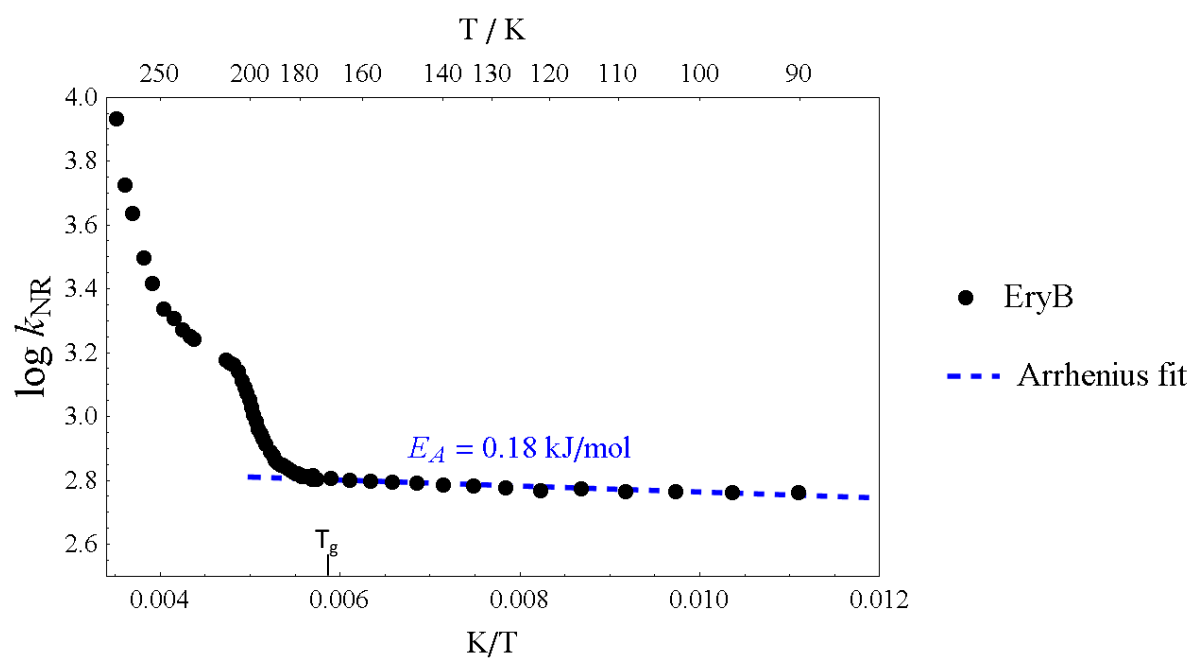
Figure II-4: Arrhenius plot of the rate of the non-radiative transition (k_{NR}) from the excited triplet state (T_1) to the ground singlet state (S_0) for erythrosine in 3:1 glycerol-water (v/v). The dashed line is an Arrhenius fit to the data at $T < T_g$. Solvent T_g is 170K.

Figure II-5

Figure II-5: Arrhenius plot of the rate of the non-radiative transition (k_{NR}) from the excited triplet state (T_1) to the ground singlet state (S_0) for erythrosine in 3:1 glycerol-water (v/v). The filled circles are the data from the previous figure, while the open circles are k_{nonvib}, the component of k_{NR} obtained after subtraction of the vibrational component (see text for details). The dashed lines are Arrhenius fit to the data.

Figure II-6
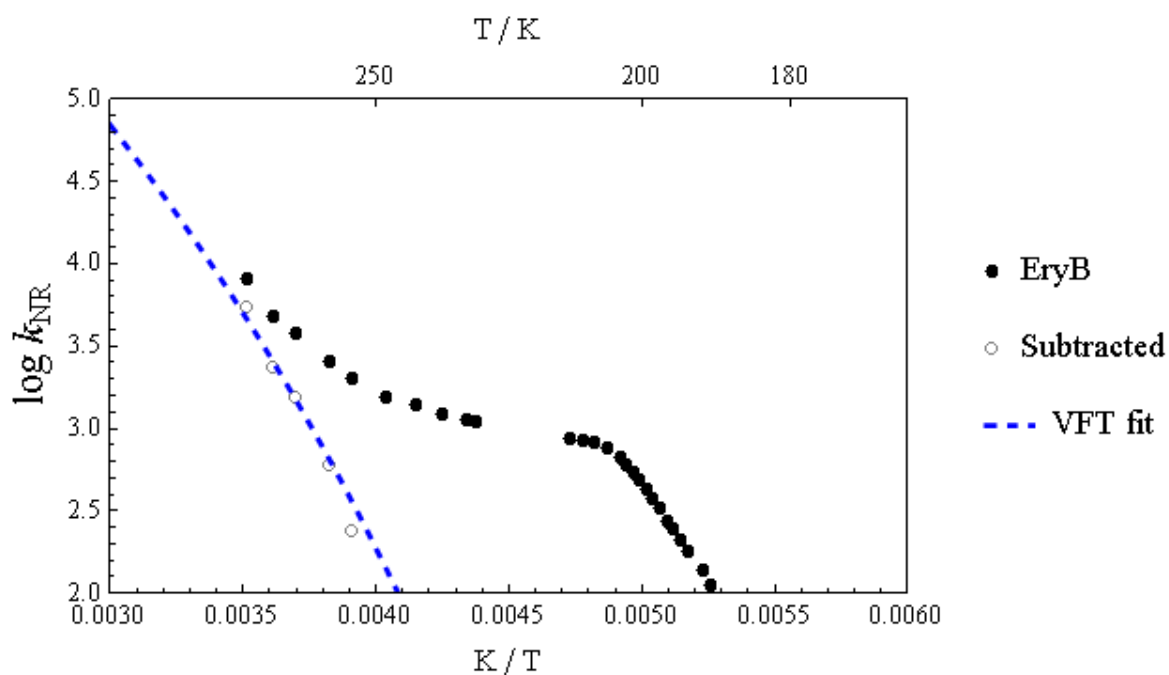
Figure II-6: Arrhenius plot of the nonvibrational component of the non-radiative transition (k_{nonvib}; filled circles) for erythrosine in 3:1 glycerol-water (v/v). The open circles are the component of k_{nonvib} obtained after subtraction of the 8.33 kJ/mol Arrhenius process from the previous figure. The dashed line is the Vogel-Fulcher-Tamman (VFT) fit of the solvent dielectric relaxation rate (k_{diel}) shifted vertically downward by 5.5 log units ($\log(k_{diel}) - 5.5$).

Figure II-7
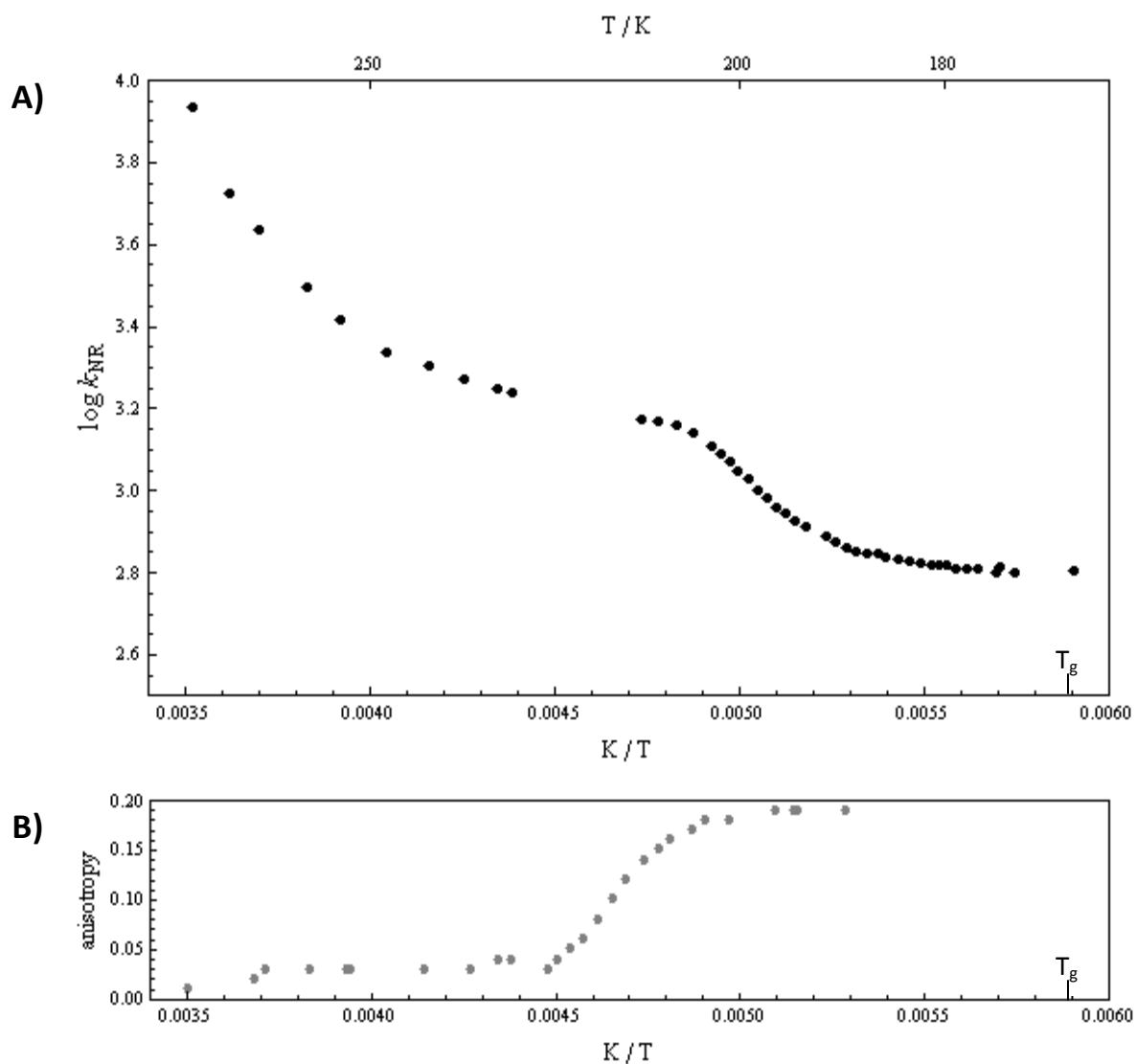
Figure II-7: (A) Arrhenius plot of the non-radiative transition (k_{NR}; filled circles) for erythrosine in 3:1 glycerol-water (v/v); (B) The steady state phosphorescence anisotropy (r_P) of erythrosine against inverse temperature.

Figure II-8

A)

B)
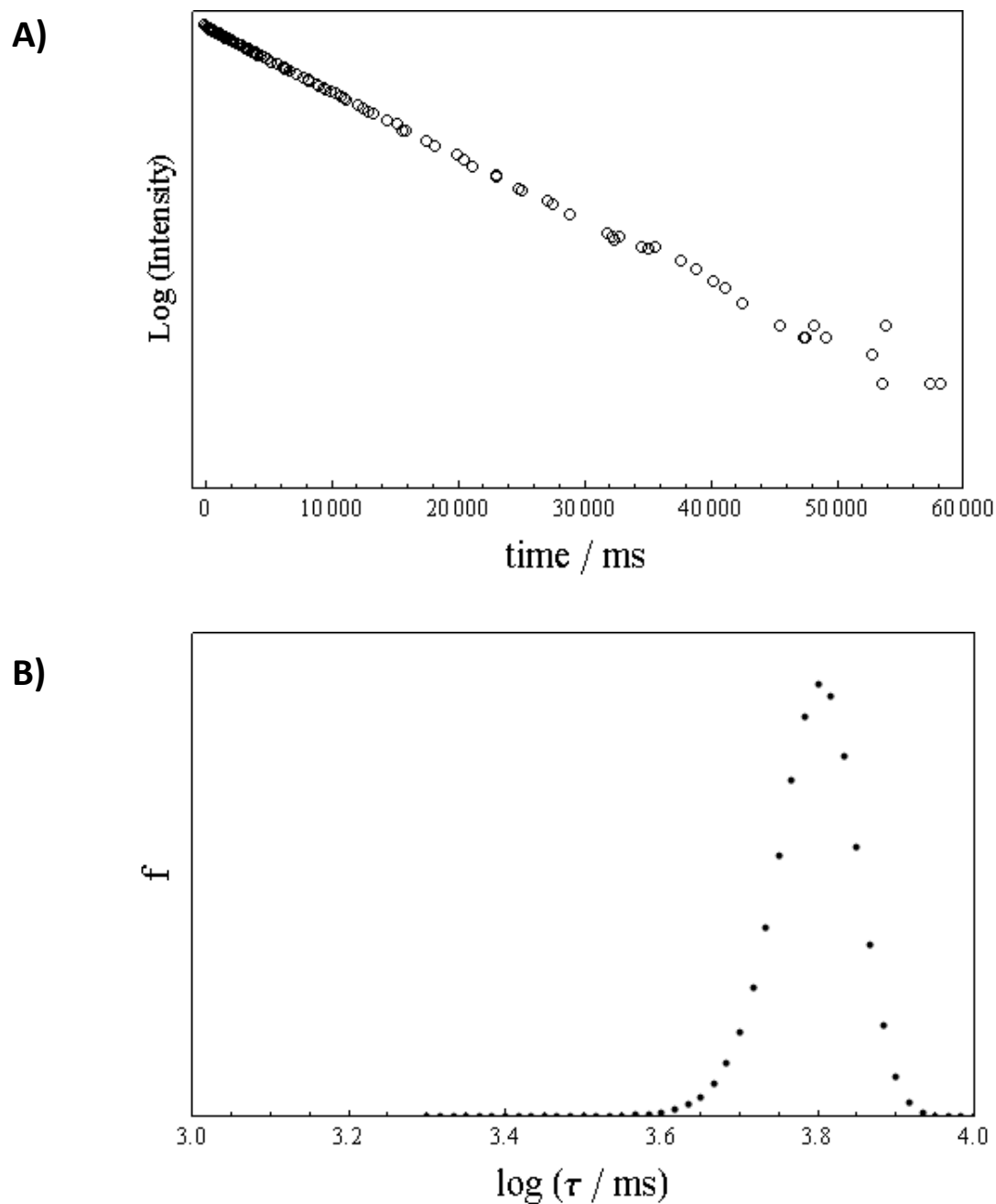
Figure II-8: (A) Phosphorescence intensity decay of tryptophan dispersed in 3:1 glycerol-water (v/v) at 77K. (B) The maximum entropy method (MEM) determined lifetime distribution of the data.

Figure II-9
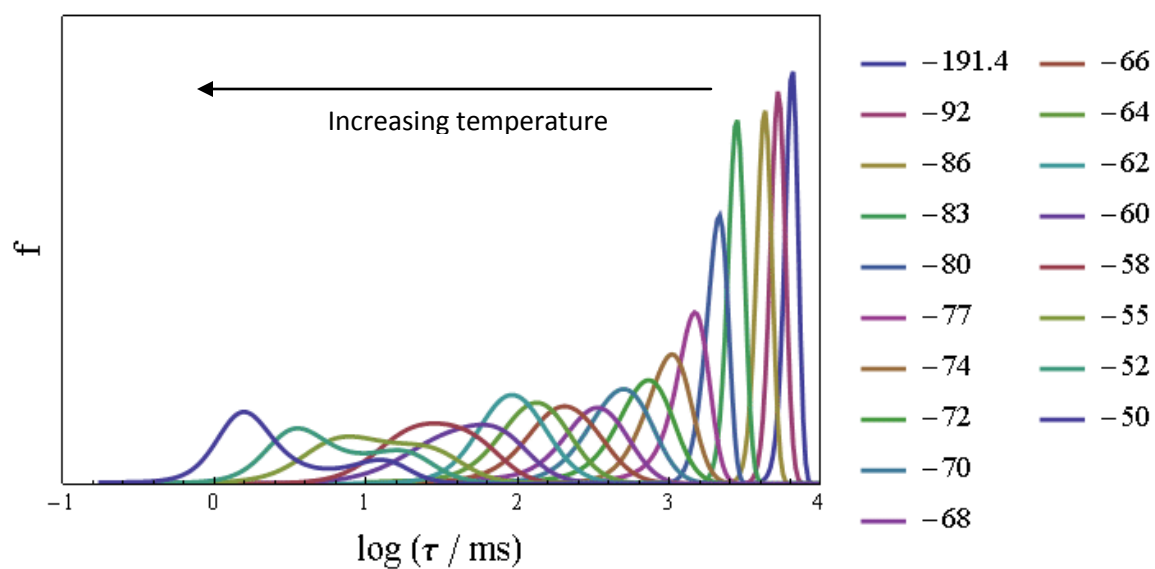
Figure II-9: Plots of the tryptophan phosphorescence MEM lifetime distribution at selected temperature points (°C). The distribution changes little from -191°C to the glass transition temperature of -103°C.

Figure II-10

A)

B)
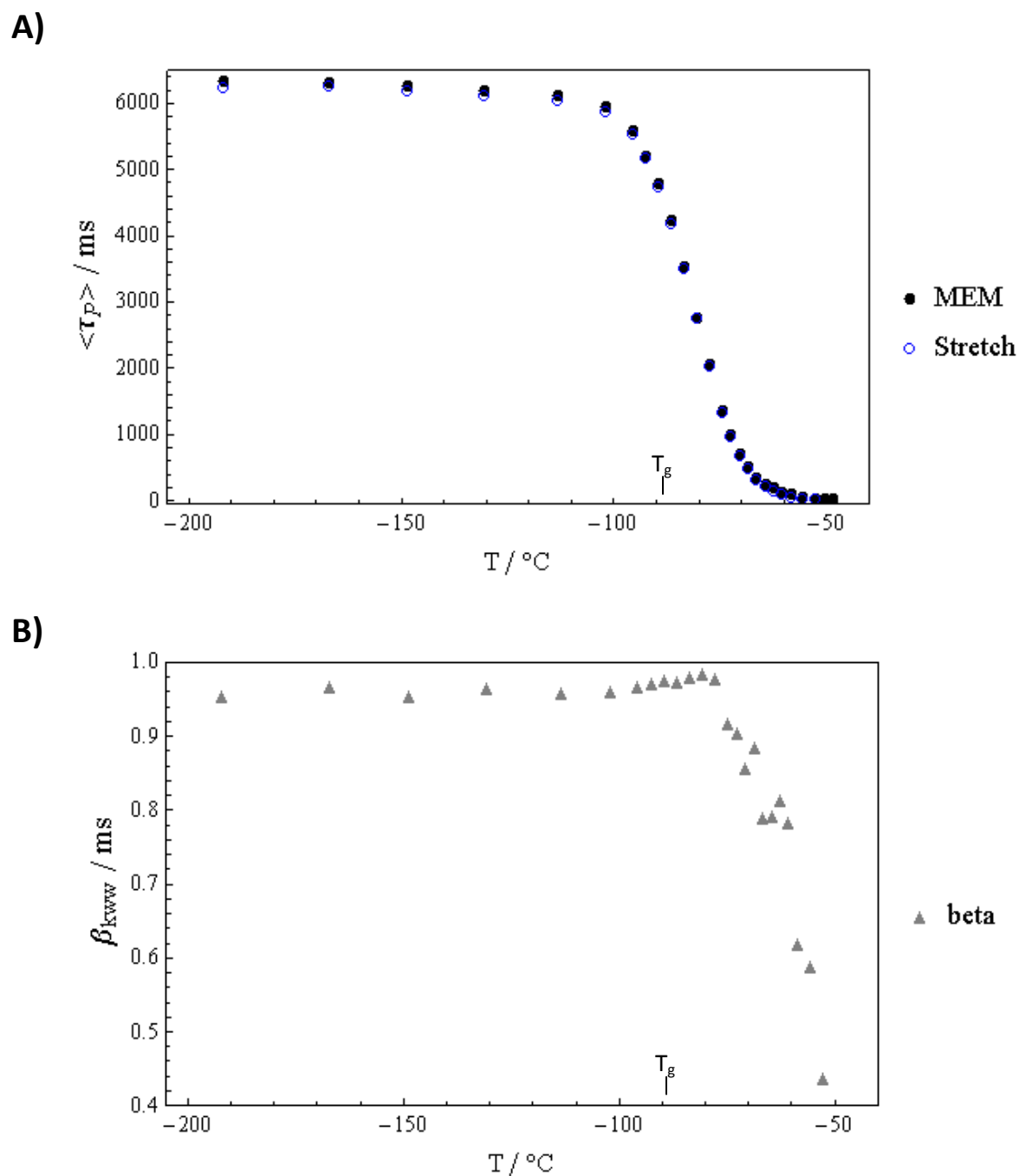
Figure II-10: Data obtained from phosphorescence of tryptophan in 3:1 glycerol-water (v/v) versus temperature. (A) Average phosphorescence lifetime of intensity decays as determined by fits to an MEM distribution of lifetimes as well as a stretched exponential function; (B) the stretching exponent beta (β) of the stretched exponential fits is an indicator of site heterogeneity.

Figure II-11
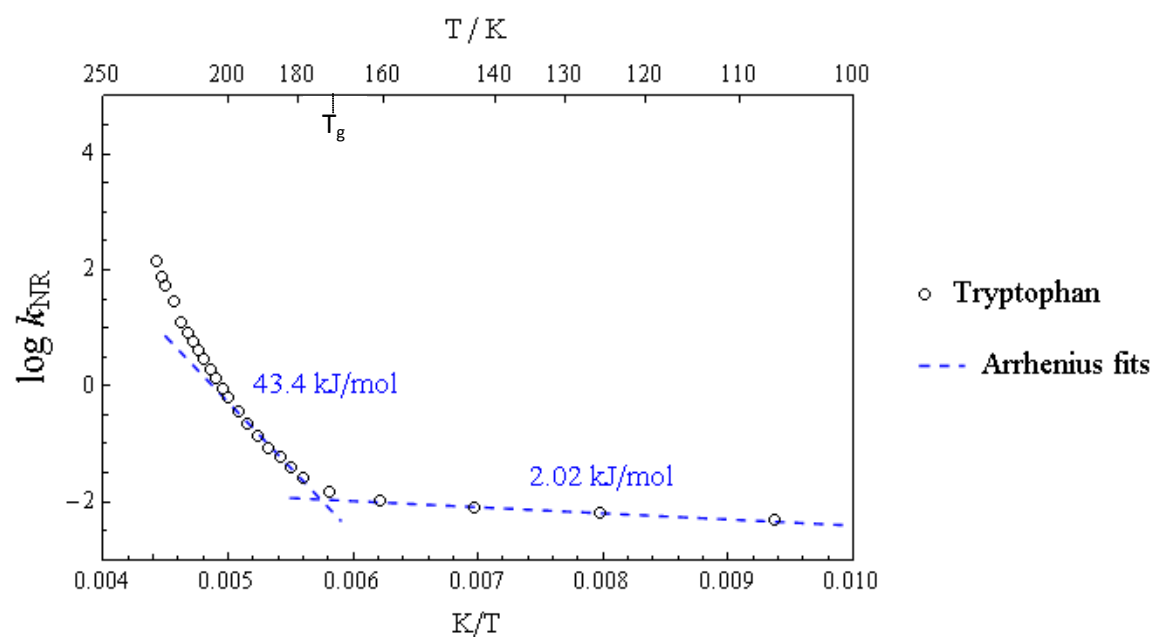
Figure II-11: Arrhenius plot of the rate of the non-radiative transition (k_{NR}) from the excited triplet state (T_1) to the ground singlet state (S_0) for tryptophan in 3:1 glycerol-water (v/v). The dashed lines are Arrhenius fits to the data at T < T_g (170K), and from T_g to T_g + 30K.

Figure II-12
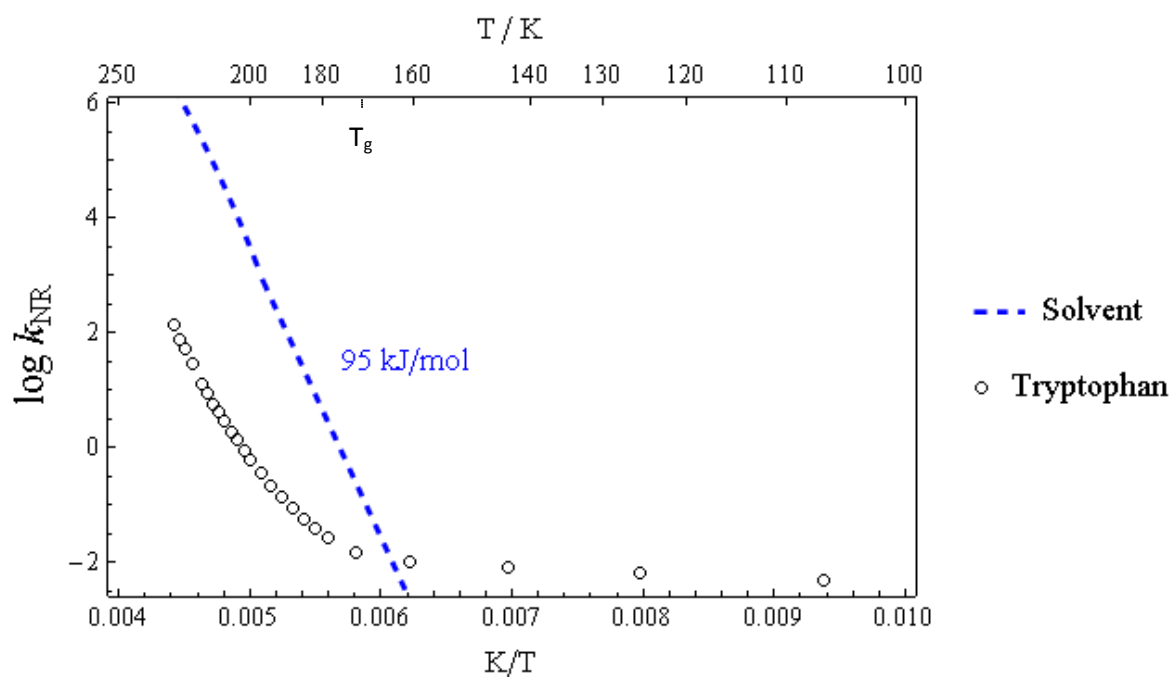
Figure II-12: Arrhenius plot of the rate of the non-radiative transition (k_{NR}) for tryptophan in 3:1 glycerol-water (v/v). The dashed lines is a fit to the rate of the primary solvent relaxation as determined by dielectric relaxation spectroscopy (k_{diel}).

Figure II-13
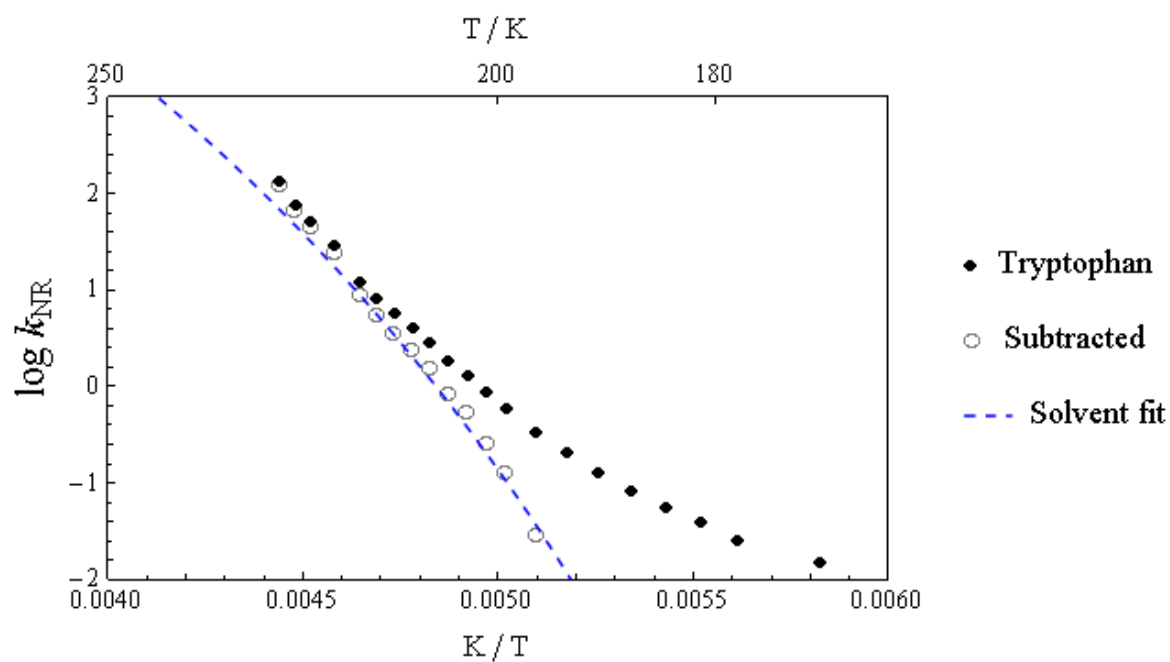
Figure II-13: Arrhenius plot of the rate of the non-radiative transition (k_{NR}, filled circles) for tryptophan in 3:1 glycerol-water (v/v). The empty circles are k_α, the component of k_{NR} that remain after subtraction of the 43.4 kJ/mol Arrhenius process from Fig. II-11. The dashed line is the VFT fit of solvent dielectric relaxation data shifted vertically downward by 4.4 log units ($\log(k_{diel}) - 4.4$).

Figure II-14

A)

B)
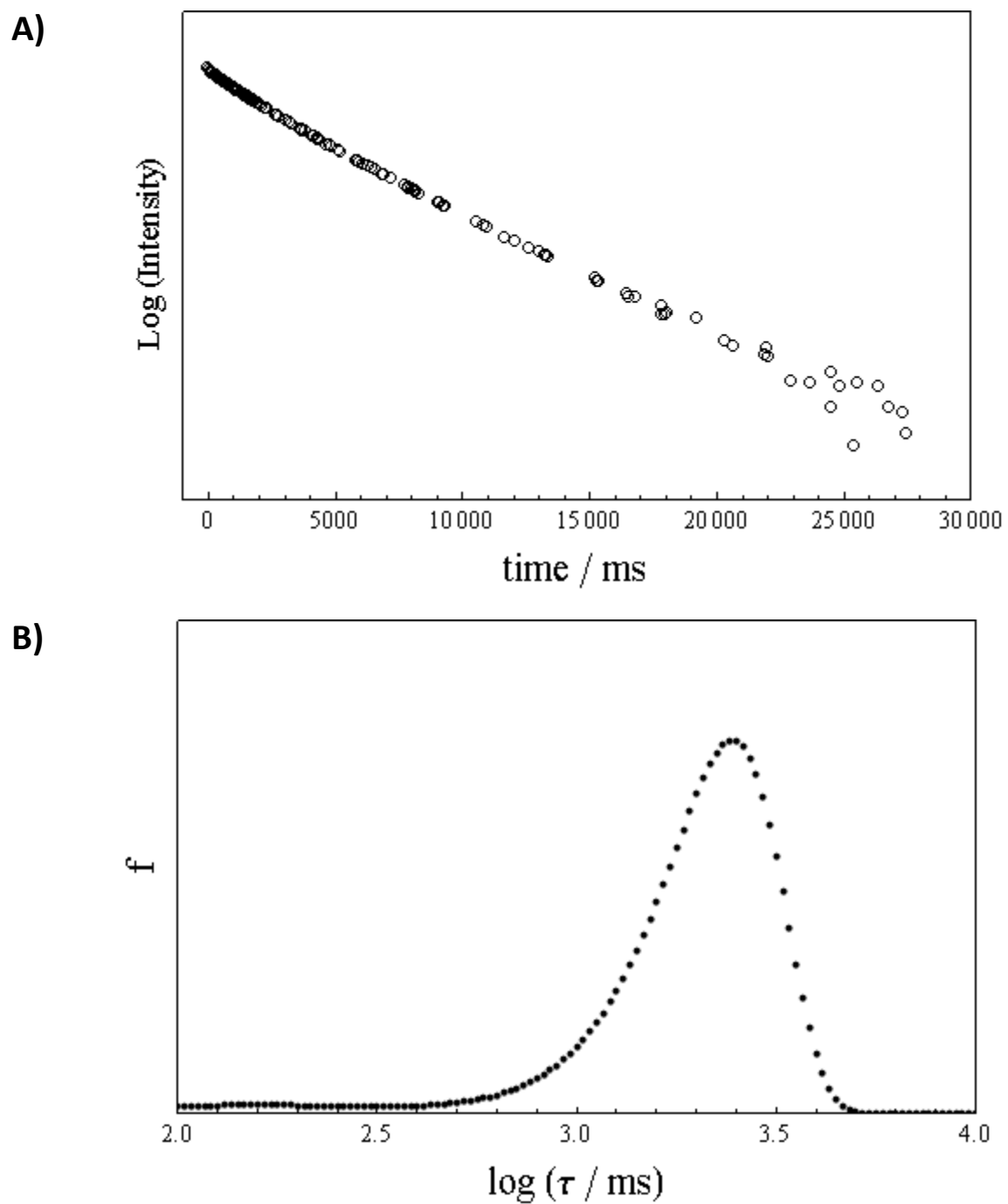
Figure II-14: (A) Phosphorescence intensity decay of tyrosine dispersed in 3:1 glycerol-water (v/v) at 77K. (B) The maximum entropy method (MEM) determined lifetime distribution of the data.

Figure II-15

A)

B)
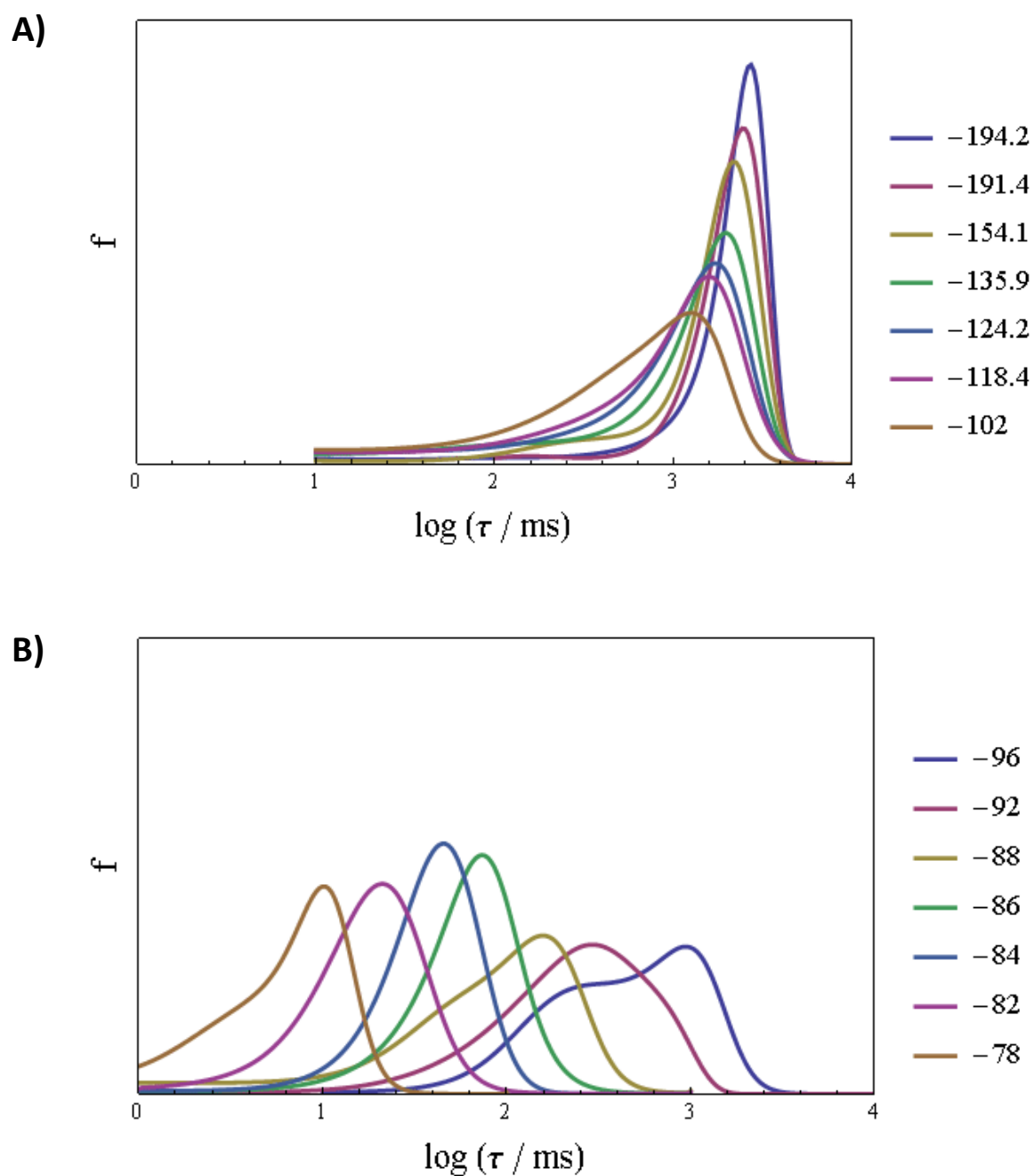
Figure II-15: Plots of the tyrosine phosphorescence MEM lifetime distribution at selected temperature points (°C): (A) For T < T_g (-103°C), the distribution becomes increasingly broad with increasing temperature; (B) once T_g is surpassed, the distribution remains broad and rapidly shifts to shorter values of log(τ).

Figure II-16

A)

B)
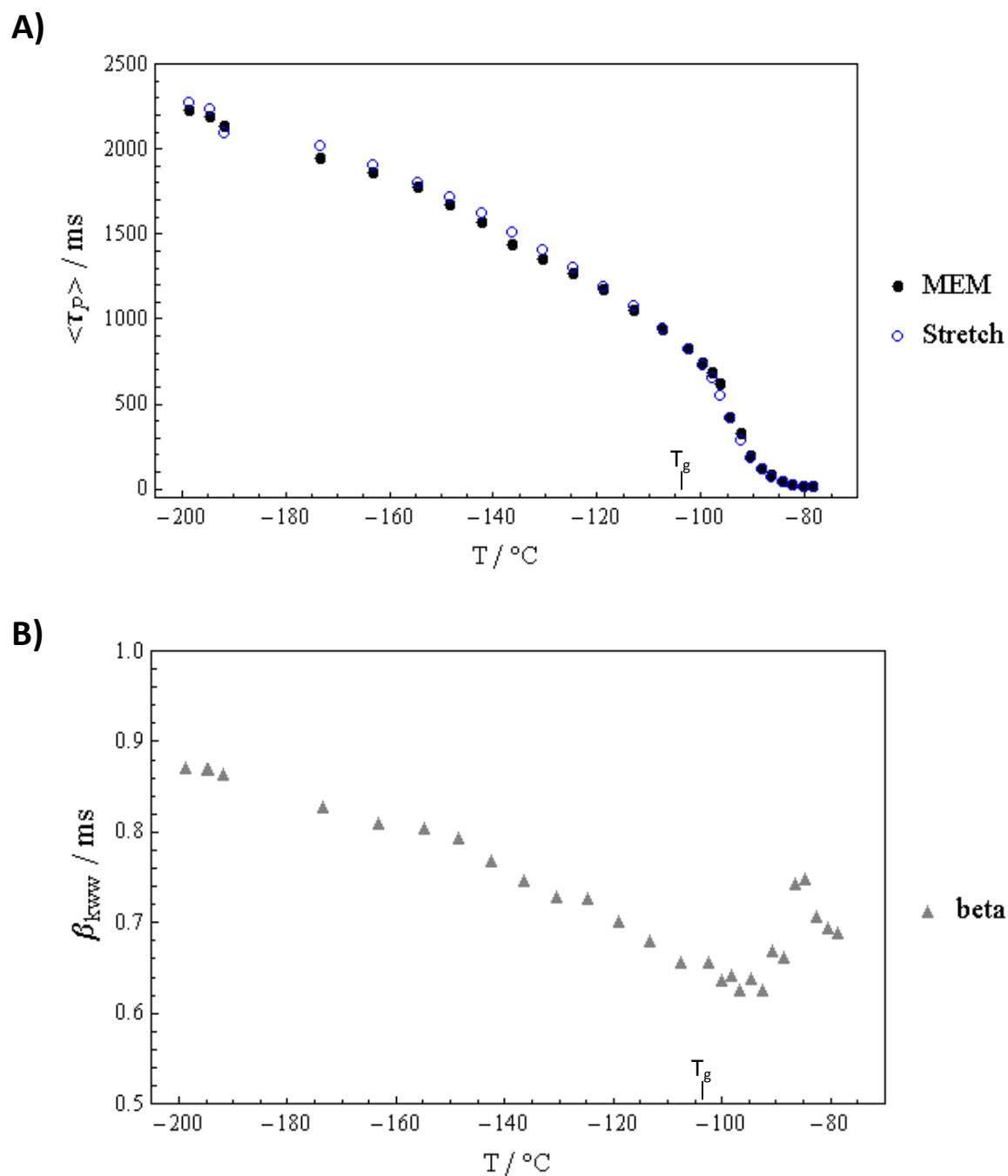
Figure II-16: Data obtained from phosphorescence of tyrosine in 3:1 glycerol-water (v/v) versus temperature. (A) Average phosphorescence lifetime of intensity decays as determined by fits to an MEM distribution of lifetimes as well as a stretched exponential function; (B) the stretching exponent beta (β) of the stretched exponential fits is an indicator of site heterogeneity.

Figure II-17
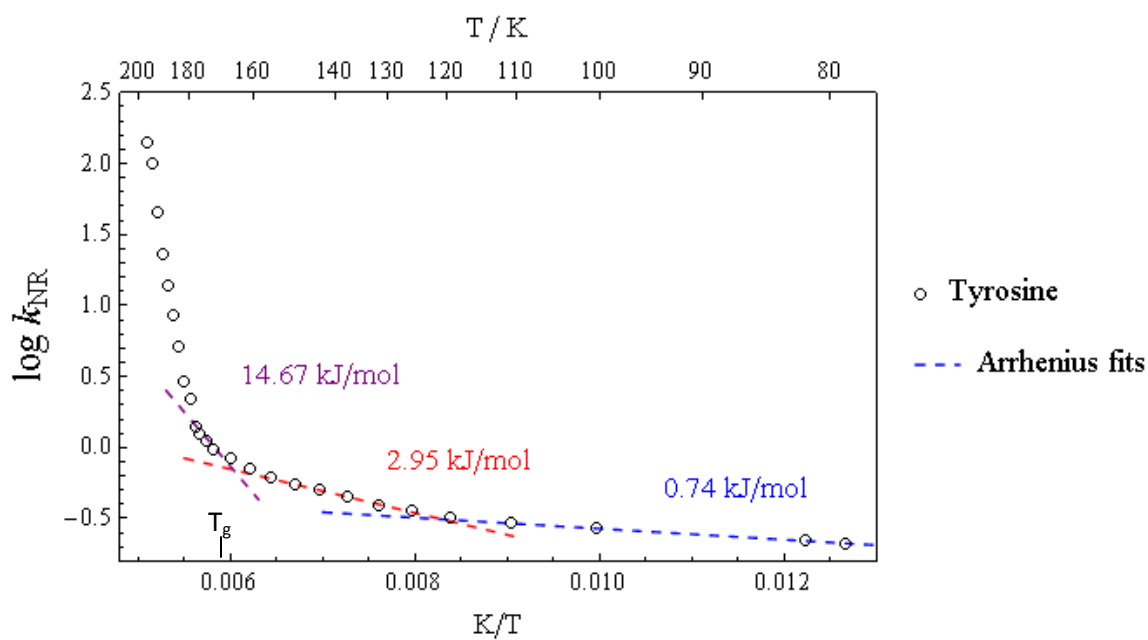
Figure II-17: Arrhenius plot of the rate of the non-radiative transition (k_{NR}) from the excited triplet state (T_1) to the ground singlet state (S_0) for tyrosine in 3:1 glycerol-water (v/v). The dashed lines are Arrhenius fits to the data at T < 120K, 125K< T < 160K, and 170K< T <180K.
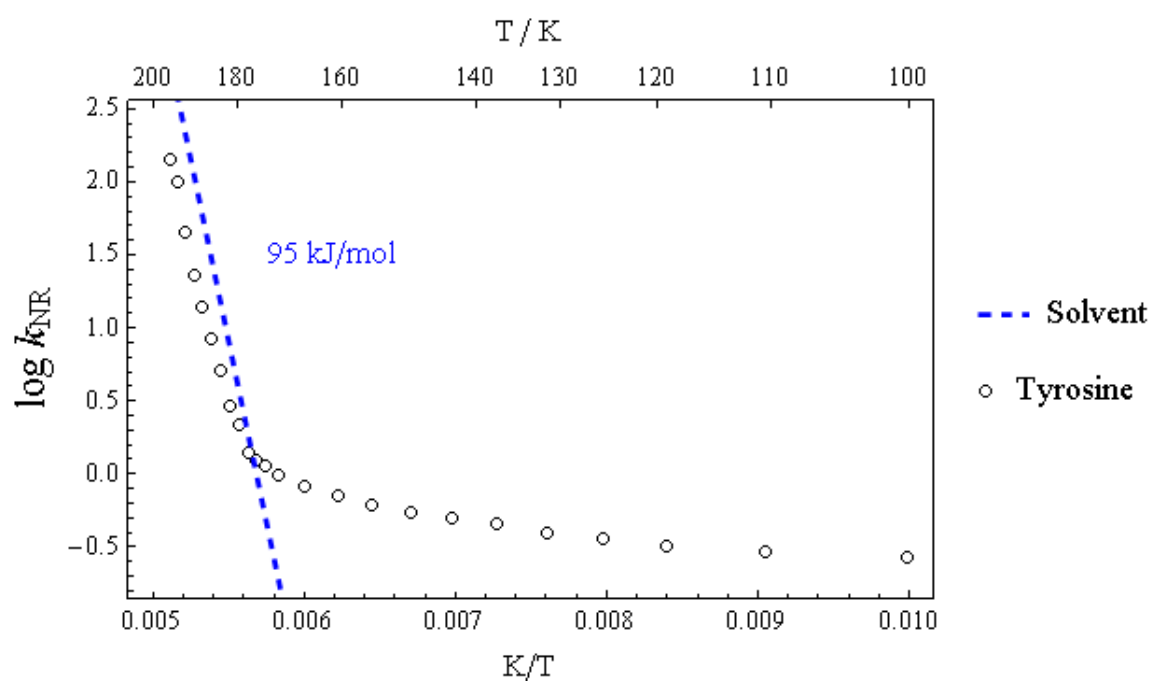
Figure II-18

Figure II-18: Arrhenius plot of the rate of the non-radiative transition (k_{NR}) from the excited triplet state (T_1) to the ground singlet state (S_0) for tyrosine in 3:1 glycerol-water (v/v). The dashed line is the VFT fit to the rate of solvent fluctuations as determined by solvent dielectric relaxation data (k_{diel}).

Figure II-19

A)

B)
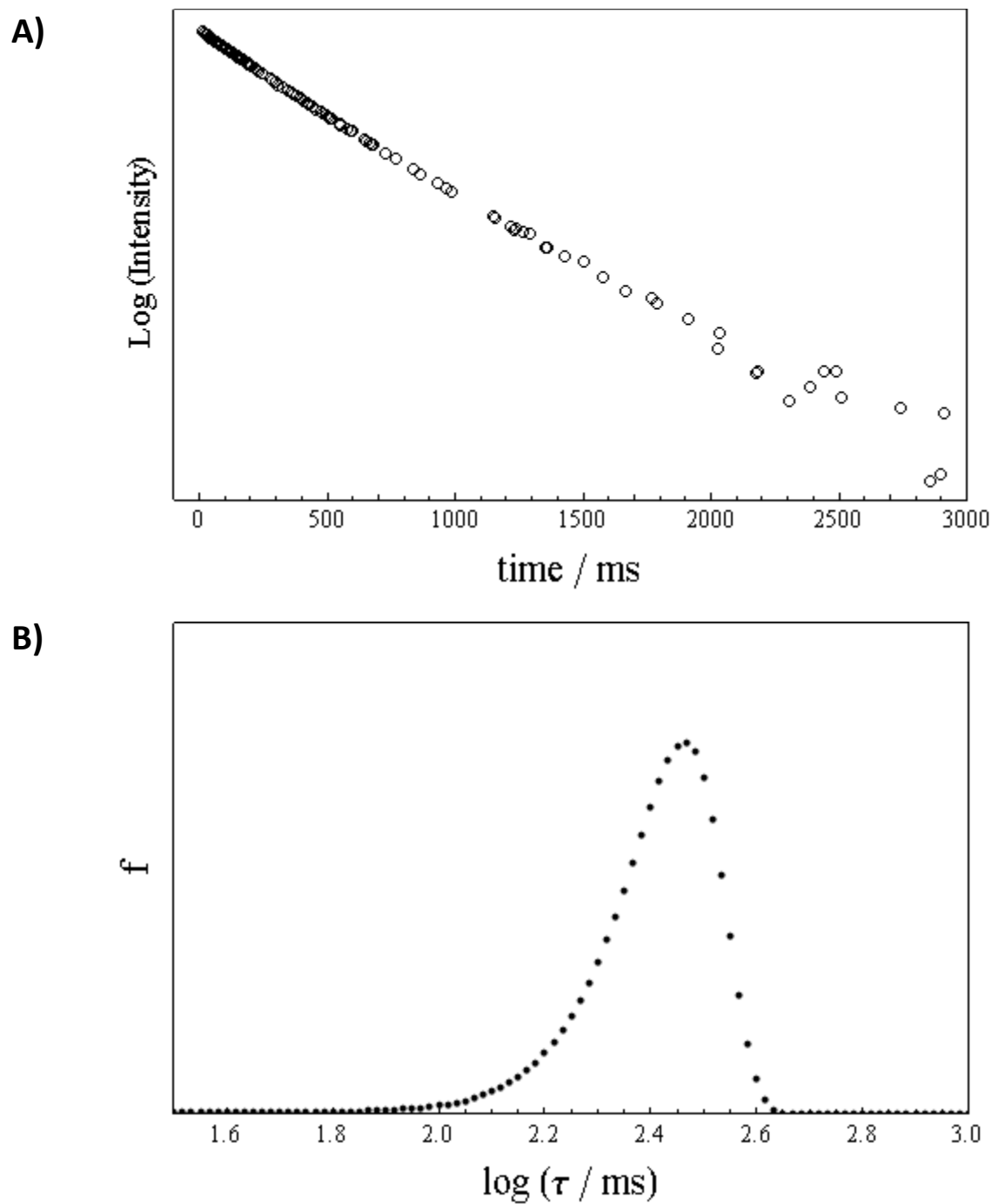
Figure II-19: (A) Phosphorescence intensity decay of vanillin dispersed in 3:1 glycerol-water (v/v) at 77K. (B) The maximum entropy method (MEM) determined lifetime distribution of the data.

Figure II-20

A)

B)
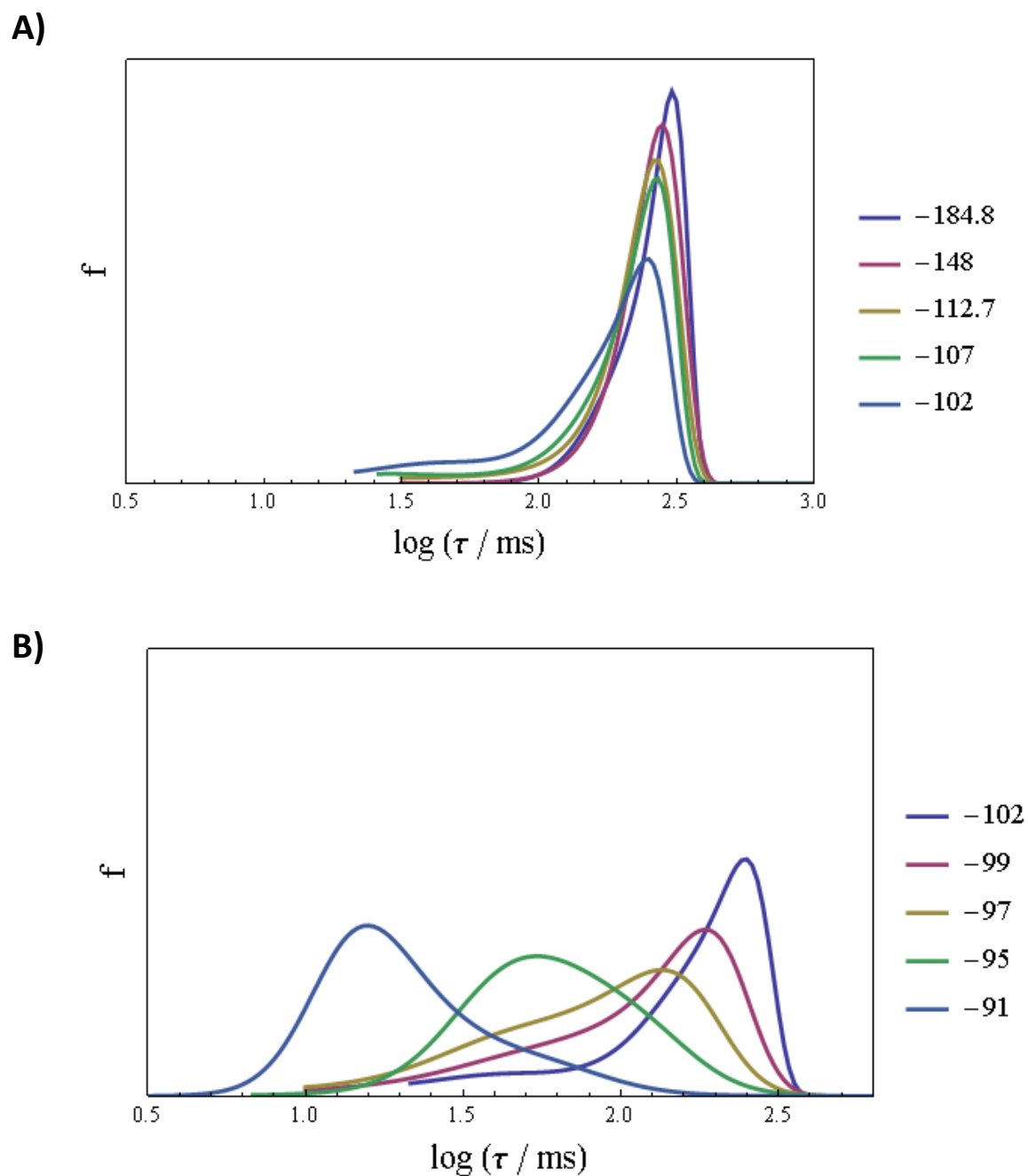
Figure II-20: Plots of the vanillin phosphorescence MEM lifetime distribution at selected temperature points (°C): (A) For T < T_g (-103°C), the distribution slightly broadens with increasing temperature; (B) once T_g is surpassed, the distribution becomes increasingly broad and rapidly shifts to shorter values of log(τ).

Figure II-21

A)

B)
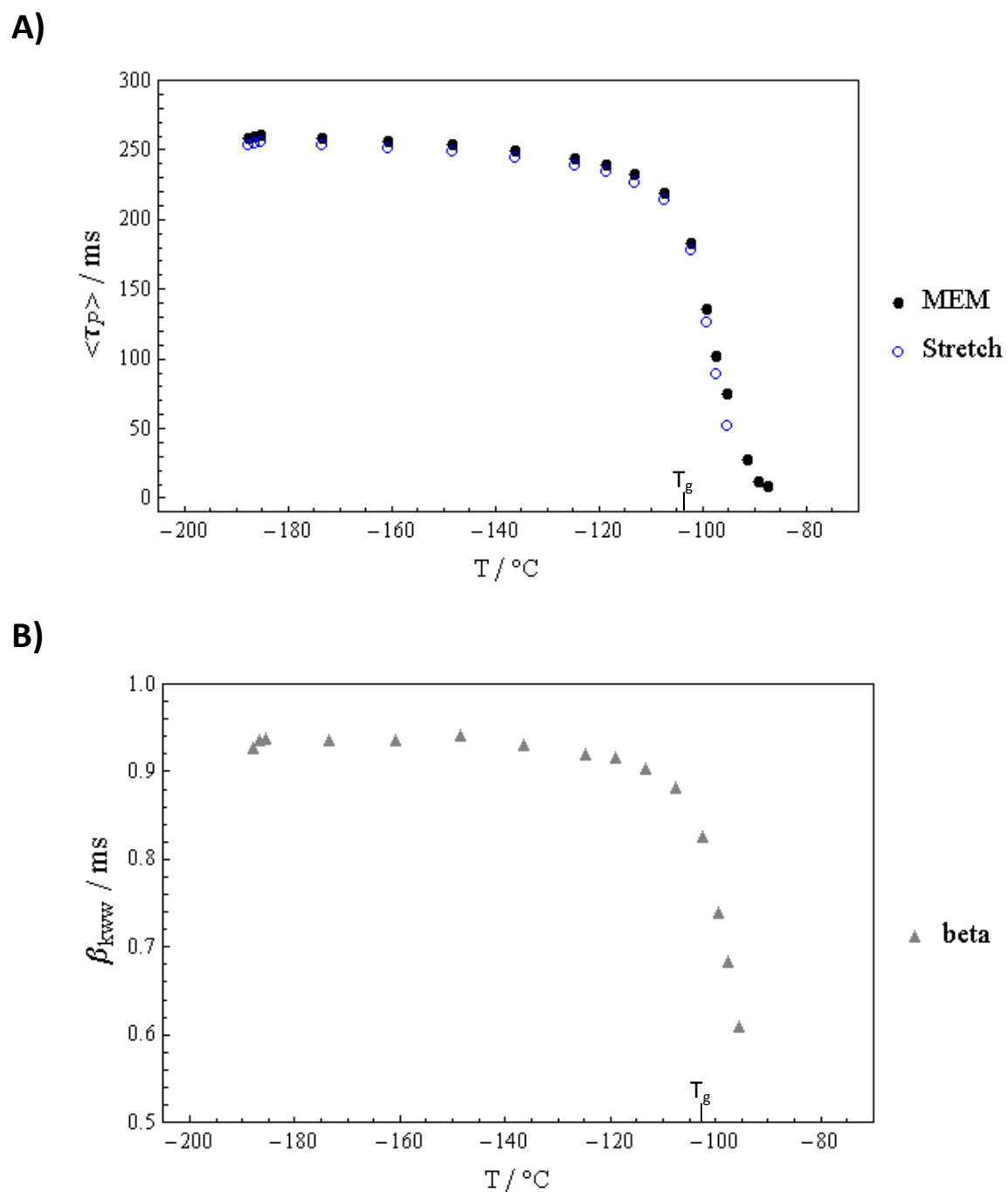
Figure II-21: Data obtained from phosphorescence of vanillin in 3:1 glycerol-water (v/v) versus temperature. (A) Average phosphorescence lifetime of intensity decays as determined by fits to an MEM distribution of lifetimes as well as a stretched exponential function; (B) the stretching exponent beta (β) of the stretched exponential fits is an indicator of site heterogeneity.
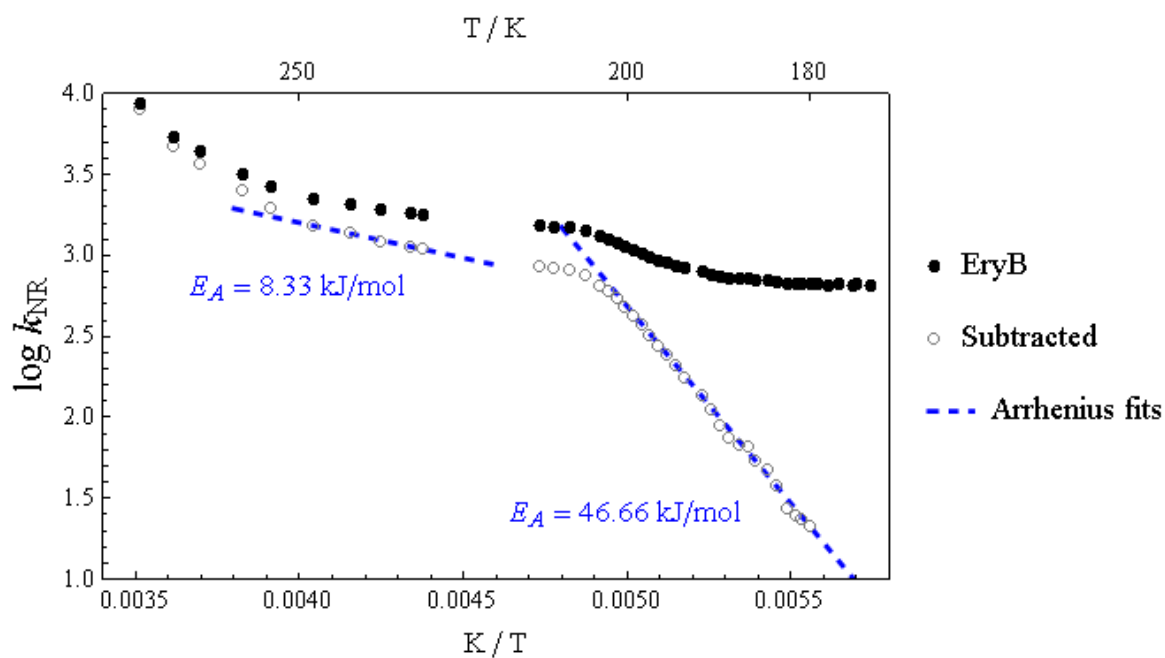
Figure II-22
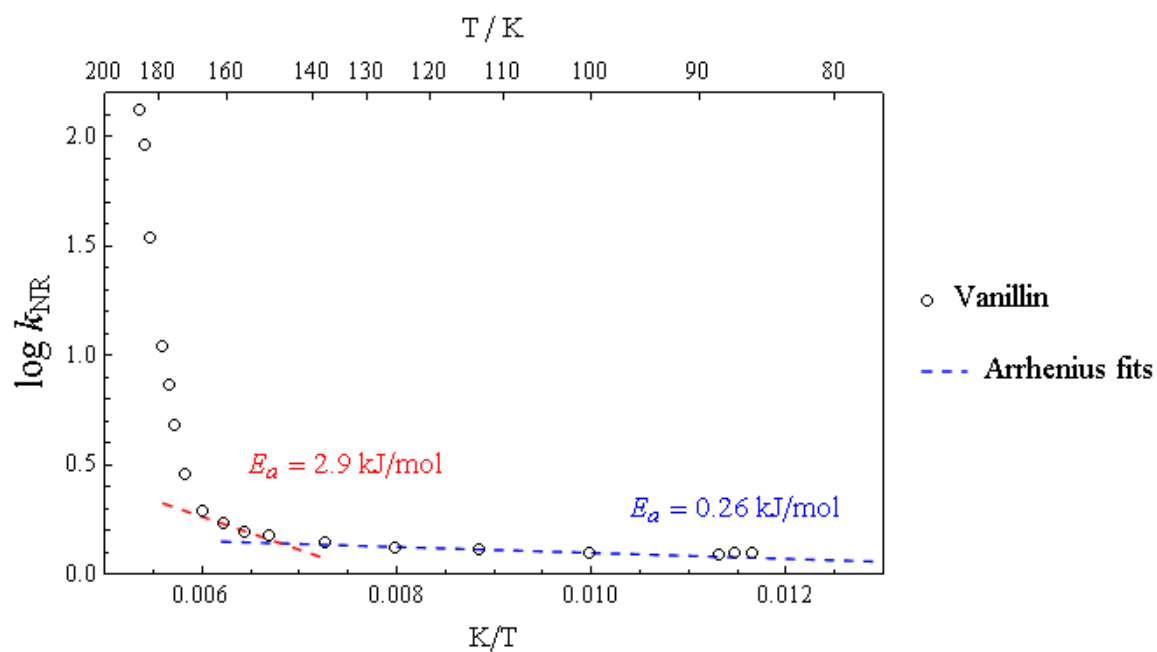
Figure II-22: Arrhenius plot of the rate of the non-radiative transition (k_{NR}) from the excited triplet state (T_1) to the ground singlet state (S_0) for vanillin in 3:1 glycerol-water (v/v). The dashed lines are Arrhenius fits to the data at T < 140K, and 150K< T <170K.

Figure II-23
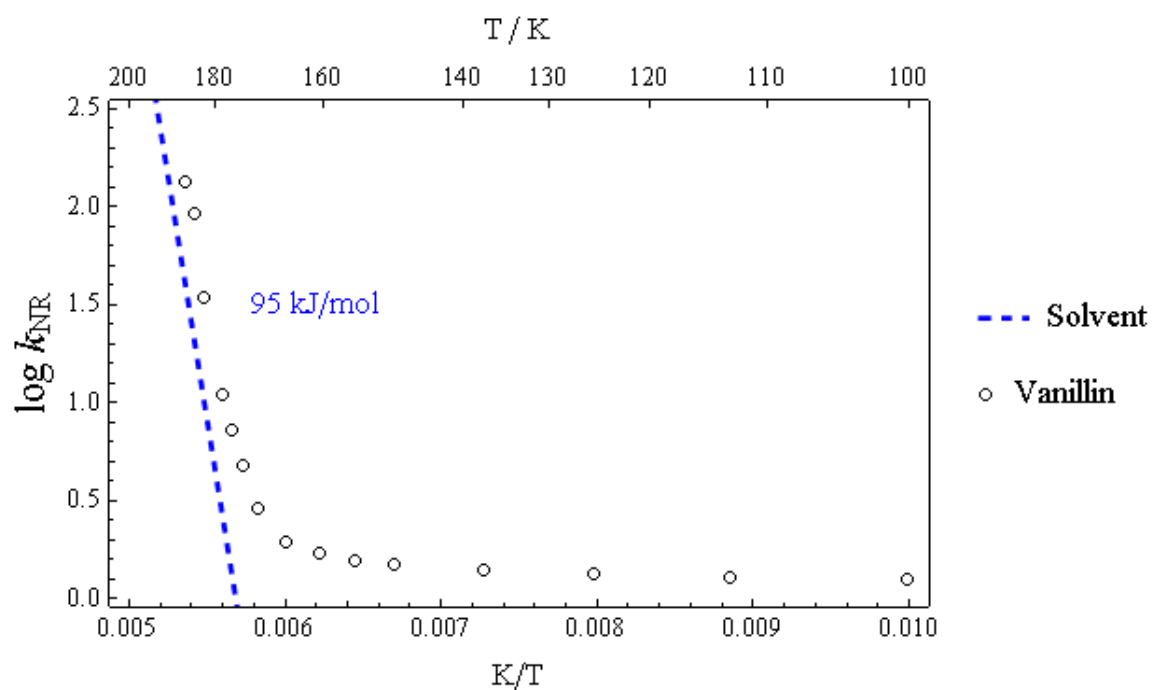
Figure II-23: Arrhenius plot of the rate of the non-radiative transition (k_{NR}) from the excited triplet state (T_1) to the ground singlet state (S_0) for vanillin in 3:1 glycerol-water (v/v). The dashed line is the VFT fit to the rate of solvent fluctuations as determined by solvent dielectric relaxation data (k_{diel}).

Figure II-24
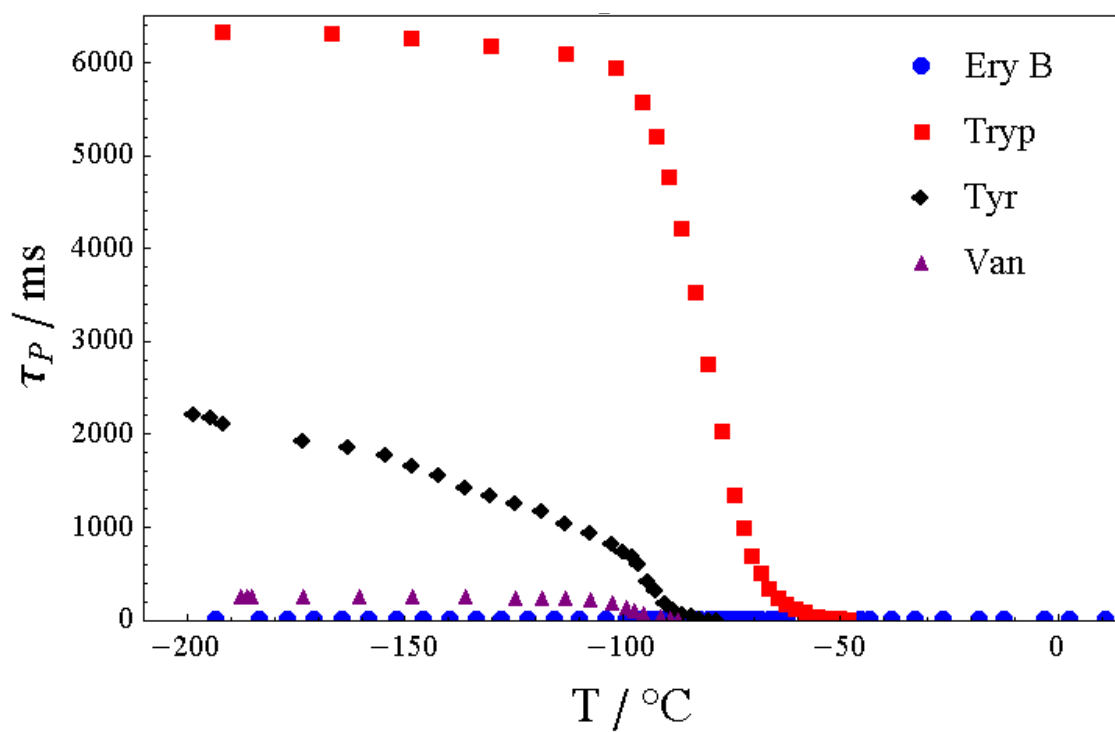
Figure II-24: Plots of the average phosphorescence lifetime vs. temperature for erythrosine, tryptophan, tyrosine, and vanillin in 3:1 glycerol-water (v/v).

Figure II-25
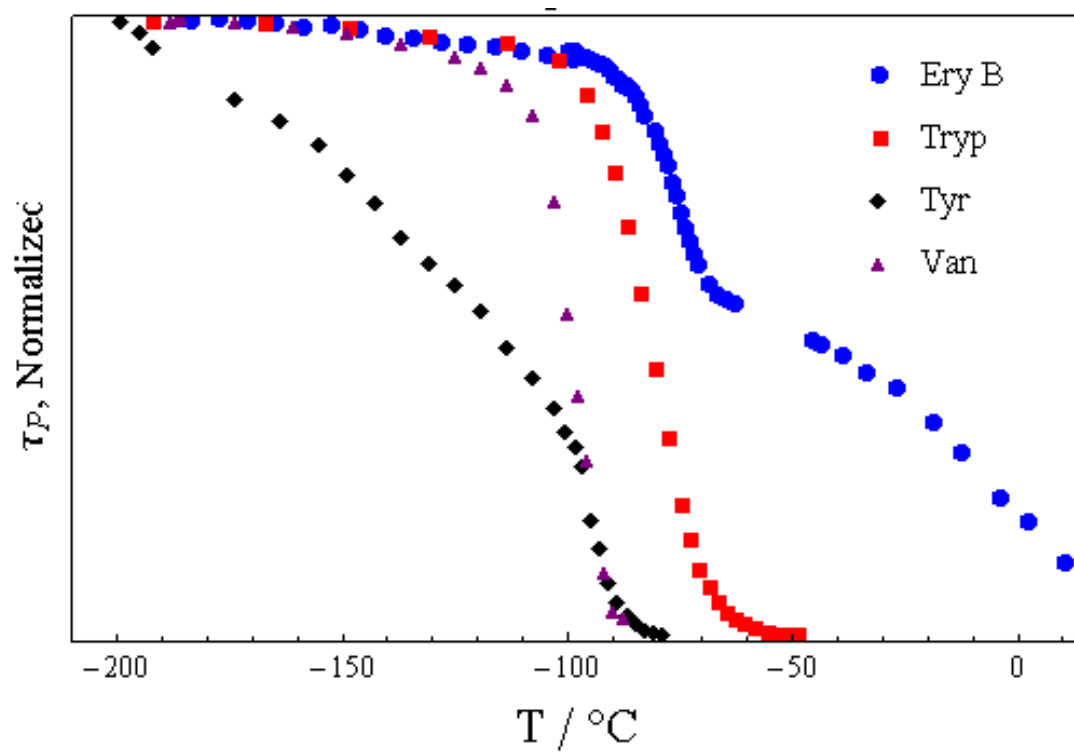
Figure II-25: Plots of the average phosphorescence lifetime normalized at -200°C for erythrosine, tryptophan, tyrosine, and vanillin in 3:1 glycerol-water (v/v).

Figure II-26
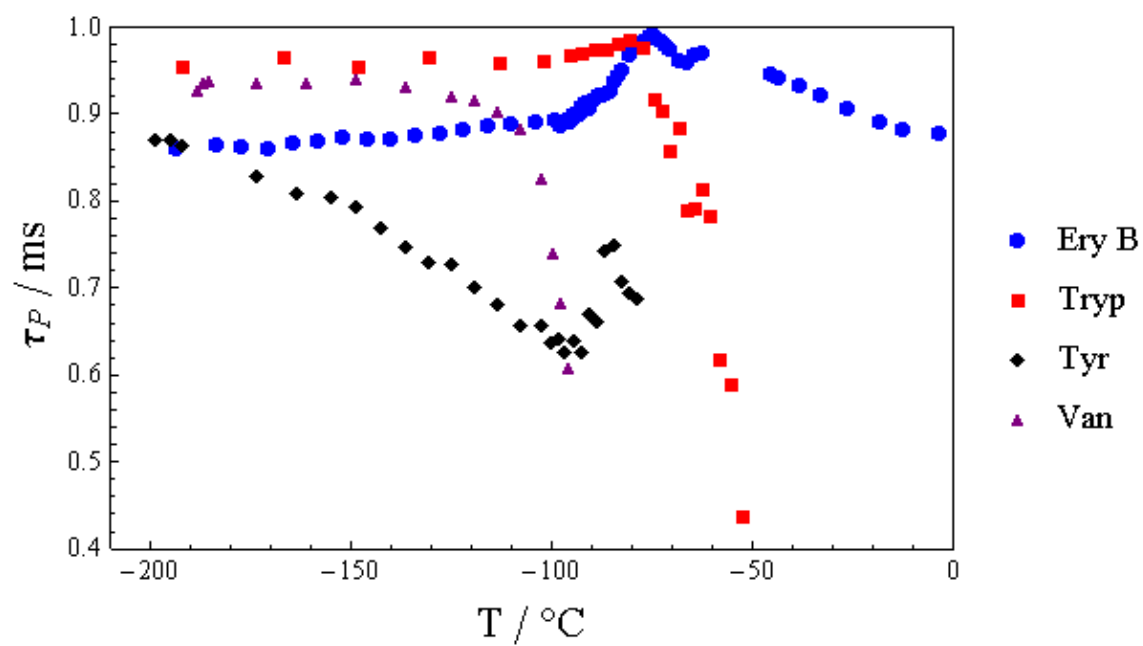
Figure II-26: The stretching exponent beta (β) of the stretched exponential fits for erythrosine, tryptophan, tyrosine, and vanillin phosphorescence decays plotted versus temperature.

Figure II-27
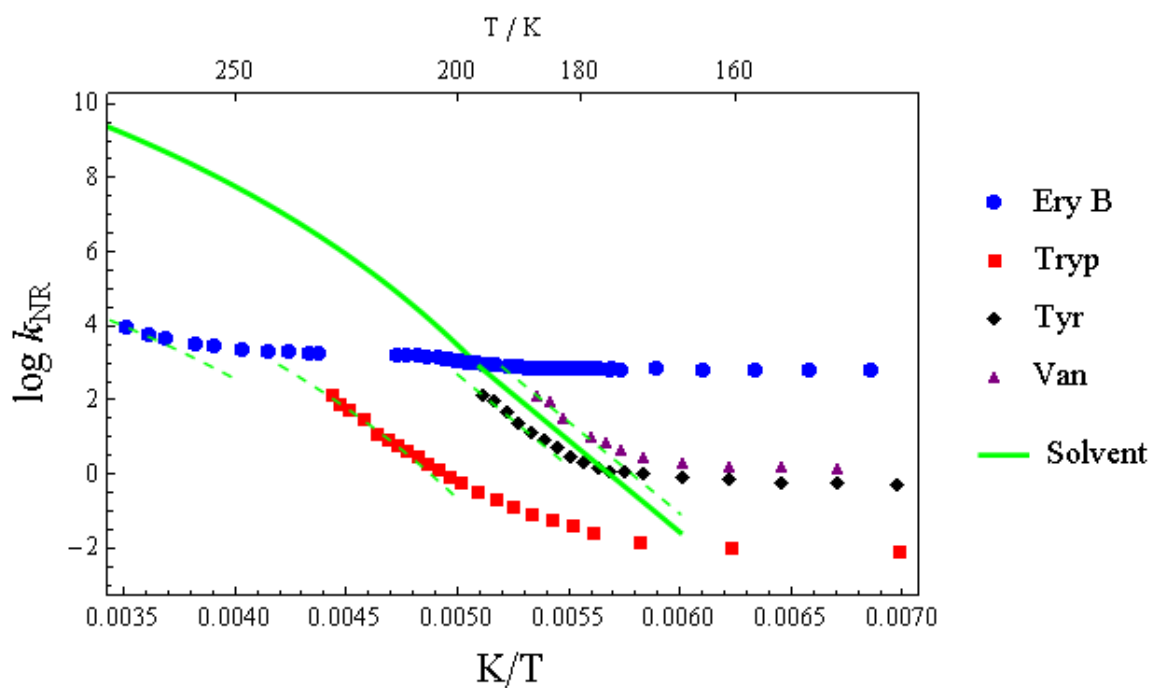
Figure II-27: Arrhenius plot of the rate of the non-radiative transition (k_{NR}) from the excited triplet state (T_1) to the ground singlet state (S_0) for erythrosine, tryptophan, tyrosine, and vanillin in 3:1 glycerol-water (v/v). The solid green line is a fit to the primary relaxation of the solvent as determined by dielectric relaxation spectroscopy experiments. The dashed lines are fits to the solvent relaxation with various downward shift to match k_{NR} of each individual probe.

Table II-1: The onset temperature (T_{onset}) of the solvent primary relaxation as detected by k_{NR}, and the ratio log (k_{diel} / k_{NR}) for erythrosine, tryptophan, tyrosine, and vanillin.

	T_{onset} / K	log (k_{diel} / k_{NR})
Erythrosine	250	5.5
Tryptophan	200	4.4
Tyrosine	185	0.4
Vanillin	175	-0.4

References

1.   Austin, R.H., et al., *Dynamics of ligand binding to myoglobin.* Biochemistry, 1975. **14**(24): p. 5355-73.
2.   Caliskan, G., et al., *Protein dynamics in viscous solvents.* Journal of Chemical Physics, 2003. **118**(9): p. 4230-4236.
3.   Sokolov, A.P., et al., *Dynamics of Strong and Fragile Glass Formers - Differences and Correlation with Low-Temperature Properties.* Physical Review Letters, 1993. **71**(13): p. 2062-2065.
4.   Frauenfelder, H., et al., *A unified model of protein dynamics.* Proceedings of the National Academy of Sciences of the United States of America, 2009. **106**(13): p. 5129-5134.
5.   Khodadadi, S., S. Pawlus, and A.P. Sokolov, *Influence of hydration on protein dynamics: combining dielectric and neutron scattering spectroscopy data.* Journal of Physical Chemistry B, 2008. **112**(45): p. 14273-80.
6.   Sudo, S. and S. Yagihara, *Universality of separation behavior of relaxation processes in supercooled aqueous solutions as revealed by broadband dielectric measurements.* The journal of physical chemistry. B, 2009. **113**(33): p. 11448-52.
7.   Sudo, S., et al., *Broadband dielectric study of alpha-beta separation for supercooled glycerol-water mixtures.* Journal of Non-Crystalline Solids, 2002. **307**: p. 356-363.
8.   Duchowicz, R., M.L. Ferrer, and A.U. Acuna, *Kinetic spectroscopy of erythrosin phosphorescence and delayed fluorescence in aqueous solution at room temperature.* Photochemistry and Photobiology, 1998. **68**(4): p. 494-501.
9.   Tsuboi, T., et al., *Photoluminescence properties of fluorone dyes in bio-related films at low temperatures.* Journal of Photochemistry and Photobiology a-Chemistry, 2011. **222**(2-3): p. 336-342.
10.   Lettinga, M.P., et al., *The orientation of the phosphorescence dipole moment of erythrosine B within its molecular frame.* Journal of Fluorescence, 1999. **9**(3): p. 265-279.
11.   Stein, R.A., et al., *Time-resolved phosphorescence anisotropy of erythrosin-EGF in the presence of membranes containing the EGF receptor: Is erythrosin EGF a good reporter of receptor dynamics?* Biophysical Journal, 1996. **70**(2): p. Mp347-Mp347.
12.   Silverstein, T.P. and H. Rottenberg, *Dynamic Protein Aggregates in the Mitochondrial Inner Membrane Probed by Time-Resolved Anisotropy Measurements of Erythrosin-Labeled-F.* Biophysical Journal, 1987. **51**(2): p. A489-A489.
13.   You, Y.M. and R.D. Ludescher, *The effect of glycerol on molecular mobility in amorphous sucrose detected by phosphorescence of erythrosin B.* Food Biophysics, 2007. **2**(4): p. 133-145.
14.   You, Y.M. and R.D. Ludescher, *The effect of sodium chloride on molecular mobility in amorphous sucrose detected by phosphorescence from the triplet probe erythrosin B.* Carbohydrate Research, 2008. **343**(2): p. 350-363.
15.   Joye, I.J., et al., *Monitoring Molecular Oxygen Depletion in Wheat Flour Dough Using Erythrosin B Phosphorescence: A Biophysical Approach.* Food Biophysics, 2012. **7**(2): p. 138-144.
16.   Draganski, A.R., et al., *Photophysical Probes of the Amorphous Solid State of Proteins.* Food Biophysics, 2010. **5**(4): p. 337-345.
17.   Simon-Lukasik, K.V. and R.D. Ludescher, *Erythrosin B phosphorescence as a probe of oxygen diffusion in amorphous gelatin films.* Food Hydrocolloids, 2004. **18**(4): p. 621-630.
18.   Lakowicz, J.R., *Principles of fluorescence spectroscopy.* 3rd ed2006, New York: Springer. xxvi, 954 p.
19.   Strambini, E.G. and G.B. Strambini, *Tryptophan phosphorescence as a monitor of protein conformation in molecular films.* Biosensors & Bioelectronics, 2000. **15**(9-10): p. 483-490.
20.   Fidy, J., B. Ullrich, and F. Tolgyesi, *Room temperature phosphorescence of tryptophan to study protein dynamics.* Biophysical Journal, 2000. **78**(1): p. 29a-29a.
21.   Subramaniam, V., A. Gafni, and D.G. Steel, *Time-resolved tryptophan phosphorescence spectroscopy: A sensitive probe of protein folding and structure.* Ieee Journal of Selected Topics in Quantum Electronics, 1996. **2**(4): p. 1107-1114.
22.   Strambini, G.B., *Tryptophan Phosphorescence as a Monitor of Protein Flexibility.* Journal of Molecular Liquids, 1989. **42**: p. 155-165.

23.   Papp, S. and J.M. Vanderkooi, *Tryptophan Phosphorescence at Room-Temperature as a Tool to Study Protein-Structure and Dynamics.* Photochemistry and Photobiology, 1989. **49**(6): p. 775-784.

24.   Creed, D., *The Photophysics and Photochemistry of the near-Uv Absorbing Amino-Acids .2. Tyrosine and Its Simple Derivatives.* Photochemistry and Photobiology, 1984. **39**(4): p. 563-575.

25.   Keiki, J.L.K. and K. Rousslang, *Phosphorescence of 3-fluoro-1-tyrosine: A spectroscopic probe for protein local structure.* Abstracts of Papers of the American Chemical Society, 2003. **225**: p. U474-U474.

26.   Tiwari, R. and R.D. Ludescher, *Molecular mobility in a homologous series of amorphous solid glucose oligomers.* Food Chemistry, 2012. **132**(4): p. 1814-1821.

27.   Tiwari, R.S. and R.D. Ludescher, *Vanillin Phosphorescence as a Probe of Molecular Mobility in Amorphous Sucrose.* Journal of Fluorescence, 2010. **20**(1): p. 125-133.

28.   Nishigaki, A., et al., *Hysteresis in the temperature dependence of phosphorescence of 4-hydroxy-3-methoxybenzaldehyde (vanillin) in ethanol.* Journal of Physical Chemistry A, 1998. **102**(7): p. 1106-1111.

29.   Richert, R., *Triplet state solvation dynamics: Basics and applications.* Journal of Chemical Physics, 2000. **113**(19): p. 8404-8429.

30.   Richert, R. and H. Wendt, *Dynamic heterogeneity of solvent response times.* Abstracts of Papers of the American Chemical Society, 2000. **220**: p. U172-U172.

31.   Steinbach, P.J., *Filtering artifacts from lifetime distributions when maximizing entropy using a bootstrapped model.* Analytical biochemistry, 2012. **427**(1): p. 102-105.

32.   Steinbach, P.J., R. Ionescu, and C.R. Matthews, *Analysis of kinetics using a hybrid maximum-entropy/nonlinear-least-squares method: Application to protein folding.* Biophysical Journal, 2002. **82**(4): p. 2244-2255.

33.   Welch, R.C., et al., *Dynamics of Glass Relaxation at Room Temperature.* Physical Review Letters, 2013. **110**(26).

34.   Swenson, J., I. Koper, and M.T.F. Telling, *Dynamics of propylene glycol and its 7-mer by neutron scattering.* Journal of Chemical Physics, 2002. **116**(12): p. 5073-5079.

35.   Wang, C.J., et al., *Relaxation dynamics and glass transition in glassy materials.* Synthetic Metals, 2003. **135**(1-3): p. 495-496.

36.   Bishai, F., E. Kuntz, and L. Augenstein, *Intra- and intermolecular factors affecting the excited states of aromatic amino acids.* Biochimica et Biophysica Acta, Protein Structure, 1967. **140**(3): p. 381-394.

37.   Schlyer, B.D., et al., *Time-Resolved Room-Temperature Protein Phosphorescence - Nonexponential Decay from Single Emitting Tryptophans.* Biophysical Journal, 1994. **67**(3): p. 1192-1202.

38.   Huang, R.H., *Phosphorescence of five amino acids.* Progress in Biochemistry and Biophysics, 1997. **24**(1): p. 60-63.

39.   Huang, J., et al., *Light induced relaxation, conformational averaging and relaxation in photodissociated COHbA.* Biophysical Journal, 1996. **70**(2): p. Su464-Su464.

40.   Gottfried, D.S., et al., *Evidence for damped hemoglobin dynamics in a room temperature trehalose glass.* Journal of Physical Chemistry, 1996. **100**(29): p. 12034-12042.

41.   Fenimore, P.W., et al., *Bulk-solvent and hydration-shell fluctuations, similar to alpha- and beta-fluctuations in glasses, control protein motions and functions.* Proceedings of the National Academy of Sciences of the United States of America, 2004. **101**(40): p. 14408-14413.

42.   Johari, G.P. and M. Goldstein, *Viscous liquids and the glass transition. II. Secondary relaxations in glasses of rigid molecules.* Journal of Chemical Physics, 1970. **53**(6): p. 2372-2388.

43.   Fischer, C.J., et al., *The triplet-state lifetime of indole in aqueous and viscous environments: Significance to the interpretation of room temperature phosphorescence in proteins.* Journal of the American Chemical Society, 2002. **124**(35): p. 10359-10366.

44.   Cioni, P., L. Erijman, and G.B. Strambini, *Phosphorescence emission of 7-azatryptophan and 5-hydroxytryptophan in fluid solutions and in alpha(2) RNA polymerase.* Biochemical and biophysical research communications, 1998. **248**(2): p. 347-351.

45.   Allen, B.D., et al., *The photophysical properties of a julolidine-based molecular rotor.* Physical Chemistry Chemical Physics, 2005. **7**(16): p. 3035-3040.

46.   Demchenko, A.P. and P.R. Callis, *Advanced fluorescence reporters in chemistry and biology I : fundamentals and molecular design*. Springer series on fluorescence,2010, Heidelberg ; New York: Springer. x, 389 p.

47.   Miura, T., et al., *Rational design principle for modulating fluorescence properties of fluorescein-based probes by photoinduced electron transfer.* Journal of the American Chemical Society, 2003. **125**(28): p. 8666-8671.

48.   Nucci, N.V., J.N. Scott, and J.M. Vanderkooi, *Coupling of complex aromatic ring vibrations to solvent through hydrogen bonds: Effect of varied on-ring and off-ring hydrogen-bonding substitutions.* Journal of Physical Chemistry B, 2008. **112**(13): p. 4022-4035.

CHAPTER III: **Evidence of solvent slaving of protein dynamics via single tryptophan phosphorescence of human serum albumin and a 20-amino acid trp-cage miniprotein**

<u>**Introduction**</u>

The goal of the field of protein dynamics is to fully characterize the transitions among protein conformational substates that ultimately are responsible for protein function[1]. Protein conformational fluctuations are distinct from normal mode harmonic vibrations as they involve some degree of structural change[2]. They may be small in scale, such as the rotation of an amino acid side group; or large, such as the hinge-like opening of a binding site. In any case, a conformational transition necessarily involves the coordinated motion of a number of atoms. It is believed that such motions are made possible by the solvent, through its bulk fluctuations as well as its modulation of the protein hydration shell[3]. It is common practice in studies of protein dynamics to slow the rate of fluctuations by conducting experiments at low temperature in glass-forming solvents such as glycerol-water[4, 5]. At a temperature below T_g, many of the solvent relaxations are too slow to drive the associated protein dynamics. Monitoring observable rates (of protein, bulk solvent, and hydration shell) as a function of temperature from the glassy state to the melt allows elucidation of the different processes at work.

One way to monitor protein dynamics is through tryptophan phosphorescence[6-9]. While phosphorescence is a complex phenomenon that does not directly measure local fluctuations, it is well established that in the absence of quenchers the rate of non-radiative decay from the triplet state (k_{NR}) is highly sensitive to local environmental fluctuations [9, 10]. By monitoring the time-resolved phosphorescence of a single-Trp protein (wild type or mutant), one can probe local mobility at a variety of sites along the polypeptide chain (e.g., surface or buried), revealing the energetics of motions at different locales. Despite its complexities, trp phosphorescence offers tremendous upside over other experimental techniques which often provide non-local/non-site specific information. Neutron scattering[11-13], dielectric relaxation[14-16], and infrared spectroscopy[17, 18] typically provide ensemble measurements; Mossbauer spectroscopy[19] and CO-stretch absorption[20] are site-specific, but the site is fixed, and limited to proteins containing a heme group. Also, many methods require an expensive radiation source and are thus impractical as a tool for multiple rapid assays. Finally, with the exception of experiments that

monitor CO-recombination in heme proteins, most of the techniques mentioned probe the environment over the sub-nanosecond timescale.

This work monitors the internal dynamics of the globular protein human serum albumin (HSA) and a 20 amino acid trp-cage miniprotein (PDB code 1L2Y) in a prototypical glass-forming solvent: a 3:1 (vol/vol) glycerol/water mixture. Phosphorescence decays of the single tryptophan residue are collected as a function of temperature. To explore the relation between internal protein motions and those in the bulk solvent, the dynamics of the bulk solvent are monitored via phosphorescence of dispersed free tryptophan. HSA is an important protein whose function as a carrier of hydrophobic molecules in the bloodstream is well characterized [21]. It is a three domain heart-shaped 66 kDa globular protein, with multiple ligand binding sites[22]. HSA contains a single tryptophan residue at position 214, which has been used extensively as an intrinsic probe of protein structure and binding properties[23]. The residue in HSA is near the surface of the protein but inaccessible to solvent, and therefore monitors mobility at an internal site. The 20 residue, 2.1 kDa trp-cage miniprotein is the smallest known folded protein[24, 25]. The synthesized polypeptide chain spontaneously folds around W6 in solution to form a hydrophobic core that renders the residue inaccessible to the bulk solvent[25]. It thus serves as an ideal counterpoint to the large and flexible HSA. While a number of recent studies have utilized tryptophan phosphorescence to explore protein dynamics [26-29], this research monitors tryptophan phosphorescence in a glass-forming solvent as a function of temperature.

Materials and Methods

Preparation of samples: Purified human serum albumin (HSA) and spectroscopic grade glycerol were

obtained from Sigma (St. Louis, MO, USA) and used as received. L(-)-tryptophan was obtained from Acros

Organics (New Jersey, USA). The 20 amino acid trp cage polypeptide was synthesized by United Peptide

(Herndon, VA, USA). In distilled deionized water HSA (3% weight), trp-cage (1% weight), or free-trp (10

mM) was dissolved; to the solution was added triple the volume of glycerol. The peptide concentration

was chosen to maximize phosphorescence intensity without causing spurious signals; in the case of the

single-tryptophan 66kDa HSA the effective tryptophan concentration was kept low to avoid protein

crowding effects. As diatomic oxygen is an efficient quencher of the triplet state, oxygen was removed by

gentle heating to 60°C followed by extensive evacuation.

Luminescence measurements: A small copper apparatus was fabricated to fit into a small dewar with a

quartz coldfinger to allow ballistic warming of the sample. About 8 µL of sample was pipetted into the

recessed area; the high viscosity, surface tension, and adhesion to the copper wall were sufficient to hold

the solution in place. After sliding into the dewar, where the sample was optically accessible, liquid

nitrogen was poured into the above reservoir, and conduction along the copper stem quickly brought the

sample temperature to 77K. Enough space between the copper apparatus and dewar remained for a thin

thermocouple wire; the thermocouple touched the copper stem at a point directly behind the sample

reservoir. It is assumed that due to the small sample volume (8 µL) in contact with large surface area of

copper (2 mm diameter x ½ mm depth) that thermostat and cryosolvent temperature were at all times in

close equilibrium. The entire apparatus was positioned with the sample along the emission light path with

front face geometry. As the sample slowly warmed to room temperature, phosphorescence decays were

collected on a Cary Eclipse fluorescence spectrophotometer (Varian Instruments, Walnut Creek, CA,

USA). The instrument contains a high-intensity pulsed lamp and collects in analog mode; excitation was at

290 nm and emission at 450 nm, both monochromator slit widths were set at a maximum of 20nm to

maximize signal. A delay time of at least 1 ms avoided the collection of scattering and prompt

fluorescence. Multiple lamp flashes, up to 15 pulses, were sometimes used to increase signal intensity. No

distortion of the collected decay due to increased excitation times (up to 200 ms) was observed as long as

the decay was sufficiently long (over 5 seconds). In the case of HSA, at T < Tg the delay time was increased to up to 2 seconds to minimize the collection of tyrosine phosphorescence. With increasing temperature, once phosphorescence decay times were below 5 seconds, excitation was limited to a single lamp flash. In this case the signal to noise ratio was improved by taking an average of increasingly more cycles with increasingly shorter decay times. Gate time (channel width) varied from 60 ms for the longest decays to 0.5 ms for the shortest decays.

Decays were collected over the temperature range of -200°C to -50°C; as the solvent glass transition temperature is -103°C[30] this temperature range allowed for observation of behavior both in the glassy state and through the glass transition. Total decay times varied greatly over this range, from as long as 60 s at liquid nitrogen temperature to as short as 500 ms at the high end of the temperature range.

Analysis of luminescence data: To eliminate the tendency of over-fitting the long tail of phosphorescence intensity decays, a simple code was written in Mathematica to remove data points from the tail. Based on random number generation, data points were selectively dropped yielding a thinned decay with points equally spaced on a log-time scale. Typically a decay of 1000 points was reduced to ≈100. Lifetime distributions of all phosphorescence decays were generated by the hybrid maximum-entropy / nonlinear-least-squares software MemExp version 3.0[31, 32], which is freely available through the NIH center for molecular modeling site (http://cmm.cit.nih.gov/memexp/). The algorithm utilizes a maximum entropy function and maximum likelihood fitting to analyze time dependent data in terms of distributed lifetimes. A discrete lifetime model is inappropriate to describe phosphorescence decays in heterogeneous environments such as found specifically in proteins[33], and more generally in the amorphous state. The collected decay is an ensemble measurement of many chromophores, each located in a similar but unique environment. A stretched exponential function, which has often been successfully used to describe relaxation processes in glassy or glass-like systems[34, 35], was first used to fit the phosphorescence decays. The simplicity of this function (a single variable describes the degree of heterogeneity around a single lifetime) holds great appeal, though typically the decays were too complex to be well described. Thus it is more appropriate to use a fitting program that allows for this spread in lifetimes. The obtained lifetime distributions frequently spread across two decades of time due to more quickly decaying

phosphorescent impurities (verified by analysis of probe-free solvent); due to its long lifetime, the component of the distribution due to tryptophan was easily distinguished from impurities. Fits were judged to be adequate when the modified residual (Poisson noise) was seen to vary randomly about zero.

According to basic photophysical principles, the inverse of the observed tryptophan phosphorescence lifetime can be expressed as a sum of rates, each of which is a potential route for the return from the excited triplet state to the ground singlet state:

$$\tau_P^{-1} = k_P = k_{RP} + k_{NR} + \sum_i (k_{Q,i}[Q_i]), \qquad\qquad \textbf{[1]}$$

k_{RP} is the intrinsic radiative rate of the triplet state, known from measurements in low-temperature glass to be roughly $1/6$ s^{-1} for tryptophan [33, 36]; each product $k_Q[Q]$ gives the rate due to collision with a quenching molecule of concentration $[Q]$. There are two potential quenchers: oxygen, which has been purged from the system, and the sulfur containing amino acids [37], which in the native folded state of HSA are fixed at distances no closer than 1.0 nm to W214 making their effective concentration zero. Therefore, $k_Q[Q] = 0$ for all molecular quenchers. The value k_{NR} may thus be calculated directly from the phosphorescence lifetime:

$$k_{NR} = <\tau>^{-1} - 1/6.5 \text{ s}^{-1} \qquad\qquad \textbf{[2]}$$

Results

Tryptophan phosphorescence decays: Tryptophan phosphorescence intensity decays of HSA (HSA-Trp), 20 amino acid tryptophan cage (trp-cage), and free amino acid (free-Trp) in glycerol/water cryosolvent were collected from 77K to 220K. Figure 2 shows the phosphorescence intensity decay of free-Trp and HSA-trp at 77K on logarithmic coordinates. It is readily apparent that the free-trp decay has a longer lifetime and more closely approaches that of a single exponential function than HSA. The resultant MEM lifetime distributions (Fig. 3) reveal primary peaks at 6300ms and 5500ms for free-trp and HSA, respectively. The smaller but significant peak at 2000ms in the HSA curve was determined to be due to tyrosine phosphorescence. Previous phosphorescence studies on HSA and BSA have demonstrated the contribution of tyrosine phosphorescence to the signal[38]. Furthermore, identical experiments conducted with RNase, a protein with similar number of tyrosine residues as HSA but without a tryptophan residue, yielded MEM lifetime distributions with the same peak at ~2000ms (data not shown).   Various small, short lifetime peaks were also seen in the MEM fits; these coincided closely with peaks seen in glycerol/water blanks and have been determined to be due to scant quantities of unidentified phosphorescent impurities in the solution. Fitting all decays with an MEM-based lifetime distribution function thus allowed for identification and isolation of the component of the signal due to tryptophan. Once the tryptophan portion of the distribution was determined, the rest of the lifetime distribution was discarded.

Heterogeneity: The width of the lifetime distributions indicate that the decays were heterogeneous, typical both of relaxation processes in glasses [39] and of phosphorescence in proteins where heterogeneity is attributed to variability in the ensemble of conformational substates that the protein can assume [33]. There was no discernible pattern of differences seen in the degree of heterogeneity from sample to sample, or at different temperature points in relation to T_g.

Average lifetimes: Figure 4 shows the thermal evolution of the free-trp MEM peak (a number of temperature points have been excluded to ease viewing); similar progressions are seen for trp-cage and HSA. As expected, the decays move to shorter times with increasing temperature. The average lifetime was calculated from the assigned tryptophan peak in the MEM distribution by calculating the center of

gravity (after converting from log (tau) to tau). Figure 5 shows the average lifetimes for free-trp, trp-cage, and HSA plotted against temperature. For all three samples, lifetime holds steady at around 6s in the glass and begins to decrease as temperature increases above T_g = -103°C. While lifetimes of all three samples follow the same general pattern with changing temperature, there are two immediately discernible differences.

At $T < T_g$: The long tryptophan lifetimes in the glass are of slightly different magnitude; they follow the trend: $\tau_{free-trp} > \tau_{trp-cage} > \tau_{HSA}$. At 77K the lifetime of free tryptophan is 6.32s, roughly the longest tryptophan phosphorescence lifetime reported in the literature[40]. The shorter lifetimes for trp-cage (5.88s) and HSA (5.65s) are likely due to slightly increased site flexibility as a result of the folded polypeptide chain. It is also unlikely that other amino acid residues (cysteine or aromatic residues) act as long-range static quenchers. Despite the difference among the samples, in all three cases the lifetimes decrease very gradually with increasing temperature, an indication that any large amplitude co-operative motions are frozen out on the timescale of the experiment.

At $T > T_g$: The lifetimes begin to rapidly decrease with increasing temperature above T_g, a clear indication that the tryptophan site has become more mobile in response to the decreasing bulk viscosity. However, the onset temperature (T_{onset}) of the sharp decrease for the three studied systems is different. The order of T_{onset} is: free-trp < trp-cage < HSA. In the case of free-trp, the decrease in lifetime closely coincides with the glass transition temperature at -103°C; the probe is in intimate contact with the cryosolvent and thus any activation of new modes of motion in the bulk are likely detected immediately by the dispersed tryptophan molecule. In contrast, the decrease in lifetime does not begin in trp-cage until T_g + 10°C (-94°C) and in HSA until T_g + 30°C (-74°C). In both of these cases, the trp residue is shielded from direct solvent exposure and thus cannot sense the glass transition in the same direct fashion as dispersed trp. The folded polypeptide plus solvent shell acts as an apparent buffer to the increased motions in the bulk. It is observed that the order of shielding scales with the size of the polypeptide (HSA: 63 kDa; trp-cage: 2.1 kDa).

Discussion

Non-radiative rate of relaxation: The trend in lifetimes vs. temperature *qualitatively* establishes the relationship between the bulk solvent viscosity and local probe mobility, but what *quantitative* information can tryptophan phosphorescence provide about the different systems being studied? For more detailed understanding, Arrhenius analysis can extract the activation energies of the motions responsible for the change in tryptophan phosphorescence lifetime.

In the absence of quencher molecules, phosphorescence lifetime is dependent upon the rate of non-radiative transition from the excited triplet state to the ground state (k_{NR}, see *material and methods* for details). In the non-radiative process the electronic energy of the excited state is lost to the surroundings as heat in the form of vibrational energy; its rate is directly dependent on the motions of the atoms that make up the chromophore center[41]. In the case of tryptophan, various bending and twisting motions of the aromatic indole ring may bring about the non-radiative transition. Briefly, there are three necessary conditions for radiationless transition, all of which are dependent on molecular mobility: (1) the nuclear geometry of the excited triplet state must closely match that of the ground singlet state; (2) some fluctuation must create a vibronic force to promote spin flip; and (3) the excess electronic energy must be able to be dissipated to the surroundings through coupled vibrations. Since the process involves an electron spin flip, it is considered *forbidden*, such that even when all three conditions are met the probability remains low; thus many promoting fluctuations are often required to effect a triplet to singlet transition. It is for this reason that phosphorescent lifetimes can be so long, and what makes phosphorescent molecules suitable probes of slower motions.

The rate k_{NR} was determined from the phosphorescent lifetime (see *methods*) and its logarithm plotted versus inverse temperature is shown in Fig. 6. The slope of the plot yields the activation energy (E_a) of the various motions surrounding the tryptophan molecule that promote the non-radiative transition. Analysis of the changing slope suggests three distinct temperature regimes:

Behavior in glass, $T < T_g$: The plots in Fig. 6 show k_{NR} to be a low energy processes in the cold temperature regime; fits to an Arrhenius model ($k_{NR} = A\exp^{(-Ea/RT)}$), shown as dashed lines in the figure, yield similar activation energies: 1.2 ± 0.3 kJ/mol for free-trp, 1.0 ± 0.18 kJ/mol for trp-cage, and 0.9 ± 0.09 kJ/mol for HSA. The low E_a indicates that k_{NR} is the product of small-amplitude vibrational motions of the indole ring, as it is too cold for any rotational or translational co-operative fluctuations in the glassy matrix. The pre-exponential value of A is highest in HSA (0.084 s^{-1}); it is roughly twice that of trp-cage (0.040 s^{-1}) and four times that of free-trp (0.021 s^{-1}).

The subtle differences in magnitude and slope seen in k_{NR} at low temperatures are not easy to unambiguously resolve. Two plausible arguments can be made to explain the observation that the tryptophan residue behaves differently in a polypeptide: the presence of static quenchers and/or increased site mobility. First, static quenching by nearby amino acids is considered. A series of experiments conducted to evaluate tryptophan phosphorescence quenching by other amino acids have established basic guidelines[37, 42]. Four amino acids were shown to quench tryptophan phosphorescence (in order of efficacy): Cys >> His+ > Tyr ~ Trp. Quenching by cysteine (or cystine) is the most effective, and has been shown to operate with exponential distance dependence and with little dependence on orientation. In contrast, the aromatic amino acids need to be in virtual direct contact in a co-planar/stacked relationship to the indole ring to have noticeable effect. In the free-trp sample the only potential quenchers are other tryptophan molecules, but probe concentration is sufficiently low to preclude this possibility, therefore there should be no quenching of free-trp. For trp-cage, there is a single tyrosine residue (Y3) that is near the tryptophan (W6); the nearest edges are 3.5 Å apart, but the orientation of the tyrosine phenol ring is both perpendicular and edge-to edge with the indole ring, a highly inefficient arrangement and thus unlikely to act as a quencher. For HSA there is a cysteine-cysteine disulfide bond in proximity to W214, roughly 11Å from the tryptophan nearest edge. The disulfide bond likely has no quenching effect in HSA: the single-trp protein azurin also has a disulfide bridge 11 Å away from the trp residue whose removal via site-directed mutagenesis had no effect on tryptophan lifetime[37]. Finally it is noted that the quenching reaction has temperature dependence, and that quenching at temperatures below -130°C is undetectable small[37]. It is thus doubtful that quenching accounts for the differences in k_{NR} observed in the glass.

More likely the different values of k_{NR} are due to variations in site mobility. The small and soluble free tryptophan molecule is expected to tightly integrate into a rigid site in the glycerol/water glass-forming matrix. On the other hand, the tryptophan residue in HSA and trp-cage is not in intimate contact with the solvent, but is instead covalently bonded into the polypeptide chain and folded into some low energy conformation; its immediate neighbors are other amino acids, all of which are subject to constraints of the polypeptide backbone, which greatly limits the ability of the adjacent residues to pack tightly around the trp. This theory is supported by a series of infrared and luminescence spectroscopy experiments on free tryptophan dispersed in glycerol/water solvent, which demonstrated the ability of solvent molecules to relax about the solvated tryptophan at temperatures as low as 20K[43]; in contrast, the buried tryptophan residue of single-trp proteins (parvalbumin and aldolase) showed no evidence of relaxation about the tryptophan with lowering temperature[18]. Tighter integration of free-trp into the matrix may also explain the slightly higher E_a: some participation of closely associated water molecules may be required to effect the non-radiative transition. Finally, examination of HSA crystal structure reveals W214 in a cavity with considerably fewer atoms located with a 4 Å radius (29 atoms) as compared to W6 of trp-cage (57 atoms).

Behavior in the melt, $T >> T_g$: A number of studies in viscous environments have demonstrated the modulation of tryptophan phosphorescence lifetime by viscosity[8, 44-47]. Since viscosity is a macroscopic manifestation of the rate of solvent relaxation—the fluctuations of solvent molecules that permit flow—it is reasonable to presume that above T_g the triplet state non-radiative mechanism involves solvent fluctuations. More specifically, it is proposed that at the microscopic level solvent fluctuations in the tryptophan environment promote the bending and twisting of the indole ring that determine k_{NR}. The frequency of the alpha fluctuations in glycerol/water at different temperatures has been determined by dielectric relaxation spectroscopy (k_{diel})[30]. This relaxation follows a super-Arrhenius process and is well described by the Vogel-Fulcher-Tamman equation: $k_{diel}(T) = A \exp[H/k_B(T - T_0)]$. The VFT fit of k_{diel} has been included in the Arrhenius plot of k_{NR} for free trp, trp-cage, and HSA in Fig. 6. While the solvent fluctuations are considerably faster than k_{NR}, the slope of the k_{NR} plots closely follow that of k_{diel} at some T

$> T_g$. The dashed lines included in the figure are VFT fits shifted downwards by adjustment of the pre-exponential factor A.

The similar temperature dependence of k_{diel} and k_{NR} suggests k_{NR} is slaved to the solvent fluctuations. The concept of solvent slaving has largely been developed around the observation that various rate coefficients in myoglobin similarly follow bulk solvent fluctuations[3, 48]. According to the theory, the protein is dynamically passive while fluctuations of the surrounding solvent drive large-scale conformational changes; it is for this reason that the activation enthalpy of many observed rates follows that of the solvent. The rate of the observed protein process is proportionately smaller than the rate of solvent fluctuations by a factor $n = k_{diel} / k_{obs}$, which gives the average number of solvent fluctuations required to bring about the observed process. The values of $\log(n)$ for the tryptophan non-radiative transition are 4.4 for free-trp, 4.6 for trp-cage, and 5.7 for HSA (Table 1). These numbers reflect the magnitude of downward shift of the dashed-line VFT fits in Fig. 6. Thus, it requires about $10^{4.4} \approx 25{,}000$ solvent fluctuations to effect the non-radiative transition of free-trp; because the free trp is in direct contact with the solvent, the inefficiency of the linkage largely reflects the forbidden nature of the non-radiative transition. On the other hand, roughly 1.6 times as many solvent fluctuations are required to effect non-radiative transition of the buried tryptophan residue in trp-cage, and 16 times as many for the trp in HSA. It is apparent that a fraction of solvent fluctuations are transmitted to the tryptophan site in the polypeptide interior. Furthermore, it is noted that the ratio of $1.6/16 = 0.1$ is almost identical to the ratio of surface area between trp cage and HSA, suggesting the size of the interface between protein and solvent is a crucial determinant in how fluctuations are transmitted from the bulk to the interior of the protein.

Behavior at T between T_g and $T_g + 40K$: The sizeable temperature window between the region where vibrational motions dominate k_{NR} ($T \leq T_g$) and the region where k_{NR} closely follows the bulk alpha fluctuations ($T \gg T_g$) suggests secondary relaxations in the matrixes affect k_{NR}. In the vicinity of T_g, k_{NR} must undergo a transition from a low E_a vibration process to a higher E_a β process. Since normal-mode vibrations and β fluctuations are independent motions, their contributions to k_{NR} are separable; thus k_{NR} consists of a vibrational and a non-vibrational component:

$$k_{NR} = k_{vib} + k_{nonvib},$$ **[3]**

At $T \ll T_g$, the matrix is "frozen" with respect to α motions while β fluctuations are too weak to compete with vibrations, i.e. $k_{nonvib} \rightarrow 0$ and $k_{vib} = k_{NR}$. Since k_{vib} is an Arrhenius process it can be extrapolated to higher temperatures and subtracted from k_{NR} to yield k_{nonvib} (Fig. 7).

Free tryptophan: With the vibrational component of k_{NR} subtracted out, a clear Arrhenius process is revealed in the free-trp plot from -110°C to -77°C with an E_a of 46.7 ± 1.1 kJ/mol. The energy matches that of the beta relaxation of the solvent as determined by dielectric relaxation[30]. This provides further evidence that the dispersed tryptophan molecule is tightly integrated into the glycerol/water matrix such that k_{NR} reflects the various fluctuations in the bulk. At -77°C is a second crossover, from β- to α-controlled. However, the bulk β and α relaxations are not separable in a straightforward way; they exist independently at Tg, and with increasing temperature β weakens until roughly -70°C where it disappears and merges into the primary α relaxation[30]. Thus the transition from β to α as reflected in k_{NR} is a more complicated function of temperature and the extrapolated β component cannot be subtracted out to yield k_α as was done for the vibrational component.

Trp-cage: A clear Arrhenius process is also revealed for trp-cage from -108°C to -75°C in Fig. 7. In contrast to free-trp, the E_a is 37 kJ/mol, notably less than the 47 kJ/mol β relaxation of the bulk. According to the solvent slaving model, internal protein motions are coupled to the protein hydration shell fluctuations and not the β fluctuations of the bulk, though the composition of the solvent ultimately determines the level of hydration[49]. The result supports the model, as the measured E_a value is within range of hydration water β fluctuations of various proteins in similar solvent compositions as determined by dielectric relaxation[50, 51].

The onset of the transition of k_{NR} from β- to α-controlled occurs at a similar temperature as it does for free-trp, roughly -75°C. However, the issue of separation of the two processes is in this case different. The α originates from the bulk, whereas the β originates from the solvent shell. They are thus statistically independent from one another, and there is no merging of β into α[3]. Rather what is observed is the sum

effect of the crossing of two distinct processes on the Arrhenius plot, and thus: $k_{nonvib} = k_\alpha + k_\beta$. At T <

T_{onset}, since the α process is too slow to affect k_{NR}, $k_\alpha = 0$. Extrapolating k_β to warmer temperatures and

subtracting from k_{nonvib} yields k_α in the transition region (Fig. 8). The downward shifted VFT fit of the

solvent α relaxation now fits smoothly across all of the temperature points.

HSA: In contrast to free-trp and trp-cage, no β-dominated k_{NR} regime is evident for HSA in Fig. 7.

Presumably because of the higher plateau of k_{NR} in the glass, and the delayed onset of the non-vibrational

effects (T_{onset} = -80°C), k_{NR} moves from the vibration controlled regime to the α-controlled regime within a

narrow temperature range of ≈20°C. This is not to say that hydration shell coupled fluctuations are not

present and affecting k_{NR}, but rather that the transition on the Arrhenius plot from k_{vib} to k_β is closely

followed by the transition from k_β to k_α. Without enough information to fit the data points, k_β has been

assumed to be a 40 kJ/mol Arrhenius process. The estimation was made based on information obtained

from various dielectric relaxation studies of proteins in glycerol/water[15, 16, 49]. In Fig. 7 the estimated

k_β is plotted to intersect the lowest temperature point. As was done for trp-cage, k_β is subtracted from k_{nonvib}

to yield k_α (Fig. 8) to yield similar results: the smooth fit of all points to the solvent α relaxation.

<u>Conclusion</u>

This study has demonstrated that the temperature dependence of the phosphorescence lifetimes from a single-tryptophan protein can be used to systematically investigate coupling between internal protein dynamics and the dynamics associated with both surface hydration waters and the bulk solvent. The results are consistent with the solvent slaving model in that the activation energy for the observed rate of non-radiative transition (k_{NR}) for the tryptophan residue matches that of specific solvent motions.   In the glassy state, Arrhenius-like behavior reveals that k_{NR} is dominated by a low-energy vibrational process. As temperature is raised above T_g, k_{NR} becomes increasingly driven first by β-fluctuations of the protein hydration shell, and eventually by α fluctuations of the bulk solvent.

Figure III-1
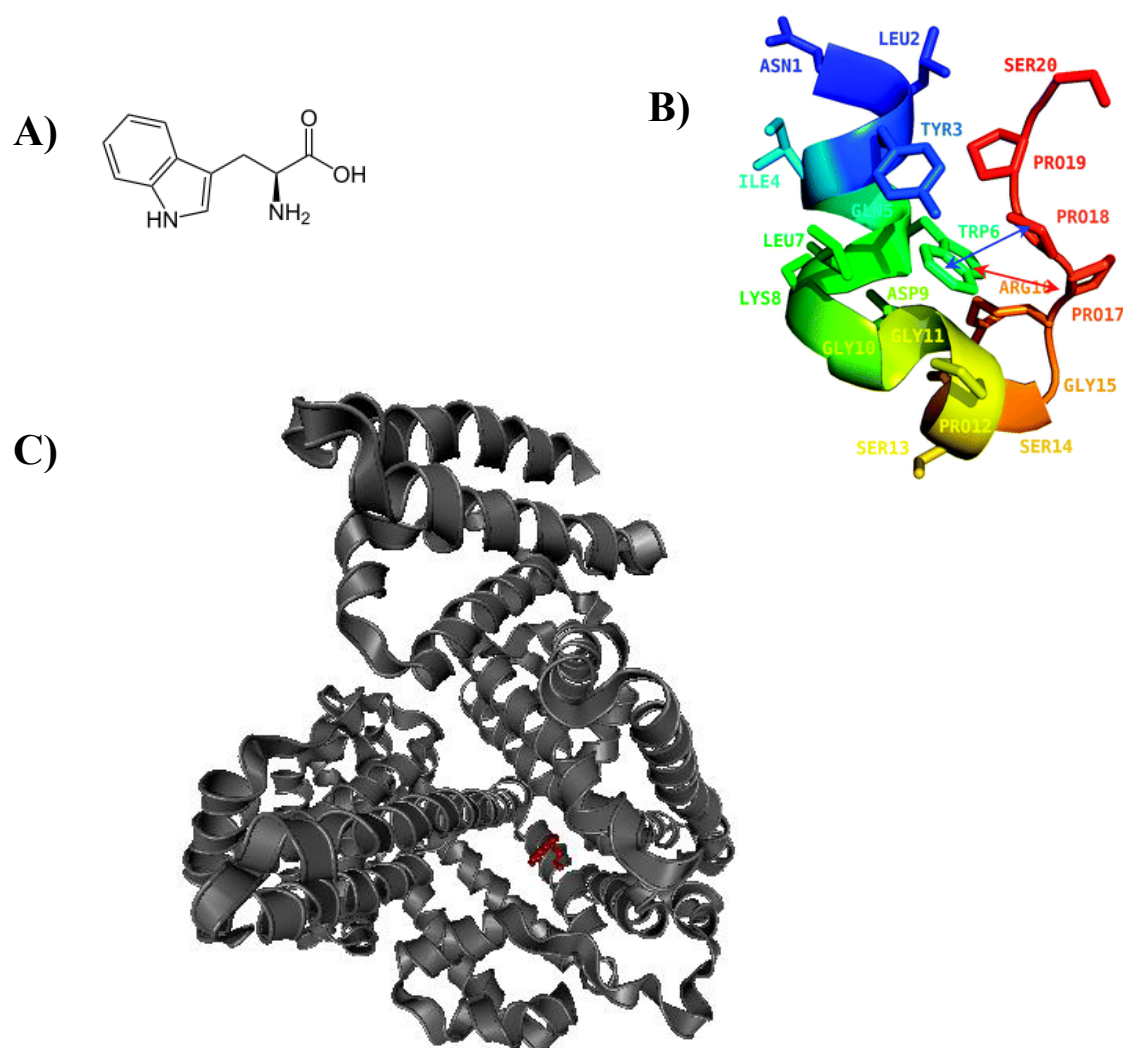
Figure III-1: Structure of (A) tryptophan, (B) 20 amino acid trp-cage miniprotein, and (C) human serum albumin (HSA), where the buried tryptophan residue is colored red.

Figure III-2
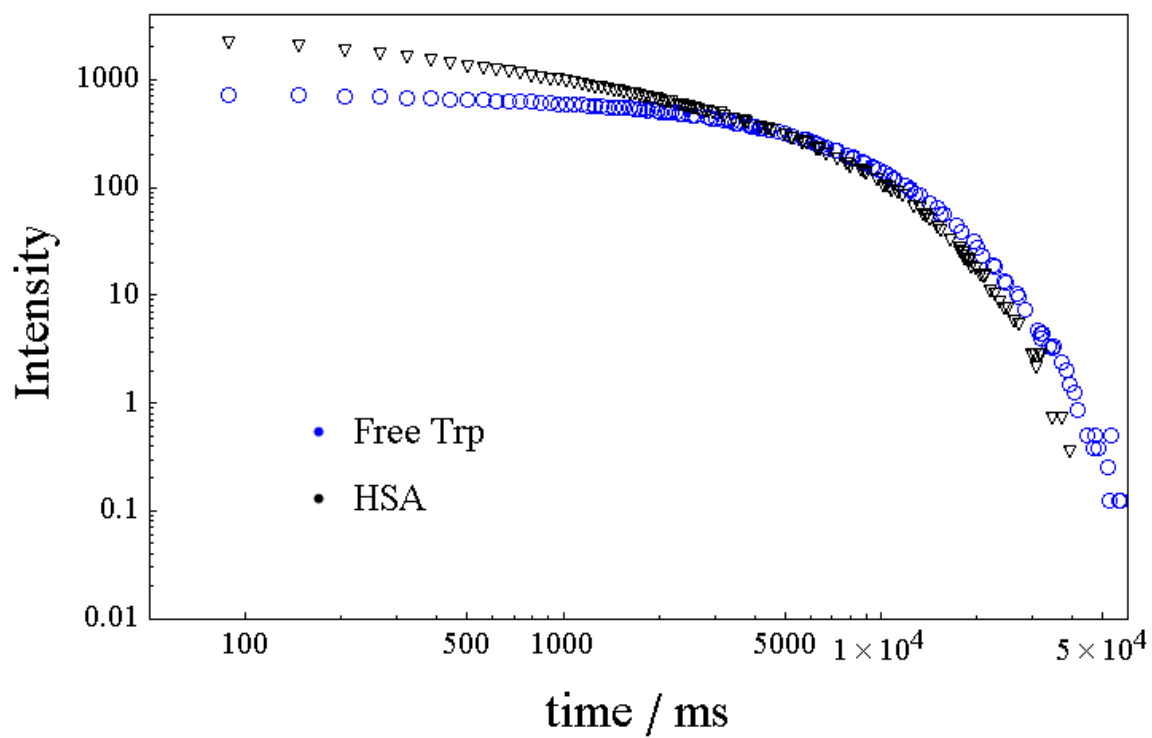
Figure III-2: Phosphorescence emission decays of dispersed free tryptophan (blue circles) and the single tryptophan (W214) of human serum albumin (HSA, black triangles) in glycerol/water (3:1 vol/vol) at 77K.

Figure III-3
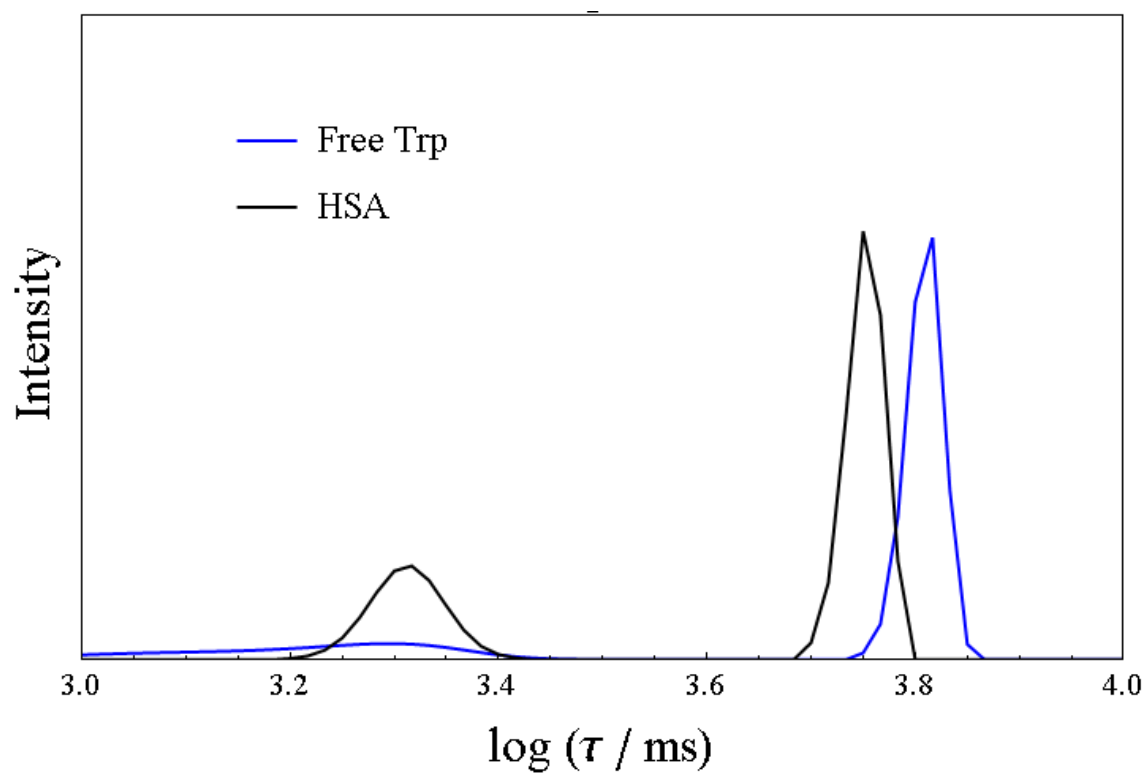
Figure III-3: Maximum entropy method (MEM) distribution analysis of the data shown in Fig. 1. The small peak at log τ = 3.3 is due to tyrosine phosphorescence.

Figure III-4
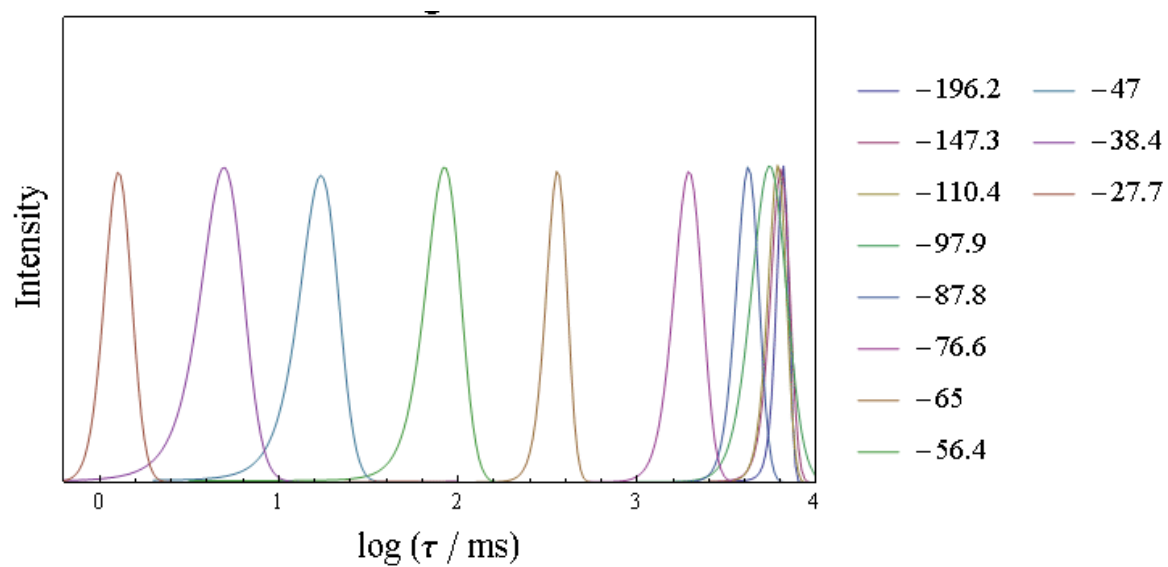
Figure III-4: Thermal evolution of the free tryptophan MEM peak. The T_g of the glycerol/water solvent is -103°C.

Figure III-5
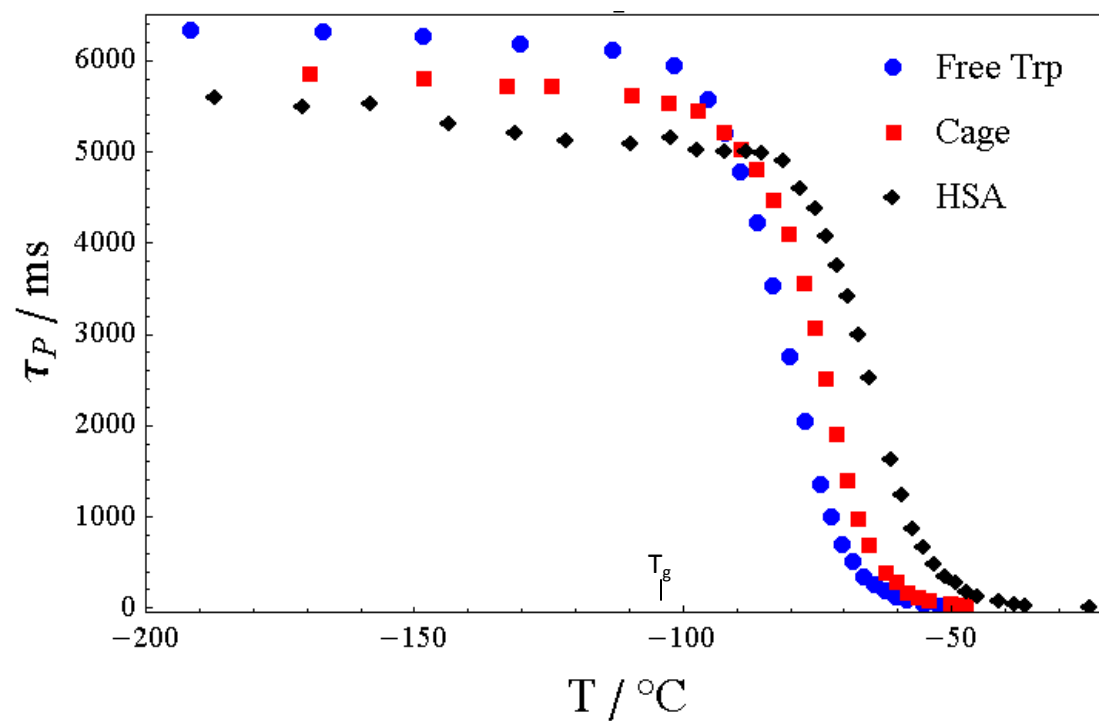
Figure III-5: The temperature dependence of the average tryptophan phosphorescence lifetime (τ_P) of dispersed free-trp (blue), trp-cage (red), and HSA (black) in glycerol/water solvent (3:1 vol/vol).

Figure III-6
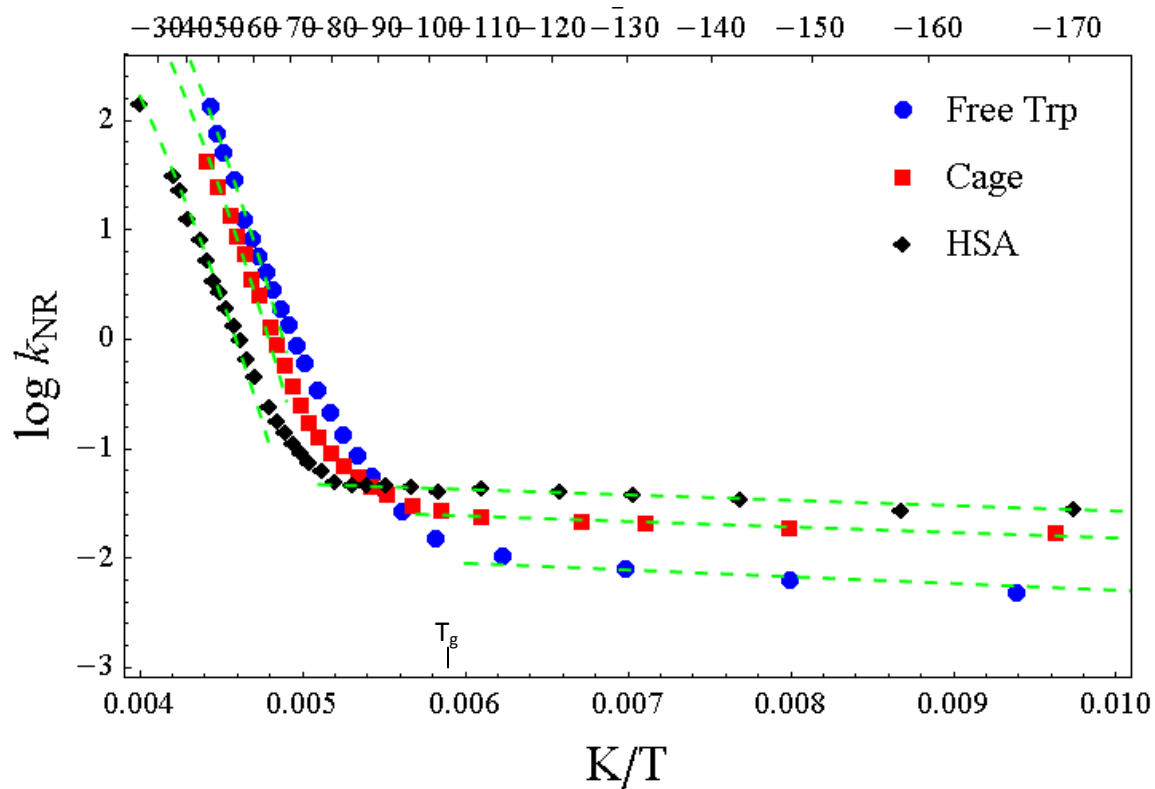
Figure III-6: Arrhenius plot of the tryptophan non-radiate transition rate (k_{NR}, as determined from data in Fig. 4) of dispersed free-trp (blue), trp-cage (red), and HSA (black). Dashed lines are Arrhenius fits to the low temperature data, where k_{NR} is a vibrationally controlled process. Dotted lines are VFT fits to high temperature data; the fits follow the dielectric α fluctuations in the solvent.

Figure III-7
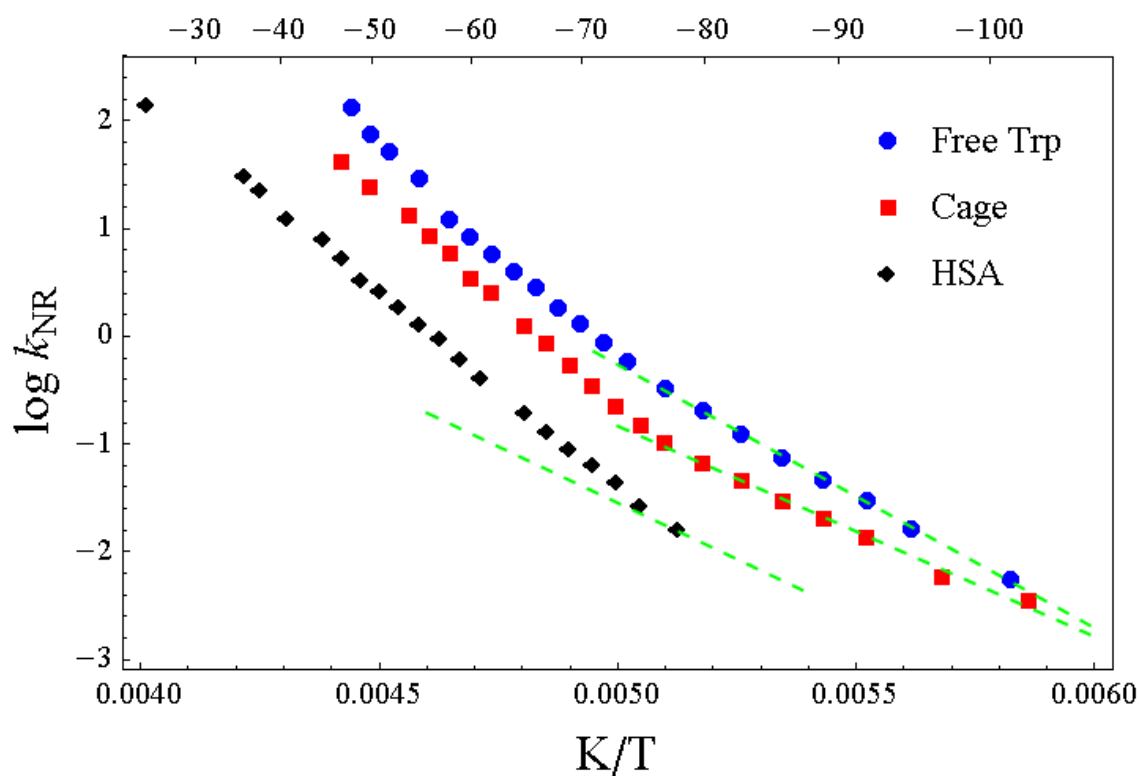
Figure III-7: Subtraction of the vibrational component from Fig. 5 yields the non-vibrational component of k_{NR}, which can be further broken down into β and α components. The dashed lines for free-trp and trp cage are Arrhenius fits (E_a of 45.6 and 37.2 kJ/mol) to the data where k_{NR} is driven by β fluctuations. The β regime is hidden in HSA; the dashed line is generated assuming an E_a of 40 kJ/mol.

Figure III-8
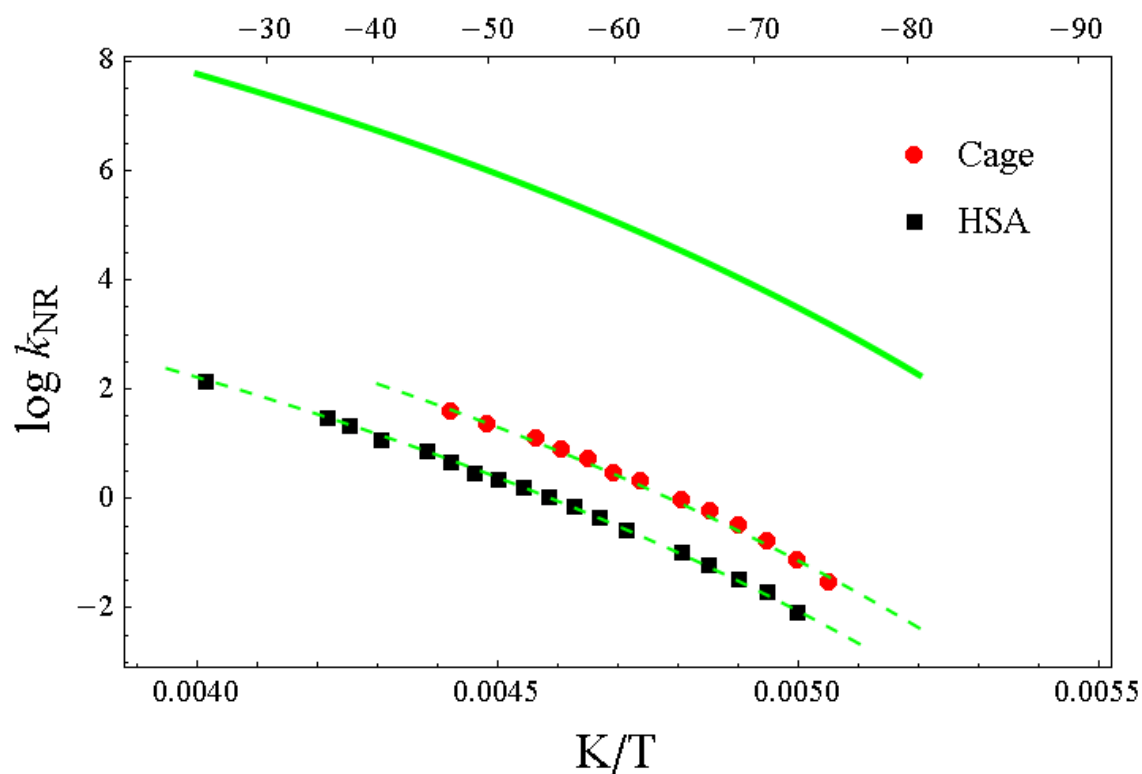
Figure III-8: Subtraction of the β component yields the α component of k_{NR} for trp-cage and HSA; the β and α fluctuations are not separable for free-trp (see text for details). The bold green line is the VFT fit of the primary relaxation in the bulk solvent as determined by dielectric relaxation spectroscopy. The dashed lines are the VFT fit shifted vertically down showing the fluctuations in the bulk drive k_{NR}.

Table III-1: Activation energy of vibrational and beta components of k_{NR}, and the ratio (k_{diel} / k_{NR}) for free-trp, trp-cage, and HSA.

	$E_{a,vib}$ / kJ/mol	$E_{a,beta}$ / kJ/mol	log (k_{diel} / k_{NR})
Free-trp	1.16 ± 0.13	45.6 ± 3.0	-4.4 ± 0.22
Trp-cage	0.60 ± 0.18	37.2 ± 0.6	-4.6 ± 0.09
HSA	0.97 ± 0.09	40.0 ± 0*	-5.7 ± 0.24

References

1.   McCammon, J.A., B.R. Gelin, and M. Karplus, *Dynamics of folded proteins.* Nature, 1977. **267**(5612): p. 585-90.
2.   Karplus, M. and J. Kuriyan, *Molecular dynamics and protein function.* Proceedings of the National Academy of Sciences of the United States of America, 2005. **102**(19): p. 6679-6685.
3.   Frauenfelder, H., et al., *A unified model of protein dynamics.* Proc Natl Acad Sci U S A, 2009. **106**(13): p. 5129-34.
4.   Fenimore, P.W., et al., *Slaving: solvent fluctuations dominate protein dynamics and functions.* Proc Natl Acad Sci U S A, 2002. **99**(25): p. 16047-51.
5.   Doster, W., *The protein-solvent glass transition.* Biochimica Et Biophysica Acta-Proteins and Proteomics, 2010. **1804**(1): p. 3-14.
6.   Gonnelli, M. and G.B. Strambini, *Structure and dynamics of proteins encapsulated in silica hydrogels by Trp phosphorescence.* Biophysical Chemistry, 2003. **104**(1): p. 155-169.
7.   Strambini, E.G. and G.B. Strambini, *Tryptophan phosphorescence as a monitor of protein conformation in molecular films.* Biosensors & Bioelectronics, 2000. **15**(9-10): p. 483-490.
8.   Gonnelli, M. and G.B. Strambini, *Glycerol effects on protein flexibility: a tryptophan phosphorescence study.* Biophysical Journal, 1993. **65**(1): p. 131-7.
9.   Papp, S. and J.M. Vanderkooi, *Tryptophan Phosphorescence at Room-Temperature as a Tool to Study Protein-Structure and Dynamics.* Photochemistry and Photobiology, 1989. **49**(6): p. 775-784.
10.   Strambini, G.B. and E. Gabellieri, *Intrinsic Phosphorescence from Proteins in the Solid-State.* Photochemistry and Photobiology, 1984. **39**(6): p. 725-729.
11.   Cordone, L., et al., *Internal dynamics and protein-matrix coupling in trehalose-coated proteins.* Biochimica Et Biophysica Acta, 2005. **1749**(2): p. 252-81.
12.   Havenith, M., et al., *An extended dynamical hydration shell around proteins.* Proceedings of the National Academy of Sciences of the United States of America, 2007. **104**(52): p. 20749-20752.
13.   Zaccai, G., *Neutron scattering perspectives for protein dynamics.* Journal of Non-Crystalline Solids, 2011. **357**(2): p. 615-621.
14.   Cametti, C., et al., *Dielectric Relaxation Spectroscopy of Lysozyme Aqueous Solutions: Analysis of the delta-Dispersion and the Contribution of the Hydration Water.* Journal of Physical Chemistry B, 2011. **115**(21): p. 7144-7153.
15.   Jansson, H. and J. Swenson, *The protein glass transition as measured by dielectric spectroscopy and differential scanning calorimetry.* Biochimica Et Biophysica Acta-Proteins and Proteomics, 2010. **1804**(1): p. 20-26.
16.   Shinyashiki, N., et al., *Glass Transitions in Aqueous Solutions of Protein (Bovine Serum Albumin).* Journal of Physical Chemistry B, 2009. **113**(43): p. 14448-14456.
17.   Cupane, A., M. Leone, and V. Militello, *Conformational substates and dynamic properties of carbonmonoxy hemoglobin.* Biophysical Chemistry, 2003. **104**(1): p. 335-344.
18.   Wright, W.W., G.T. Guffanti, and J.M. Vanderkooi, *Protein in sugar films and in glycerol/water as examined by infrared spectroscopy and by the fluorescence and phosphorescence of tryptophan.* Biophysical Journal, 2003. **85**(3): p. 1980-1995.
19.   Frauenfelder, H. and G.A. Petsko, *Structural dynamics of liganded myoglobin.* Biophysical Journal, 1980. **32**(1): p. 465-83.
20.   Ansari, A., et al., *Co Stretching Frequency as a Probe of Relaxation in Sperm Whale Carboxymyoglobin .1.* Biophysical Journal, 1987. **51**(2): p. A289-A289.
21.   Fasano, M., et al., *The extraordinary ligand binding properties of human serum albumin.* Iubmb Life, 2005. **57**(12): p. 787-796.
22.   Curry, S., *Beyond expansion: Structural studies on the transport roles of human serum albumin.* Vox Sanguinis, 2002. **83**: p. 315-319.
23.   Mao, S.Y. and A.H. Maki, *Optical-Detection of Triplet-State Magnetic-Resonance Studies on Individual Tryptophan Residues of Serum-Albumin - Correlation between Phosphorescence and Zero-Field Splittings.* Biochemistry, 1987. **26**(11): p. 3106-3114.
24.   Neuweiler, H., S. Doose, and M. Sauer, *A microscopic view of miniprotein folding: Enhanced folding efficiency through formation of an intermediate.* Proceedings of the National Academy of Sciences of the United States of America, 2005. **102**(46): p. 16650-16655.

25. Barua, B., et al., *The Trp-cage: optimizing the stability of a globular miniprotein.* Protein Engineering Design & Selection, 2008. **21**(3): p. 171-185.

26. Mazhul, V.M.T., Alexander V.; Zaitseva, Ekaterina M.; Loznikova, Svetlana G.; Halets, Inessa V.; Chernovets, Tatsiana S., *Room temperature tryptophan phosphorescence of proteins in the composition of biological membranes and solutions*, in *Reviews in Fluorescence 2008*, C.D. Geddes, Editor 2010, Springer: New York. p. 37-67.

27. Kerwin, B.A., et al., *Differentiation of the local structure around tryptophan 51 and 64 in recombinant human erythropoietin by tryptophan phosphorescence.* Photochemistry and Photobiology, 2008. **84**(5): p. 1172-1181.

28. Schay, G., et al., *Millisecond Time-Scale Protein Dynamics Exists Prior to the Activation of the Bulk Solvent Matrix.* Journal of Physical Chemistry B, 2011. **115**(19): p. 5707-5715.

29. D'Auria, S., et al., *The tryptophan phosphorescence of porcine and mutant bovine odorant-binding proteins: A probe for the local protein structure and dynamics.* Journal of Proteome Research, 2008. **7**(3): p. 1151-1158.

30. Sudo, S., et al., *Broadband dielectric study of alpha-beta separation for supercooled glycerol-water mixtures.* Journal of Non-Crystalline Solids, 2002. **307**: p. 356-363.

31. Steinbach, P.J., R. Ionescu, and C.R. Matthews, *Analysis of kinetics using a hybrid maximum-entropy/nonlinear-least-squares method: Application to protein folding.* Biophysical Journal, 2002. **82**(4): p. 2244-2255.

32. Steinbach, P.J., *Filtering artifacts from lifetime distributions when maximizing entropy using a bootstrapped model.* Analytical biochemistry, 2012. **427**(1): p. 102-105.

33. Schlyer, B.D., et al., *Time-Resolved Room-Temperature Protein Phosphorescence - Nonexponential Decay from Single Emitting Tryptophans.* Biophysical Journal, 1994. **67**(3): p. 1192-1202.

34. Baysal, C. and A.R. Atilgan, *Relaxation kinetics and the glassiness of native proteins: coupling of timescales.* Biophys J, 2005. **88**(3): p. 1570-6.

35. Welch, R.C., et al., *Dynamics of Glass Relaxation at Room Temperature.* Physical Review Letters, 2013. **110**(26).

36. Bishai, F., E. Kuntz, and L. Augenstein, *Intra- and intermolecular factors affecting the excited states of aromatic amino acids.* Biochimica et Biophysica Acta, Protein Structure, 1967. **140**(3): p. 381-394.

37. Gonnelli, M. and G.B. Strambini, *Phosphorescence Lifetime of Tryptophan in Proteins.* Biochemistry, 1995. **34**(42): p. 13847-13857.

38. Waldmeyer, J., K. Korkidis, and N.E. Geacintov, *Relative contributions of tryptophan and tyrosine to the phosphorescence emission of human serum albumin at low temperatures.* Photochemistry and Photobiology, 1982. **35**(3): p. 299-304.

39. Richert, R., *Molecular dynamics analyzed in terms of continuous measures of dynamic heterogeneity.* Journal of Non-Crystalline Solids, 1998. **235**: p. 41-47.

40. Huang, R.H., *Phosphorescence of five amino acids.* Progress in Biochemistry and Biophysics, 1997. **24**(1): p. 60-63.

41. Turro, N.J., V. Ramamurthy, and J.C. Scaiano, *Modern molecular photochemistry of organic molecules*2010, Sausalito, Calif.: University Science Books. xxxiii, 1084 p.

42. Strambini, G.B. and M. Gonnelli, *Protein Phosphorescence Quenching: Distinction between Quencher Penetration and External Quenching Mechanisms.* Journal of Physical Chemistry B, 2010. **114**(29): p. 9691-9697.

43. Dashnau, J.L., B. Zelent, and J.M. Vanderkooi, *Tryptophan interactions with glycerol/water and trehalose/sucrose cryosolvents: infrared and fluorescence spectroscopy and ab initio calculations.* Biophysical Chemistry, 2005. **114**(1): p. 71-83.

44. Richert, R., *Triplet state solvation dynamics: Basics and applications.* Journal of Chemical Physics, 2000. **113**(19): p. 8404-8429.

45. Fischer, C.J., et al., *The triplet-state lifetime of indole in aqueous and viscous environments: Significance to the interpretation of room temperature phosphorescence in proteins.* Journal of the American Chemical Society, 2002. **124**(35): p. 10359-10366.

46. Okutsu, T., et al., *Excited state dynamics of p-chlorotoluene in rigid glass matrices.* Journal of Photochemistry and Photobiology a-Chemistry, 1998. **115**(3): p. 243-247.

47.   Cioni, P., L. Erijman, and G.B. Strambini, *Phosphorescence emission of 7-azatryptophan and 5-hydroxytryptophan in fluid solutions and in alpha(2) RNA polymerase.* Biochemical and biophysical research communications, 1998. **248**(2): p. 347-351.

48.   Austin, R.H., et al., *Dynamics of ligand binding to myoglobin.* Biochemistry, 1975. **14**(24): p. 5355-73.

49.   Fenimore, P.W., et al., *Bulk-solvent and hydration-shell fluctuations, similar to alpha- and beta-fluctuations in glasses, control protein motions and functions.* Proc Natl Acad Sci U S A, 2004. **101**(40): p. 14408-13.

50.   Swenson, J., et al., *Properties of hydration water and its role in protein dynamics.* Journal of Physics-Condensed Matter, 2007. **19**(20): p. -.

51.   Bergman, R. and J. Swenson, *Dynamics of supercooled water in confined geometry.* Nature, 2000. **403**(6767): p. 283-286.

CHAPTER IV: Protein dynamics in glassy sugar matrixes via human serum albumin single-tryptophan phosphorescence.

<u>Introduction</u>

Preservation of proteins and other biological materials is often realized when stored in a dry, glassy state[1-3]. When a protein is embedded in a glass-forming solvent at a temperature below T_g, solvent relaxations are too slow to drive any large-amplitude protein conformational motions. At cold temperatures the rates of various processes such as enzymatic activity and degradation are greatly reduced; thus protein stability is improved [4]. It is an especially challenging problem to achieve room-temperature stabilization of proteins and other biological materials, as the macroscopic attainment of the glassy state is not in itself a sufficient condition. Slow degradation processes can still occur [5] and mounting evidence suggests that the requisite mobility is provided by small-amplitude fluctuations that can persist in the glassy state [6, 7]. Minimization of these motions is a challenge: in addition to surrounding the protein with a sufficiently rigid matrix, its surface must be well integrated into that matrix. Small saccharides, which are often used as excipients in lyopholization treatments of pharmaceuticals, are preferentially excluded from the protein surface [8]. Even when embedded in a dry amorphous solid, significant amounts of water may remain in the protein's hydration shell [9]. If there are several layers of water that are not tightly integrated into the hydrogen-bonded network of the surrounding matrix, the protein and its hydration shell will to some degree fluctuate independently of the relatively rigid bulk matrix [7, 10]. To effectively minimize these motions, a glassy matrix should replace [11] and/or immobilize [10, 12, 13] water at the surface of the protein. Thus a basic first step in developing formulations for long-term storage of a protein at room temperature is monitoring and establishing the extent to which the protein surface and its hydration shell are integrated into its surrounding rigid matrix. This objective is experimentally challenging as the amorphous solid state is especially difficult to characterize.

In this study, the kinetics of phosphorescent optical probes are demonstrated to provide an effective approach to the problem. While phosphorescence is a complex phenomenon that does not directly measure local fluctuations, it is well established that the rate of non-radiative decay from the triplet state (k_{NR}) is highly sensitive to local environmental fluctuations [14, 15]. By measuring k_{NR} as a function of

temperature, tryptophan can be utilized as a long-lived and site-specific probe of local dynamics. With single-Trp proteins (wild type or mutant), local mobility can be probed at a variety of sites along the polypeptide chain (e.g., surface or buried), revealing the energetics of motions at different locales within proteins

The internal dynamics of human serum albumin (HSA) embedded in sugar glasses (glucose, sucrose, maltose, and trehalose) are monitored by measuring phosphorescence decays of the single tryptophan residue as a function of temperature. To explore the relation between internal protein motions and those in the bulk, the dynamics of the sugar glass have been monitored via phosphorescence of dispersed free tryptophan. To establish the presence or absence of water in the hydration shell of the protein, and to demonstrate what effects surface water has on internal protein dynamics, the water-sensitive charge transfer probe pyranine (8-hydroxypyrene 1,3,7-trisulfonate) has been employed. The fluorescence emission of pyranine depends on its protonation state[16] and thus when bound to HSA probes the interface between the binding site and local solvent shell[17]. HSA is an important protein whose function as a carrier of hydrophobic molecules in the bloodstream is well characterized [18]. Its structure is established (a three domain heart-shaped 66 kDa globular protein, with multiple ligand binding sites) [19]. HSA contains a single tryptophan residue at position 214, which has been used extensively as an intrinsic probe of HSA structure and binding properties [20]. The residue in HSA is near the surface of the protein but inaccessible to solvent, and therefore monitors mobility at an internal site.

Materials and Methods

Preparation of glassy protein/sugar samples: Purified human serum albumin (HSA), pyranine, maltose, and glucose were obtained from Sigma (St. Louis, MO, USA) and used as received. Purified sucrose was obtained from Fisher Scientific (Fair Lawn, NJ, USA); L(-)-tryptophan and trehalose were obtained from Acros Organics (New Jersey, USA). Glass transition temperatures (T_g) for glucose (32°C) [25-28], sucrose (67°C) [27-29], maltose (92°C) [25, 26], and trehalose (114°C) [27-29] are averages of experimental studies from the literature.

To make samples of HSA in sugar glasses, HSA was dissolved in distilled deionized water to make a 12.5% (w/v) solution that was passed through a 0.2 μm Puradisc™ nylon membrane filter (Whatman Inc., Florham Park, NJ, USA). To assure complete loss of the crystalline state, sugars were dissolved in distilled deionized water by gentle heating to concentrations just below saturation (glucose = 44 wt. %, sucrose = 64 wt. %, maltose = 44 wt. %, trehalose = 48 wt. %); final concentration at room temperature was checked with an Atago hand-held refractometer (Tokyo, Japan). To minimize the potential for protein-protein contact in the amorphous samples and maximize phosphorescence signal, protein was added to sugar in the ratio of 1:10 HSA:sugar by weight and thoroughly mixed. Protein and sugar amorphous films were then made by pipetting 8 μL of the solution onto quartz slides (13 x 30 x 0.6 mm; custom made by NSG Precision Cells, Farmingdale, NY, USA) and spreading over an area approximately 15 mm x 10 mm. After spreading, the slides were dried for ~1 hour under a steady stream of room temperature air and then checked for the formation of sugar crystals by viewing through a dissecting microscope under cross polarized light. The slides were then transferred to a desiccator over phosphorous pentoxide at ~23°C and protected from light to prevent any photobleaching from occurring. Samples were stored for a minimum of two weeks, and desiccant was refreshed as needed to maintain a relative humidity close to 0%.

The same procedure as above was followed in preparing samples of pyranine bound HSA in sugar glasses, with the additional step of adding a 1 mM aqueous solution of pyranine to the 12 % (w) HSA solution in a 1:1 molar ratio. From titration of bovine serum albumin by pyranine, pyranine has been shown to bind to serum albumin at three distinct sites{Clement, 1981 #476}. The experiment was repeated with HSA with

nearly identical results. It was found that all added pyranine was bound to HSA, with none free in solution, at a probe to protein ratio below 1.5:1. Thus the ratio of 1:1 was chosen to ensure that pyranine fluorescence only probes the binding sites of HSA and not the bulk sugar phase.

The procedure for preparing samples of free tryptophan in sugar glasses was similar to the above, with a few important modifications. In the absence of protein, the pure sugar systems more readily crystallized upon drying. The sugar solutions also tended to bead up upon spreading on slides, due to an apparently higher surface tension in the absence of protein, which slowed the drying time and thus increased crystallization. The problem was solved by working at about 60°C which allowed for a greater solubility (glucose = 66 wt. %, sucrose = 70 wt. %, maltose = 58 wt. %, trehalose = 64 wt. %). A 50 mM aqueous stock solution of tryptophan was made and added to the sugars at a probe to sugar monomer ratio of 1:1000 (i.e. a mole ratio of 1:1000 to the monosaccharide glucose, and 1:500 to the disaccharides sucrose, maltose, and trehalose). Slides were placed on a heated dry bath after spreading with sugar solutions, and hot air was blown from a heat gun across the surface to quickly evaporate water. Slides were then stored desiccated.

Luminescence measurements: To prevent oxygen quenching of the triplet state, a steady stream of high purity nitrogen gas flushed the quartz cuvette throughout the experiment. To ensure oxygen was eliminated, the sample was purged with nitrogen for a period of at least 30 minutes. At low temperatures, a stream of dry air was used to prevent condensation on the cuvette faces. Measurements were made on a Cary Eclipse fluorescence spectrophotometer (Varian Instruments, Walnut Creek, CA, USA) equipped with a temperature controlled multicell holder. The instrument contains a high-intensity pulsed lamp and collects in analog mode.

Phosphorescence decays of tryptophan were collected with an excitation wavelength of 280 nm and emission wavelength of 450 nm, with slit widths of both monochromators set at 20 nm. A 0.2 ms delay was used to avoid any fluorescence during the lamp pulse. To maximize the signal to noise ratio of the longest-lived component of the decay, the photomultiplier tube voltage was set to high (800 V). Decays were collected over the temperature range from -10°C to 130°C with increments of 10°C. Total decay times

varied greatly over this range, from as long as 35 s at low temperatures to as short as 200 ms at high temperatures. In all cases the gate time was equal to the decay time divided by 1000; this procedure produced decays with 1000 data points. Each measurement was an average of decays typically collected over 5 minutes; thus for a 30 second decay time, the measurement was an average of 10 cycles. This technique consistently provided an acceptable signal to noise ratio, as the faster decays needed more cycles due to decreased signal levels.

Pyranine fluorescence emission spectra were measured from 400 to 600 nm, with an excitation wavelength of 350 nm, a 0.5 s averaging time, and 2.5 nm slit widths of both monochromators. The excitation wavelength, which is between the two major excitation peaks at 290 nm and 415, was chosen to not excite tryptophan while minimizing scattering, especially water Raman. Because scattering was still prevalent in measuring fluorescence in the solid state, spectra of sample blanks (HSA in sugars without pyranine) were subtracted.

Analysis of luminescence data: Phosphorescence decays were analyzed by nonlinear least-squares fitting with the statistical curve fitting program Igor (Wavemetrics, Inc., Lake Oswego, OR, USA). Because the decays were highly non-exponential (e.g., see Fig. 1), a sum of exponentials model was used to fit the curves:

$$I(t) = I(0) \sum_i \alpha_i \exp[-(t/\tau_i)] + c. \qquad \textbf{[1]}$$

Here I(t) is the intensity as a function of time following excitation, I(0) is the initial intensity at time zero, and α_i and τ_i are the individual normalized pre-exponential and lifetime components. As fits were judged to be adequate when the modified residual was seen to vary randomly about zero, it was found necessary to fit almost all decays to a sum of five exponentials. In a few cases at high temperature the shorter decays fit well to a sum of four exponentials. The amplitude-weighted average was used to calculate the average lifetimes:

$$<\tau> = \sum_i \alpha_i \tau_i / \sum_i \alpha_i. \qquad \textbf{[2]}$$

The pre-exponential values represent the relative number of chromophores in a given environment [30], and weighting by α_i gives equal weight to each chromophore. The phosphorescence average lifetime is the

inverse sum of the average rate constants associated with the various processes that depopulate the excited triplet state [31]:

$$\langle\tau\rangle^{-1} = k_P = k_{RP} + \langle k_{NR}\rangle + \langle k_Q[Q]\rangle. \tag{3}$$

The brackets $\langle\ \rangle$ indicate that both the non-radiative decay and collisional quenching are average quantities. This equation can be used to calculate $\langle k_{NR}\rangle$, the average rate of non-radiative transition to the ground state due to vibrational losses to the medium, if k_{RP} and $\langle k_Q[Q]\rangle$ are known; k_{RP} is the intrinsic radiative rate of the triplet state, known from measurements in low-temperature glass to be $1/6$ s^{-1} for tryptophan [32, 33], and $\langle k_Q[Q]\rangle$ is the average value of the product of the bimolecular quenching constant and the quencher concentration. There are two potential quenchers: oxygen, which has been purged from the system, and the sulfur containing amino acids [34], which in the native folded state of HSA are no closer than 1.0 nm to W214 making their effective concentration zero[35, 36]. Therefore, $\langle k_Q[Q]\rangle = 0$ for all quenchers and $\langle k_{NR}\rangle$ may be calculated directly.

Results

Tryptophan phosphorescence decays: Tryptophan phosphorescence intensity decays of HSA (HSA-Trp) and free amino acid (free-Trp) dispersed in amorphous glucose, maltose, sucrose, and trehalose were collected from -10°C to 130°C at 10°C intervals. The decays were without exception non-exponential which reflects a heterogeneous distribution of probe site mobilities. This behavior is typical for relaxation processes in glasses [37] and for tryptophan phosphorescence in proteins where heterogeneity is attributed to the ensemble of conformational substates that the protein can assume [33]. A representative decay and fit for HSA-Trp in sucrose at 0°C are plotted in log fashion in Fig. 1. As the plot is clearly non-linear, a distribution of rates is appropriate to describe the decay [38]. At the lowest temperatures, in the high viscosity regime, the decays were well fit to a stretched exponential function. With increasing temperature, the stretching exponent decreased indicating an increase of the width of the distribution. At temperatures approaching the matrix T_g, where the α process became significant on the experimental timescale, the decay became too complex to fit with a simple distribution function. In the interest of consistency, a sum of five exponential terms (Eq. 1, see Methods) has been used to fit the data at all temperatures. The function used fit all decays well, and thus provided an acceptable approximation for a distribution of rates from which the average rate may be calculated; this approach has been used in previous studies of protein phosphorescence [33, 34]. For each fit, the normalized pre-exponential value αi can be considered to represent the fraction of chromophores occupying local environments of similar mobility as characterized by the corresponding lifetime τ_i [30].

Lifetime distributions: In the glassy state of all four sugars, the distribution of free-Trp lifetimes (τ_i) is extremely broad with lifetimes ranging over 2.5 orders of magnitude (from ~ 25 ms to 4 s) and approximately equal fractional amplitudes (pre-exponentials); that is, $\alpha_1 \sim \alpha_2 \sim \alpha_3 \sim \alpha_4 \sim \alpha_5 \sim 0.2$. Due to extensive dynamic heterogeneity in the glassy matrix, it appears that probes are evenly distributed among highly mobile (short lifetime) and highly rigid (long lifetime) sites. At temperatures near the sugar glass transition temperature (T_g), the temperature at which the α-fluctuations exceed ~0.01 s^{-1}, the lifetime distribution narrows as the fraction of probes in more mobile environments (shorter lifetimes) increases. This change in the distribution of lifetime components occurs over a narrow temperature range of about

30K in both glucose and sucrose. However, in maltose and trehalose the lifetime distribution from 30°C to 90°C is of intermediate and constant heterogeneity. In contrast, the distribution of fit lifetimes for HSA-Trp in the sugar matrices did not change as the temperature (and the rate of α-fluctuations) increased through the sugar T_g.

Average lifetimes: The amplitude-average lifetime $<\tau>$ for each phosphorescence decay was calculated from the fit coefficients α_i and τ_i (Eq. 2, see *Methods*). In Fig. 2a the average lifetimes of free-Trp dispersed in glassy sugar matrices are plotted as a function of temperature. The value of $<\tau>$ provides an ensemble average measure of local site mobility as seen by the probe in the bulk sugar matrix. In all cases $<\tau>$ decreased with increasing temperature, with a sharp decrease seen around each sugar's T_g where sugar α-fluctuation rates sharply increase. The lifetime plots of HSA-Trp in sugar matrices are presented in Fig. 2b. As for free-Trp, $<\tau>$ for HSA-Trp decreased with temperature in all matrices; however, there is no *sharp* decrease around the T_g of the embedding sugar. Nevertheless, despite the difference in the rate of change near T_g, the $<\tau>$ values of HSA-Trp loosely tracked those of free-Trp. This correspondence indicates that the surrounding sugar matrix has a modulated effect on the internal mobility of the protein as detected by W214.

Non-radiative rates: Average non-radiative decay rates of dispersed free-Trp ($<k_{NR,bulk}>$) and intrinsic HSA-Trp ($<k_{NR,protein}>$) have been calculated (Eq. 3, see *Methods*). The rate of triplet state deactivation is sensitive to the local site mobility of each probe [14, 15, 39]. The mobility is due to an assortment of thermally activated modes of motion and therefore the slope of an Arrhenius plot of $<k_{NR}>$ reveals the average activation energy of these motions [40]. For each sugar matrix, the rate in the bulk $<k_{NR,bulk}>$ and in the protein $<k_{NR,protein}>$ have been plotted in Arrhenius fashion (Figs. 3a-d). These plots allow for direct comparison of the motions detected by tryptophan in the bulk matrix with motions detected by tryptophan inside the protein. Each pair of Arrhenius curves exhibits similar general trends.

The behavior at temperatures well below the sugar T_g is considered first. At -10°C $<k_{NR,protein}>$ is about 6 times larger than $<k_{NR,bulk}>$, indicating that in the glassy state the protein interior is more mobile than in the

bulk. However, the Arrhenius curves have similar slopes, implying that the energetics of probe deactivation are similar despite the significant difference in $<k_{NR}>$. The matching slopes are especially evident in the trehalose and maltose samples. The plots are also concave upward, which is common behavior for relaxation processes in glassy systems [40]. At low temperatures the rate of the α-fluctuation in the glass is very slow relative to the tryptophan triplet state lifetime; consequently, only lower energy/lower amplitude yet faster β-type relaxations deactivate the triplet state. The change in slope with increasing temperature indicates that no single Arrhenius process is responsible for probe deactivation, but rather a collection of processes, that is, secondary relaxations, having a distribution of activation energies. Increasing temperature increases the relative contribution to $<k_{NR}>$ from higher energy relaxations of the distribution. Such a scenario is expected for these highly heterogeneous protein/sugar systems, which are characterized by a broad distribution of phosphorescence lifetimes representative of a broad distribution of mobile environments.

At some point, typically near the sugar T_g, $<k_{NR,bulk}>$ grows larger than $<k_{NR,protein}>$, indicating that the bulk matrix has become more mobile than the interior of the protein. At higher temperatures in glucose and sucrose, but not in maltose or trehalose, the plots become concave downwards, indicative of a temperature regime where triplet state deactivation is dominated by α-fluctuations [41]. The overall shape of each plot demonstrates the separability of α and β fluctuations as seen in previous works [42]: β-fluctuations at low temperatures have Arrhenius temperature dependence while α-fluctuations at high temperatures may be approximated with a Vogel-Tammann-Fulcher relation [43]. The increasing influence of the α relaxation as T_g is approached is further demonstrated by the increasing complexity of the phosphorescence decays (as discussed above). The behavior at high temperatures (above T_g) is not the subject of this study due to low signal levels in these highly mobile environments; this topic will be the focus of a future study designed to generate the required signal/noise levels.

Activation Energies: Activation energies have been calculated at each temperature by measuring the slope of the Arrhenius plots using the points T-10°C, T, and T+10°C. In Fig. 4A E_a versus temperature is plotted for free-Trp dispersed in glucose, sucrose, maltose, and trehalose. At 0°C in all four sugars, the value

converges to about 25 kJ/mol, indicating that the probe responds similarly to the bulk glassy matrix regardless of composition. The value in glucose is likely higher because at this temperature the probe can already sense the α-relaxation whose rate is rapidly increasing with temperature. The E_a values gradually increase with temperature with a jump to higher values as the temperature approaches T_g. The E_a at $T \sim T_g$ peaks at about 120 kJ/mol for glucose, 140 kJ/mol for sucrose, 160 kJ/mol for maltose, and 190 kJ/mol for trehalose. At temperatures above T_g, E_a decreases as evident in the E_a plots of glucose and sucrose.

In Fig. 4B E_a is plotted versus temperature for $<k_{NR,protein}>$ in glucose, sucrose, maltose, and trehalose. Similar to the $E_{a,bulk}$ values, the $E_{a,protein}$ values converge to about 22 kJ/mol at 0°C. This is within the range of typical values reported for the β-fluctuations in proteins of 10-30 kJ/mol [43]. In the glass, $E_{a,protein}$ also increases with temperature in similar fashion to $E_{a,bulk}$. Notably, in maltose and trehalose the activation energies for bulk and protein are almost identical from 0°C to 50°C. This is a significant result that indicates that the dynamics of the dispersed tryptophan and the protein tryptophan are governed by the same processes over this temperature range, despite their entirely different local environments. Finally, as exemplified by the glucose and sucrose systems, as temperature approaches T_g, $E_{a,protein}$ increases but to a smaller extent than $E_{a,bulk}$. The motion of the protein's internal tryptophan responds to the onset of the bulk α-relaxations, yet to a smaller degree than the motions of the dispersed tryptophan.

Several of these results lead to the important conclusion that many of the same processes are operative in both HSA and the bulk matrix. This point is primarily demonstrated by the matching slopes of the Arrhenius plots, and hence activation energies, at low temperature. Additionally, as the sugar glass transition temperature is approached, the E_a for the protein and bulk rise in similar fashion towards their peak values.

Analysis of pyranine fluorescence shows water at surface of protein: Excitation of pyranine to its first excited singlet state converts the compound from a weak base to a strong acid. The dissociation of the proton is a fast reaction ($k = 1 \times 10^{10}$ s^{-1}) in pure water, and is slowed (via an exponential function) by the chemical activity of water, as demonstrated in concentrated salt solutions [44]. As fluorescence occurs on a

similar timescale, pyranine emission from both protonated (ROH*; λ_{max} = 425 nm) and unprotonated (RO⁻ *; λ_{max} = 511) species may be observed, and the relative height of the two peak intensities provides a qualitative measure of microenvironment water activity. When added to HSA prior to embedding in sugar glasses, pyranine is tightly bound to the protein (see materials and methods), and probes the activity of water at a site on the surface of the protein.

Figure 5 shows the emission spectra of pyranine in various environments (free in water, bound to HSA in water, HSA-bound in 66% sucrose, and HSA-bound in amorphous sucrose). When free in solution, because the acidic proton is readily accepted by water, the O⁻ peak dominates the spectrum at 511 nm while the OH peak at 425 nm is about 30 times as small. When bound to HSA in solution, the spectrum changes significantly: the ratio of O⁻ to OH peak decreases to about 2 and both peaks are significantly blue-shifted. These are indications that the bound probe is in a site that is only partially accessible to water and of lower polarity. Both trends continue when the water is replaced by 66% sucrose solution, and even further after desiccation at 0% RH for 2 weeks where the ratio of O⁻ to OH peaks has decreased to 0.61 and the O⁻ peak has blue shifted some 30 nm.

In Fig. 6 is plotted the normalized pyranine emission bound to HSA embedded in each of the sugar matrices as well as free pyranine dispersed in amorphous sucrose (spectra of free pyranine in all four sugars are indistinguishable from each other). Evidence of the dryness of the sugar glass is established by the absence of any O⁻ peak at 511 nm in the pyranine emission. In comparison, when HSA is embedded in this bone-dry sugar matrix, there is water that remains bound to the surface of the protein. There is also a clear difference, as shown by the differing O⁻/OH peak ratios, in the amount of surface-bound water when the protein is dried in different sugars. In order of "wettest" to "driest": maltose = 0.77, sucrose = 0.61, trehalose = 0.59, and glucose = 0.35.

The pyranine emission was also measured across the temperature range studied (data not included). While the emission intensity increased with temperature, which was attributed to a blue-shift in the excitation band, the normalized shape of the spectra did not noticeably change. This indicates that the activity of the

bound water seen by the probe on the surface of the protein was not affected by temperature or the glass to melt phase change.

Discussion

Dynamic behavior in the bulk: The k_{NR} of tryptophan phosphorescence is sensitive to various relaxation processes that occur in the amorphous sugar environment of the probe [40]. These relaxations include the large-scale primary α-relaxation as well as localized secondary β-relaxations [45]. Dielectric relaxation [46] and DSC [29] studies on mono- and disaccharide sugar glasses have revealed two secondary relaxations: the lower energy γ, with estimated average E_a of ~50 kJ/mol, and the intermediate energy β with an E_a of ~90 kJ/mol [46]; the primary or α-relaxation has a reported E_a of >200 kJ/mol [29].

At low temperature, the observed $E_{a,bulk}$ of 25 kJ/mol is well below the reported 50 kJ/mol of the γ-relaxation in amorphous sugars, indicating the presence of additional low energy modes of motion that cause probe de-excitation. These motions are expected to be local, of small amplitude, and not reflective of bulk matrix relaxation processes. Even after extensive drying, the tryptophan solvation shell will retain some hydration waters whose number and mobility likely depend on how effectively the tryptophan molecule is incorporated into the extended hydrogen bond network of the sugar matrix [47]. It is likely that the fluctuations of these solvation waters enable the low energy processes detected at low temperatures. The librational motions of water in various confined environments, monitored by IR absorption [48], dielectric relaxation [49, 50], quasi-elastic neutron scattering [51], and molecular dynamics simulation [52], have energies in the range 14 to 30 kJ/mol, similar to the E_a observed here at low temperature. This lower-energy process dominates k_{NR} in extremely rigid matrixes because the higher-energy bulk relaxations occur with very low frequency. As temperature increases, the observed $E_{a,bulk}$ values increase as the rates of the γ- and β-relaxations in the amorphous sugar matrix become fast enough to deactivate the probe. Under these conditions, the observed E_a is an average of multiple processes.

Comparison with protein: The matching activation energies in bulk and in protein at low temperature, especially evident in trehalose and maltose, suggest that the same relaxation processes drive probe deactivation in both environments. As the protein is expected to be significantly hydrated in the glass [8, 9, 53], it is likely that small amplitude fluctuations of these waters drive internal protein dynamics that deactivate the tryptophan triplet state in a similar fashion to the deactivation of free-Trp in the bulk. This is

consistent with the model proposed by Cordone and others where in dry conditions an embedded protein is tightly anchored via a hydrogen bond network to the glass and its dynamics depend on "flickering" of the hydration shell water-dipole network [10, 13, 54]. Since the rate of probe deactivation (k_{NR}) is ~6 times faster in the protein than in the bulk, there are clearly differences in the efficiency of the quenching process. The larger protein contains many more surface waters and thus provides more pathways connecting their motions to internal protein motions that deactivate the triplet state. The result is an increase in the observed efficiency of probe deactivation (larger $<k_{NR}>$) with no change in E_a. The two observations $E_{a,bulk} = E_{a,protein}$ and $k_{NR,bulk} < k_{NR,protein}$ thus provide evidence for solvent slaving of protein motions. In the language of the energy landscape, the entropic search is more rapid on the protein landscape, though in both cases the transient lowering of enthalpic barriers is due to similar localized small amplitude water motions (librations).

In maltose and trehalose, over the temperature range of –10°C to 50°C, $E_{a,bulk}$ and $E_{a,protein}$ gradually increase together from 25 kJ/mol to 50 kJ/mol, indicating that both the dispersed probe and the embedded protein respond in the same way to the dynamically changing matrix. Over this temperature range, the motions driving probe deactivation progress from solvent shell water motions (~25 kJ/mol) to local relaxations of the sugar matrix (~50 kJ/mol). At ~50°C, the protein and its hydration shell sense the motions in the matrix, which is no longer immobile on the lifetime of the triplet state. This protein-matrix interaction may be through direct contact between sugar and protein or may be mediated by hydration waters. Both situations likely exist, as molecular dynamics simulations of trehalose-myoglobin-water systems have illustrated [9].

Above 50°C in maltose and trehalose, 10°C in sucrose, and -10°C in glucose (presumably), $E_{a,protein}$ does not rise as quickly as $E_{a,bulk}$ with increasing temperature, indicating that the protein begins to respond to relaxations in the matrix to a smaller degree than does the dispersed tryptophan. This may be the result of the free-Trp being more tightly integrated into the extensive hydrogen-bonded network of the matrix than the protein, which is reasonable given the protein's extensive and highly textured surface. The protein will certainly contain more mobile waters in its hydration shell than tryptophan; this larger solvent shell may

also dampened the larger-amplitude bulk motions, in effect decoupling them from protein motions. A similar effect is seen at constant temperature with increasing hydration where the hydrogen bonding network anchoring the protein to the matrix becomes softer and the coupling of protein and bulk dynamics becomes increasingly short-lived and short-range [9, 10]. In each amorphous matrix this divergence of bulk and protein E_a occurs at a temperature approximately 50°C below the sugar T_g, presumably coinciding with the increase in the rate of larger amplitude β-relaxations of the bulk.

The trend of diverging E_a continues with increasing temperature until the sugar glass transition temperature is reached, as demonstrated in the glucose and sucrose data: at $T = T_g$, $E_{a,bulk} \sim 120$ kJ/mol while $E_{a,protein} \sim$ 80 kJ/mol in both sugars. $E_{a,protein}$ also reaches its peak value near the sugar T_g, providing further evidence for coupling of bulk and matrix motions. The lower E_a in protein is likely due to the fundamentally different nature of the primary α-relaxation in a folded protein versus a sugar glass. In the absence of a physical change akin to unfolding, the limited motions within a protein cannot match the extent of co-operative motions in the sugar matrix. Thus, the onset of translational motion in the bulk matrix may affect the deactivation rate of free-Trp more dramatically than that of the HSA-Trp.

Water in the solvation shell: In the dried amorphous state, the presence of water in a protein's hydration shell is believed to be a crucial determinant of fast fluctuations in the protein[55]. These are known as hydration-shell-coupled or β-fluctuations. In the effort to monitor the presence and mobility of HSA hydration shell water in the matrixes, pyranine was bound to HSA prior to embedding in solid amorphous sugars. The probe is sensitive to the replacement of water by sugar molecules: the ratio of the two fluorescence peaks changes with extent of drying, and after extensive desiccation becomes constant. The differences in the spectra of pyranine bound to HSA in the four sugars indicate differences in the availability of water in the protein's solvation shell. Admittedly the ratio of the heights of the two fluorescence peaks only provide a qualitative value of water activity at a single site (in the binding cavity or cavities) on the surface of the protein. Despite this, there are clear and meaningful differences in the activity of water when HSA is embedded in different sugars.

It is evident from the small pyranine [O⁻] peak in Fig. 6 that HSA embedded in solid amorphous glucose has the least amount of mobile water in its hydration shell compared to HSA in the other sugars. It therefore may be said that glucose is the most effective sugar of those studied at replacing water from the protein's hydration shell. Likely this is so because glucose is a monosaccharide and the other sugars are disaccharides. The smaller sugar experiences a much greater degree of translational and rotational freedom which allows it to more efficiently form hydrogen bonds with the polar groups on the surface of the protein. Furthermore, the absence of a glycosidic linkage provides additional hydrogen bond donors and acceptors on a mass basis.

There are also differences among the ability of the three disaccharides to replace water. While trehalose and sucrose produced similar results, maltose is clearly less effective at water replacement. No readily apparent explanation for this observation exists, however it is perhaps relevant that sucrose and trehalose are the two sugars that are commonly found in nature that provide desiccation tolerance in a variety of organisms[56-59]. There may be some correlation between overall stability in the dry amorphous state and the surrounding matrix's ability to replace water in a protein's solvation shell.

Finally, the pyranine data was compared with the data obtained from Trp phosphorescence and no consistent meaningful correlations were discovered. For example, when considering the pyranine data, one might expect the maltose/HSA system with its (qualitatively) greater activity of hydration shell waters to be more mobile as measured by $<k_{NR}>$ than that of the HSA/trehalose system. If this were the case, it would stand to reason that the additional water in the protein's hydration shell effectively plasticized the protein's motion, much as it has been argued that fast fluctuations in a protein's hydration shell are coupled with motions of hydration waters[55]. However the internal HSA motion local to the Trp residue is in fact slightly lower in the maltose system at temperatures all the way up to T_g. It thus appears that the mobility as measured by Trp phosphorescence is not affected by the differences in hydration shell water. In reference to the argument made by Frauenfelder, it is possible that in the solid state the effect of hydration shell water is different, that the fast fluctuations are not detected by the tryptophan residue. It is also possible that the fluctuations of the waters are the same in all systems, but that the pyranine—which only

measures the water in a specific local environment—does not provide a reliable measure of the entire

solvent shell.

<u>Conclusions</u>

This study shows how the temperature dependence of the phosphorescence lifetimes from a buried

tryptophan within a glass-embedded protein can be used to systematically investigate coupling between

internal protein dynamics and the dynamics associated with both surface hydration waters and the bulk

glassy matrix. The results are consistent with the solvent slaving model in that the activation energy for the

protein motion matches that of specific solvent motions.   In the glassy state, Arrhenius-like behavior

reveals a steady evolution of protein dynamics with temperature. Comparison of activation energies

suggests a model where protein dynamics are independent of the glassy matrix at low temperatures and are

instead driven by β-fluctuations of water molecules in the hydration shell. As temperature is raised, the

protein increasingly is driven by higher energy β-fluctuations of the bulk sugar glass. As the T_g of the

matrix is approached there is a gradual climb in activation energy over a broad temperature range. The

results are also supported from comparison with other studies. Activation energies in the glassy state as

determined by Trp-phosphorescence ranged from ~20 – 50 kJ/mol. Dynamical studies over a broad

temperature range on a variety of proteins in numerous glass-forming solvents have utilized neutron-

scattering [60, 61], dielectric relaxation [42, 62, 63], CO rebinding to Mb [38, 64], Fe-Mb Mossbauer

spectroscopy [65], and IR vibrational echo [66]; these have similarly provided Ea measurements ranging
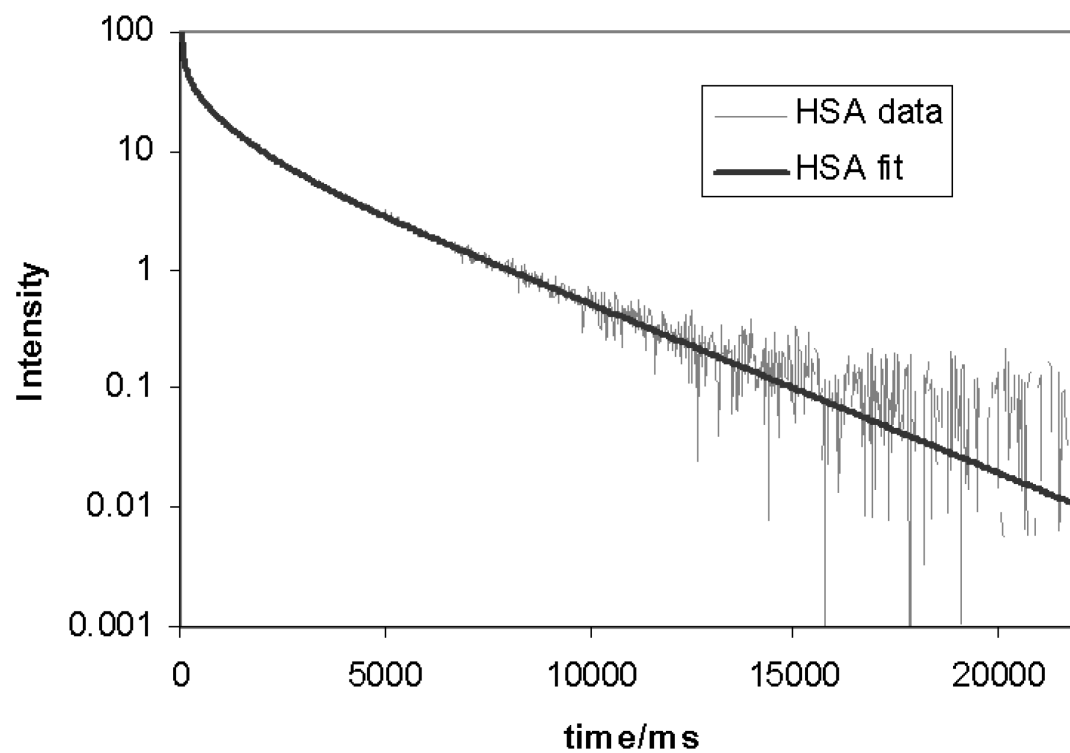
from 12 – 45 kJ/mol.

Figure IV-1

Figure IV-1: Phosphorescence emission decay of the single tryptophan (W214) of human serum albumin embedded in glassy sucrose matrix at 0°C. The fit is a sum of five exponentials.
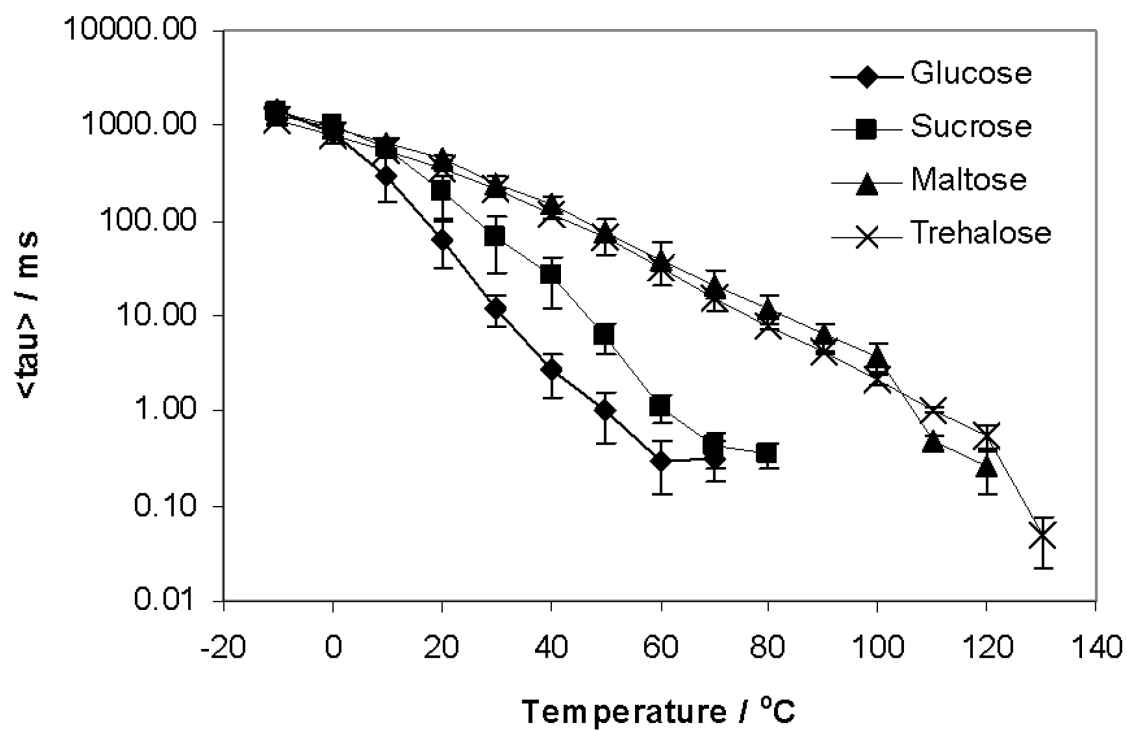
Figure IV-2a

Figure IV-2A: Amplitude-averaged phosphorescence lifetime of tryptophan amino acid dispersed in amorphous solid glucose, sucrose, maltose, or trehalose.
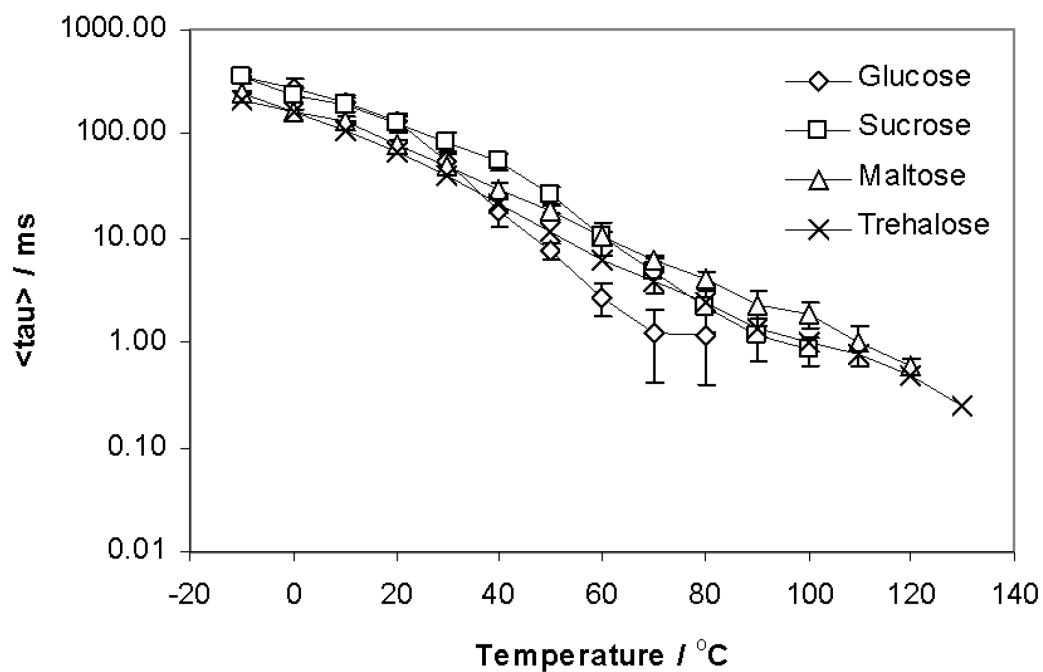
Figure IV-2b

Figure IV-2B: Average phosphorescence lifetime of the single tryptophan of human serum albumin embedded in amorphous solid glucose, sucrose, maltose, and trehalose.

Figure IV-3a

Figure IV-3A: Arrhenius plots of the average non-radiative decay rate $\langle k_{NR} \rangle$ (calculated from the amplitude-averaged lifetime) for de-excitation of the tryptophan triplet state in free amino acid (solid symbols) and in human serum albumin (open symbols) embedded in amorphous solid glucose. Data replotted from Figure 2.
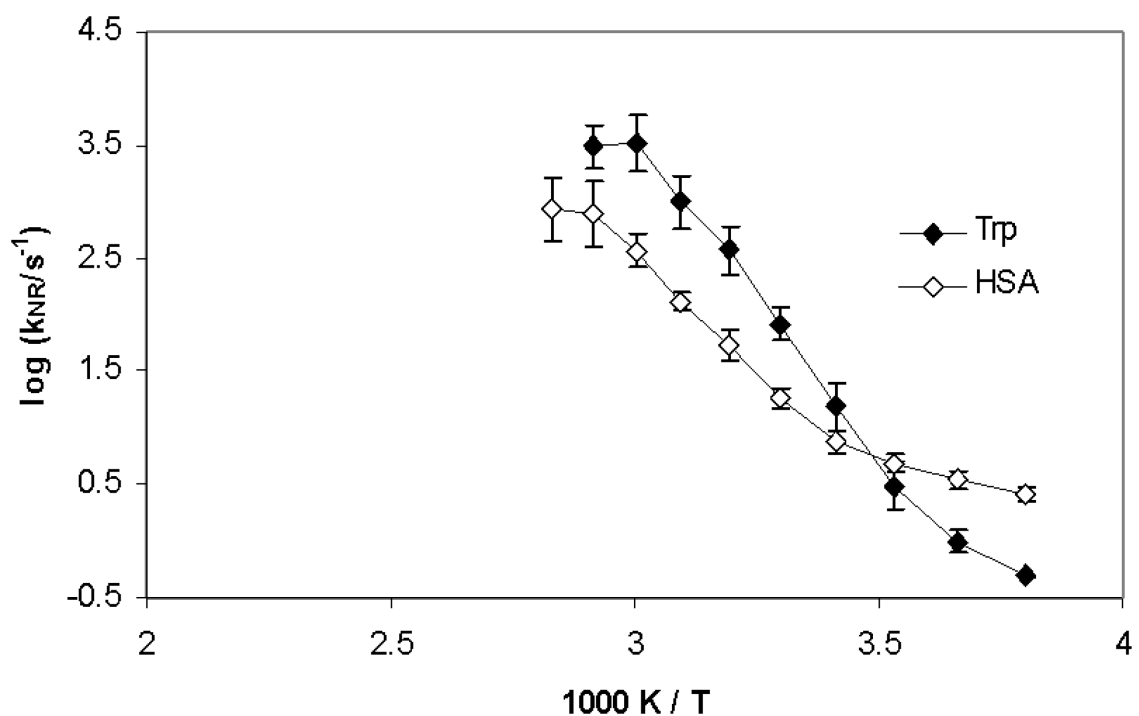
Figure IV-3b

Figure IV-3B: Arrhenius plots of the average non-radiative decay rate $\langle k_{NR} \rangle$ (calculated from the amplitude-averaged lifetime) for de-excitation of the tryptophan triplet state in free amino acid (solid symbols) and in human serum albumin (open symbols) embedded in amorphous solid sucrose. Data replotted from Figure 2.

Figure IV-3c

Figure IV-3C: Arrhenius plots of the average non-radiative decay rate $\langle k_{NR} \rangle$ (calculated from the amplitude-averaged lifetime) for de-excitation of the tryptophan triplet state in free amino acid (solid symbols) and in human serum albumin (open symbols) embedded in amorphous solid maltose. Data replotted from Figure 2.
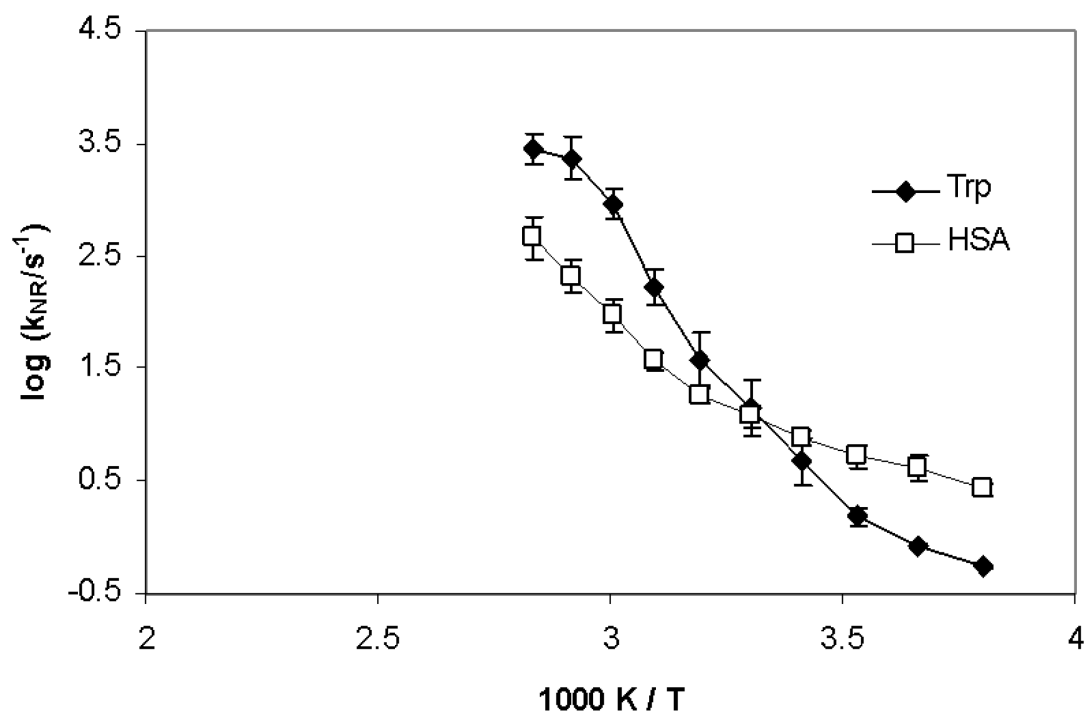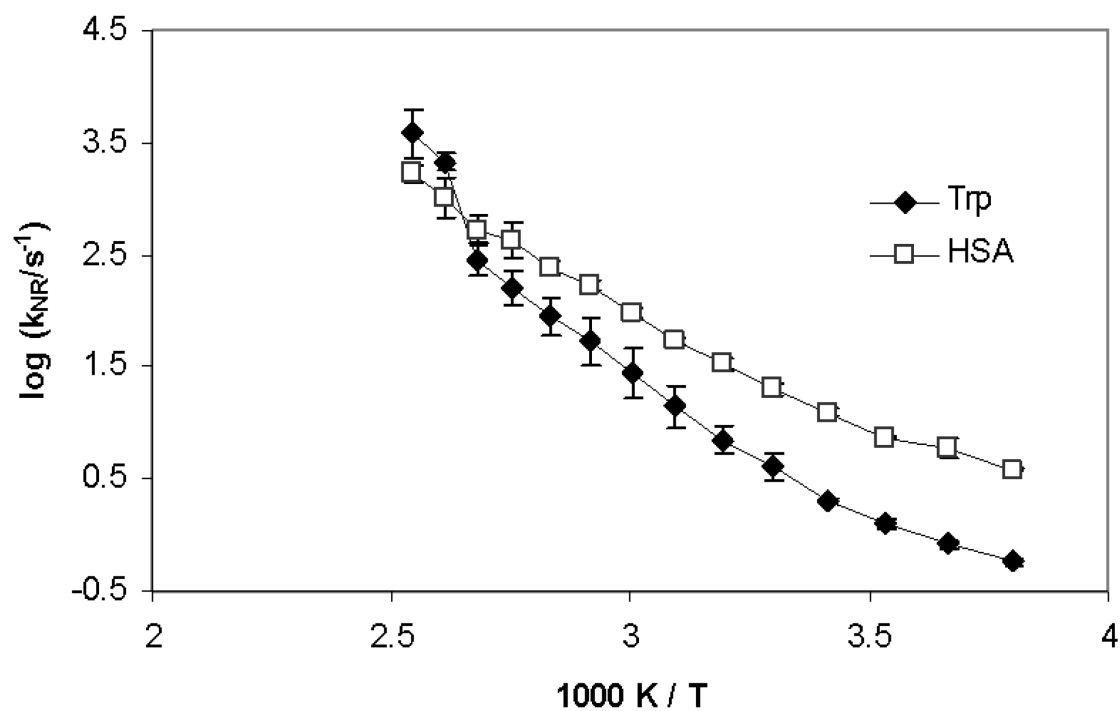
Figure IV-3d

Figure IV-3D: Arrhenius plots of the average non-radiative decay rate $\langle k_{NR} \rangle$ (calculated from the amplitude-averaged lifetime) for de-excitation of the tryptophan triplet state in free amino acid (solid symbols) and in human serum albumin (open symbols) embedded in amorphous solid trehalose. Data replotted from Figure 2.

Figure IV-4a
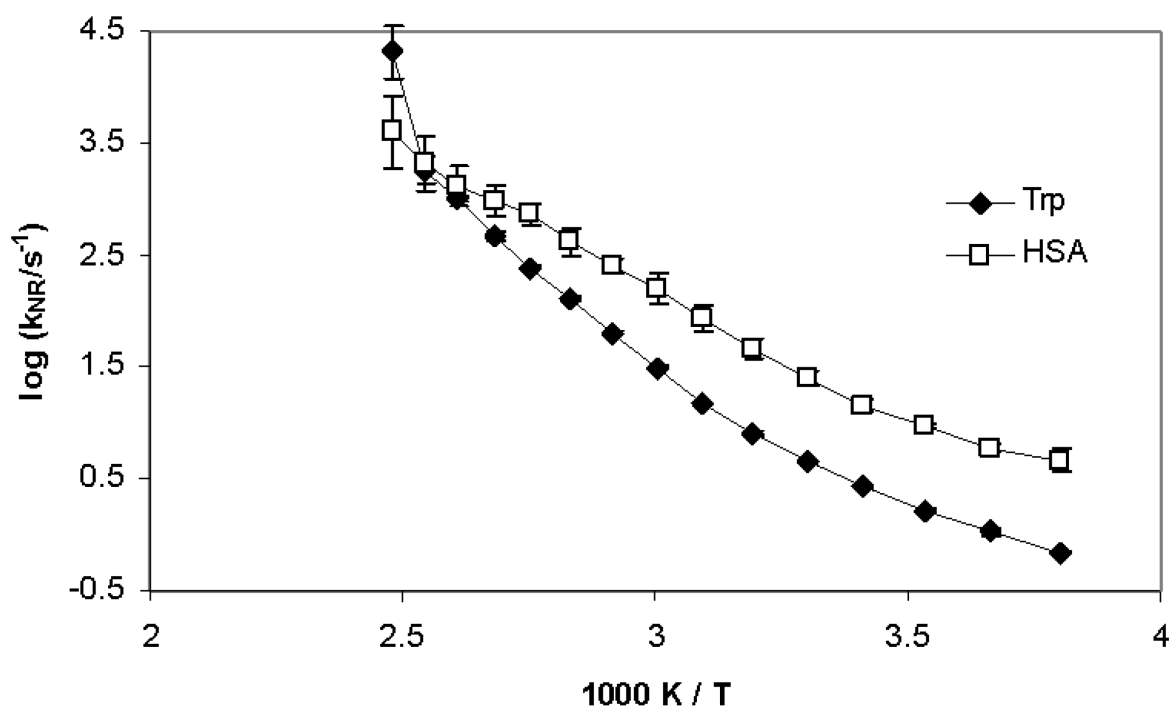

Figure IV-4A: Activation energy (E_a) for non-radiative decay of free tryptophan amino acid embedded in amorphous solid glucose, sucrose, maltose, and trehalose. E_a values calculated from the slopes of the Arrhenius plots of Fig. 3.

Figure IV-4b

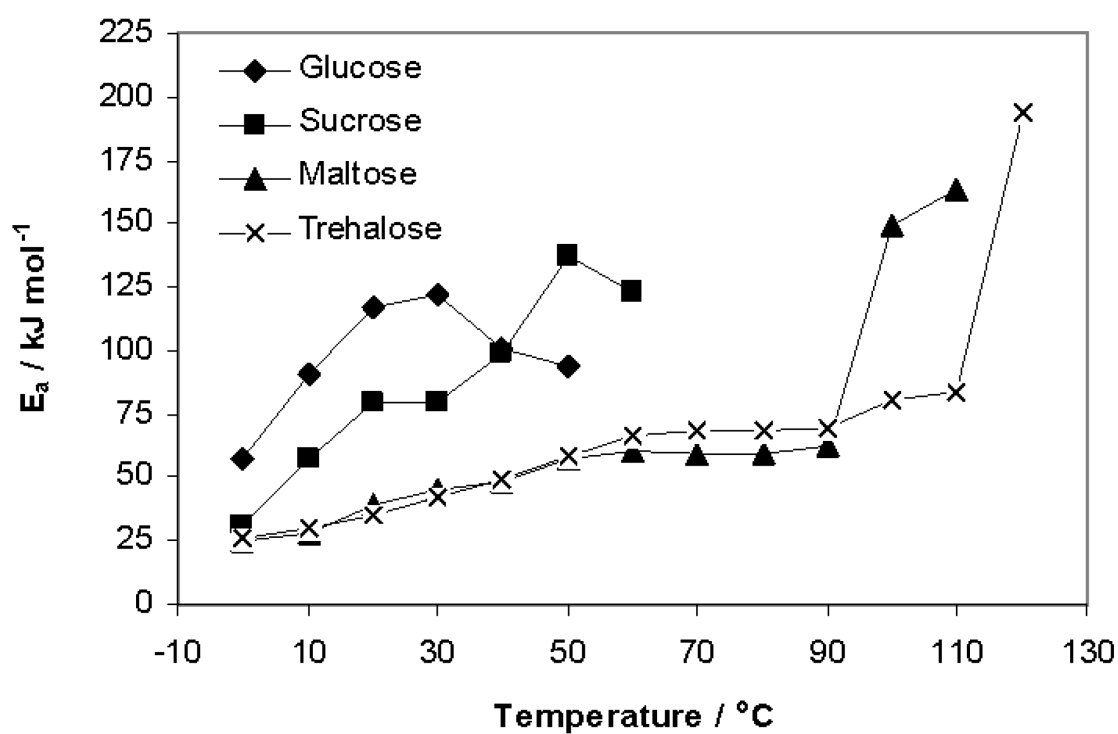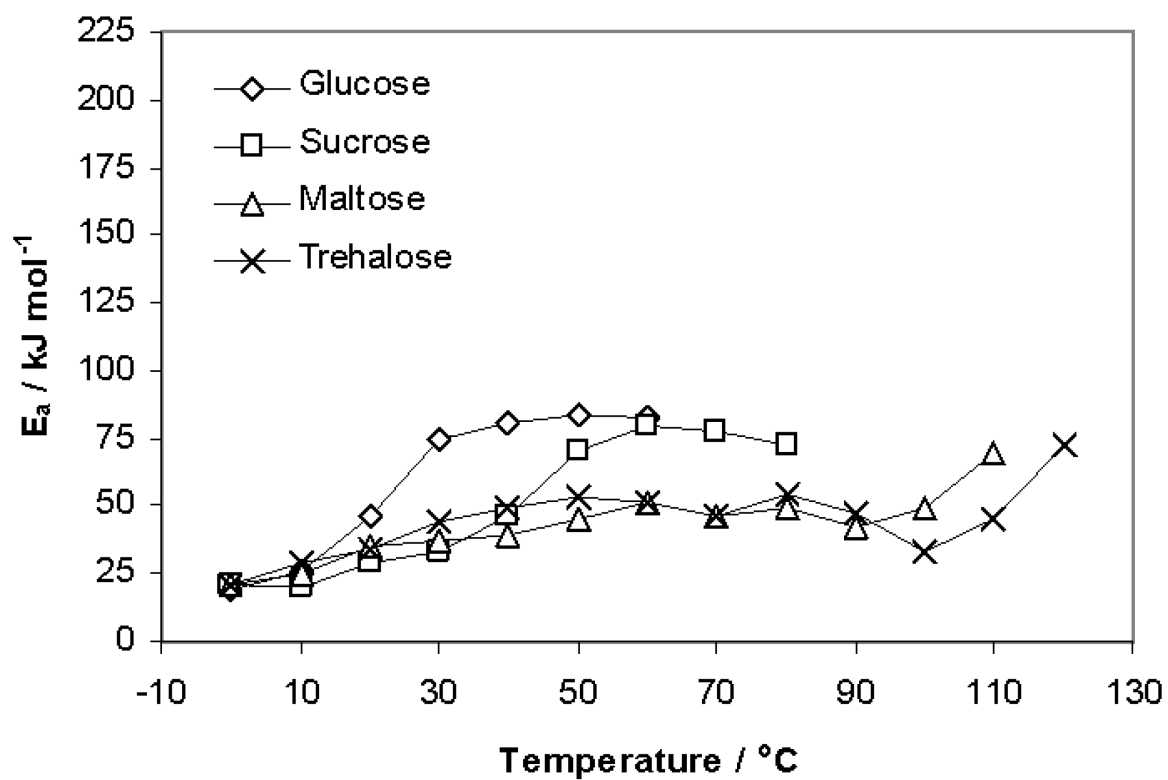**Figure IV-4B:** Activation energy (E_a) for non-radiative decay of tryptophan in human serum albumin embedded in amorphous solid glucose, sucrose, maltose, and trehalose. E_a values calculated from the slopes of the Arrhenius plots of Fig. 3.

Figure IV-5
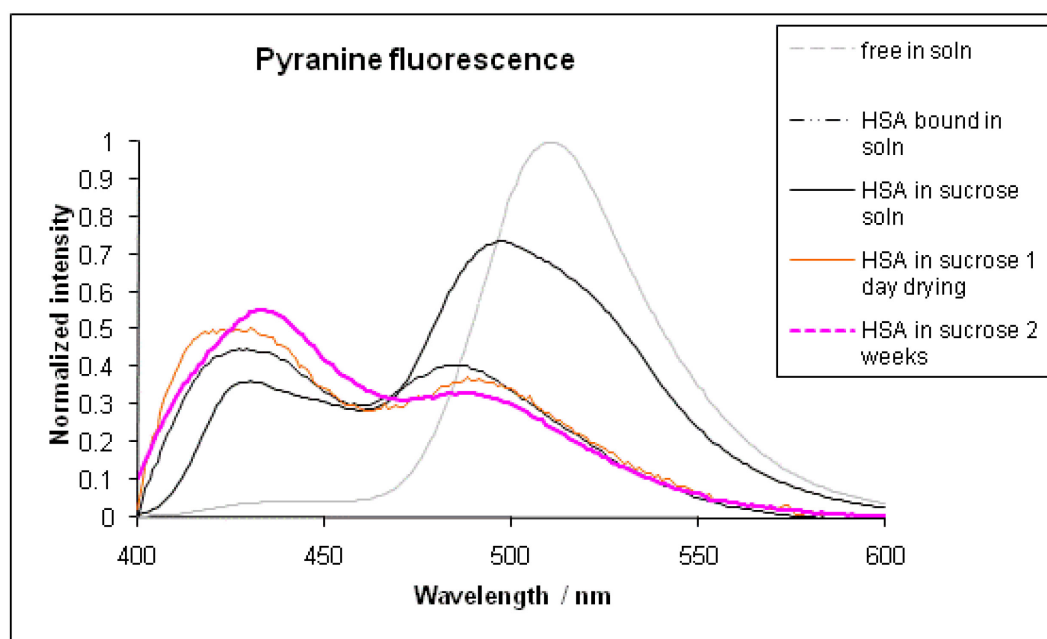
Figure IV-5: Pyranine fluorescence emission: free in water, HSA-bound in water, and HSA-bound in sucrose at different drying times.

Figure IV-6

Figure IV-6: Normalized pyranine fluorescence emission bound to HSA and embedded in glassy sugar matrices (glucose, sucrose, maltose, and trehalose).

References

1. Salnikova, M.S., C.R. Middaugh, and J.H. Rytting, *Stability of lyophilized human growth hormone.* International journal of pharmaceutics, 2008. **358**(1-2): p. 108-113.

2. Schule, S., et al., *Stabilization of IgG1 in spray-dried powders for inhalation.* European Journal of Pharmaceutics and Biopharmaceutics, 2008. **69**(3): p. 793-807.
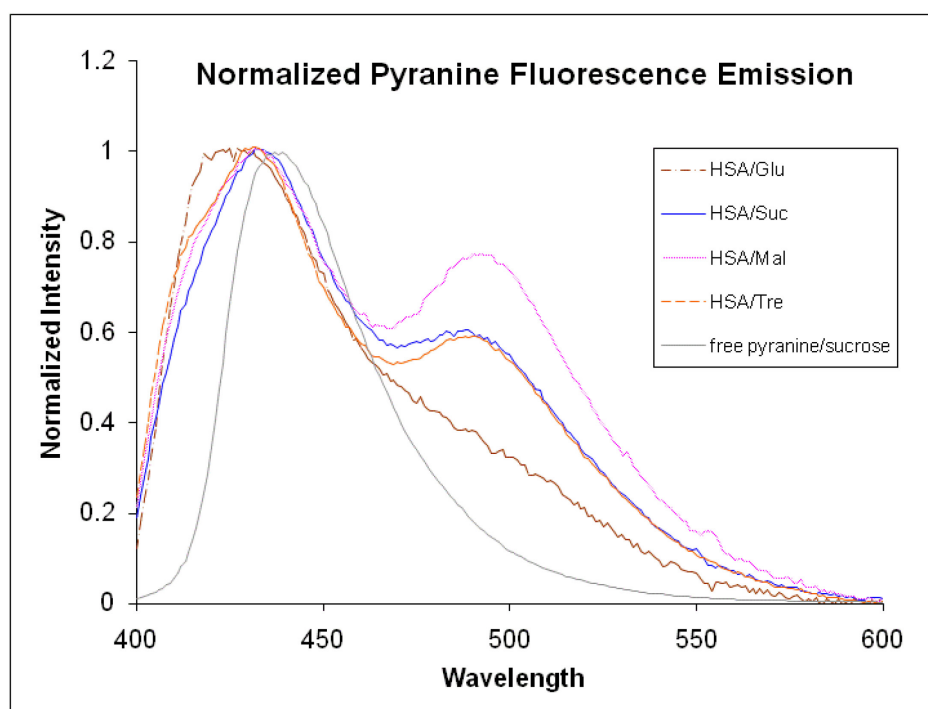
3. Curtin, V., et al., *Investigation of the Capacity of Low Glass Transition Temperature Excipients to Minimize Amorphization of Sulfadimidine on Comilling.* Molecular Pharmaceutics, 2013. **10**(1): p. 386-396.

4. Cicerone, M.T., et al., *Increased protein stabilization in optimally plasticized glass.* Abstracts of Papers of the American Chemical Society, 2002. **224**: p. U226-U226.

5. Lai, M.C. and E.M. Topp, *Solid-state chemical stability of proteins and peptides.* Journal of Pharmaceutical Sciences, 1999. **88**(5): p. 489-500.

6. Yoshioka, S. and Y. Aso, *Correlations between molecular mobility and chemical stability during storage of amorphous pharmaceuticals.* Journal of Pharmaceutical Sciences, 2007. **96**(5): p. 960-981.

7. Hill, J.J., E.Y. Shalaev, and G. Zografi, *Thermodynamic and dynamic factors involved in the stability of native protein structure in amorphous solids in relation to levels of hydration.* Journal of Pharmaceutical Sciences, 2005. **94**(8): p. 1636-1667.

8. Timasheff, S.N., *Protein hydration, thermodynamic binding, and preferential hydration.* Biochemistry, 2002. **41**(46): p. 13473-13482.

9. Cottone, G., G. Ciccotti, and L. Cordone, *Protein-trehalose-water structures in trehalose coated carboxy-myoglobin.* Journal of Chemical Physics, 2002. **117**(21): p. 9862-9866.

10. Cordone, L., G. Cottone, and S. Giuffrida, *Role of residual water hydrogen bonding in sugar/water/biomolecule systems: a possible explanation for trehalose peculiarity.* Journal of Physics-Condensed Matter, 2007. **19**(20): p. 205110/1-16.

11. Carpenter, J.F. and J.H. Crowe, *An Infrared Spectroscopic Study of the Interactions of Carbohydrates with Dried Proteins.* Biochemistry, 1989. **28**(9): p. 3916-3922.

12. Belton, P.S. and A.M. Gil, *Ir and Raman-Spectroscopic Studies of the Interaction of Trehalose with Hen Egg-White Lysozyme.* Biopolymers, 1994. **34**(7): p. 957-961.

13. Giuffrida, S., et al., *Coupling between the thermal evolution of the heme pocket and the external matrix structure in trehalose coated carboxymyoglobin.* Journal of Physical Chemistry B, 2003. **107**(47): p. 13211-13217.

14. Strambini, G.B. and E. Gabellieri, *Intrinsic Phosphorescence from Proteins in the Solid-State.* Photochemistry and Photobiology, 1984. **39**(6): p. 725-729.

15. Papp, S. and J.M. Vanderkooi, *Tryptophan Phosphorescence at Room-Temperature as a Tool to Study Protein-Structure and Dynamics.* Photochemistry and Photobiology, 1989. **49**(6): p. 775-784.

16. Chakraborty, R. and K.A. Berglund, *Steady-State Fluorescence Spectroscopy of Pyranine as a Trace Extrinsic Probe to Study Structure in Aqueous Sugar Solutions.* Journal of Crystal Growth, 1992. **125**(1-2): p. 81-96.

17. Roche, C.J., F. Guo, and J.M. Friedman, *Molecular level probing of preferential hydration and its modulation by osmolytes through the use of pyranine complexed to hemoglobin.* Journal of Biological Chemistry, 2006. **281**(50): p. 38757-38768.

18. Fasano, M., et al., *The extraordinary ligand binding properties of human serum albumin.* Iubmb Life, 2005. **57**(12): p. 787-796.

19. Curry, S., *Beyond expansion: Structural studies on the transport roles of human serum albumin.* Vox Sanguinis, 2002. **83**: p. 315-319.

20. Mao, S.Y. and A.H. Maki, *Optical-Detection of Triplet-State Magnetic-Resonance Studies on Individual Tryptophan Residues of Serum-Albumin - Correlation between Phosphorescence and Zero-Field Splittings.* Biochemistry, 1987. **26**(11): p. 3106-3114.

21. Mazhul, V.M.T., Alexander V.; Zaitseva, Ekaterina M.; Loznikova, Svetlana G.; Halets, Inessa V.; Chernovets, Tatsiana S., *Room temperature tryptophan phosphorescence of proteins in the composition of biological membranes and solutions*, in *Reviews in Fluorescence 2008*, C.D. Geddes, Editor 2010, Springer: New York. p. 37-67.

22. Kerwin, B.A., et al., *Differentiation of the local structure around tryptophan 51 and 64 in recombinant human erythropoietin by tryptophan phosphorescence.* Photochemistry and Photobiology, 2008. **84**(5): p. 1172-1181.

23. Schay, G., et al., *Millisecond Time-Scale Protein Dynamics Exists Prior to the Activation of the Bulk Solvent Matrix.* Journal of Physical Chemistry B, 2011. **115**(19): p. 5707-5715.

24. D'Auria, S., et al., *The tryptophan phosphorescence of porcine and mutant bovine odorant-binding proteins: A probe for the local protein structure and dynamics.* Journal of Proteome Research, 2008. **7**(3): p. 1151-1158.

25. Imamura, K., et al., *Temperature scanning FTIR analysis of hydrogen bonding states of various saccharides in amorphous matrixes below and above their glass transition temperatures.* Journal of Physical Chemistry B, 2006. **110**(31): p. 15094-15099.

26. Orford, P.D., R. Parker, and S.G. Ring, *Aspects of the Glass-Transition Behavior of Mixtures of Carbohydrates of Low-Molecular-Weight.* Carbohydrate Research, 1990. **196**: p. 11-18.

27. Seo, J.A., et al., *The glass transition temperatures of sugar mixtures.* Carbohydrate research, 2006. **341**(15): p. 2516-20.

28. Simperler, A., et al., *Glass transition temperature of glucose, sucrose, and trehalose: An experimental and in silico study.* Journal of Physical Chemistry B, 2006. **110**(39): p. 19678-19684.

29. Dranca, I., et al., *Implications of Global and Local Mobility in Amorphous Sucrose and Trehalose as Determined by Differential Scanning Calorimetry.* Pharmaceutical Research, 2009. **26**(5): p. 1064-1072.

30. Lakowicz, J.R., *Principles of Fluorescence Spectroscopy.* 3rd ed2006, New York: Springer.

31. Parker, C.A., *Photoluminescence of Solutions*1968, Amsterdam, New York etc.: Elsevier Pub. Co.

32. Bishai, F., E. Kuntz, and L. Augenstein, *Intra- and intermolecular factors affecting the excited states of aromatic amino acids.* Biochimica et Biophysica Acta, Protein Structure, 1967. **140**(3): p. 381-394.

33. Schlyer, B.D., et al., *Time-Resolved Room-Temperature Protein Phosphorescence - Nonexponential Decay from Single Emitting Tryptophans.* Biophysical Journal, 1994. **67**(3): p. 1192-1202.

34. Gonnelli, M. and G.B. Strambini, *Phosphorescence Lifetime of Tryptophan in Proteins.* Biochemistry, 1995. **34**(42): p. 13847-13857.

35. Strambini, G.B. and M. Gonnelli, *Tryptophan Phosphorescence in Fluid Solution.* Journal of the American Chemical Society, 1995. **117**(29): p. 7646-7651.

36. Strambini, G.B. and M. Gonnelli, *Protein Phosphorescence Quenching: Distinction between Quencher Penetration and External Quenching Mechanisms.* Journal of Physical Chemistry B, 2010. **114**(29): p. 9691-9697.

37. Richert, R., *Molecular dynamics analyzed in terms of continuous measures of dynamic heterogeneity.* Journal of Non-Crystalline Solids, 1998. **235**: p. 41-47.

38. Austin, R.H., et al., *Dynamics of ligand binding to myoglobin.* Biochemistry, 1975. **14**(24): p. 5355-73.

39. Fischer, C.J., et al., *The triplet-state lifetime of indole in aqueous and viscous environments: Significance to the interpretation of room temperature phosphorescence in proteins.* Journal of the American Chemical Society, 2002. **124**(35): p. 10359-10366.

40. Christoff, M. and T.D.Z. Atvars, *Phosphorescent probes in studies of secondary relaxation of amorphous polystyrene and poly(n-alkyl methacrylate)s.* Macromolecules, 1999. **32**(19): p. 6093-6101.

41. Ferrer, M.L., et al., *Supercooled liquids and the glass transition: Temperature as the control variable.* Journal of Chemical Physics, 1998. **109**(18): p. 8010-8015.

42. Frauenfelder, H., et al., *A unified model of protein dynamics.* Proceedings of the National Academy of Sciences of the United States of America, 2009. **106**(13): p. 5129-5134.

43. Fenimore, P.W., et al., *Bulk-solvent and hydration-shell fluctuations, similar to alpha- and beta-fluctuations in glasses, control protein motions and functions.* Proceedings of the National Academy of Sciences of the United States of America, 2004. **101**(40): p. 14408-14413.

44. Clement, N.R. and J.M. Gould, *Pyranine (8-hydroxy-1,3,6-pyrenetrisulfonate) as a probe of internal aqueous hydrogen ion concentration in phospholipid vesicles.* Biochemistry, 1981. **20**(6): p. 1534-8.

45. Johari, G.P. and M. Goldstein, *Viscous liquids and the glass transition. II. Secondary relaxations in glasses of rigid molecules.* Journal of Chemical Physics, 1970. **53**(6): p. 2372-2388.

46. Kaminski, K., et al., *Identifying the Origins of Two Secondary Relaxations in Polysaccharides.* Journal of Physical Chemistry B, 2009. **113**(30): p. 10088-10096.

47. Wang, J.S. and R.J. Hurtubise, *Phosphorescence properties of 2-amino-1-methyl-6-phenylimidazo[4,5-b]pyridine and benzo[f]quinoline in glucose glasses via temperature variation and spectral characterization.* Analytical Chemistry, 1997. **69**(10): p. 1946-1951.

48. Swanepoel, J. and A.M. Heyns, *MF2 Vibrations and Librations of Water-Molecules in the Series MF2.4H2O (M=Fe,Co,Ni or Zn).* Spectrochimica Acta Part A, 1990. **46**(11): p. 1629-1638.

49. Cerveny, S., J. Colmenero, and A. Alegria, *Dynamics of confined water in different environments.* European Physical Journal, 2007. **141**: p. 49-52.

50. Jansson, H., et al., *Dynamics of water in strawberry and red onion as studied by dielectric spectroscopy.* Physical Review E, 2005. **71**(1): p. -.

51. Malardier-Jugroot, C. and T. Head-Gordon, *Separable cooperative and localized translational motions of water confined by a chemically heterogeneous environment.* Physical Chemistry Chemical Physics, 2007. **9**(16): p. 1962-1971.

52. Kumar, P., S.H. Han, and H.E. Stanley, *Anomalies of water and hydrogen bond dynamics in hydrophobic nanoconfinement.* Journal of Physics-Condensed Matter, 2009. **21**(50): p. 504108/1-9.

53. Longo, A., et al., *Myoglobin embedded in saccharide amorphous matrices: water-dependent domains evidenced by small angle X-ray scattering.* Physical Chemistry Chemical Physics, 2010. **12**(25): p. 6852-6858.

54. Cordone, L., et al., *Internal dynamics and protein-matrix coupling in trehalose-coated proteins.* Biochimica Et Biophysica Acta-Proteins and Proteomics, 2005. **1749**(2): p. 252-281.

55. Fenimore, P.W., et al., *Bulk-solvent and hydration-shell fluctuations, similar to alpha- and beta-fluctuations in glasses, control protein motions and functions.* Proc Natl Acad Sci U S A, 2004. **101**(40): p. 14408-13.

56. Blackman, S.A., R.L. Obendorf, and A.C. Leopold, *Maturation Proteins and Sugars in Desiccation Tolerance of Developing Soybean Seeds.* Plant Physiology, 1992. **100**(1): p. 225-230.

57. Drennan, P.M., et al., *The Occurrence of Trehalose in the Leaves of the Desiccation-Tolerant Angiosperm Myrothamnus-Flabellifolius Welw.* Journal of Plant Physiology, 1993. **142**(4): p. 493-496.

58. Leslie, S.B., et al., *Trehalose and Sucrose Protect Both Membranes and Proteins in Intact Bacteria during Drying.* Applied and Environmental Microbiology, 1995. **61**(10): p. 3592-3597.

59. Crowe, J.H., J.F. Carpenter, and L.M. Crowe, *The role of vitrification in anhydrobiosis.* Annual Review of Physiology, 1998. **60**: p. 73-103.

60. Ferrand, M., et al., *Thermal Motions and Function of Bacteriorhodopsin in Purple Membranes - Effects of Temperature and Hydration Studied by Neutron-Scattering.* Proceedings of the National Academy of Sciences of the United States of America, 1993. **90**(20): p. 9668-9672.

61. Tsai, A.M., D.A. Neumann, and L.N. Bell, *Molecular dynamics of solid-state lysozyme as affected by glycerol and water: A neutron scattering study.* Biophysical Journal, 2000. **79**(5): p. 2728-2732.

62. Singh, G.P.P., F.; Hunklinger, S.; Dransfeld, K, *Role of adsorbed water in the dynamics of metmyoglobin.* Phys. Rev. Lett., 1981. **47**: p. 685-688.

63. Bergman, R. and J. Swenson, *Dynamics of supercooled water in confined geometry.* Nature, 2000. **403**(6767): p. 283-6.

64. Kleinert, T., et al., *Solvent composition and viscosity effects on the kinetics of CO binding to horse myoglobin.* Biochemistry, 1998. **37**(2): p. 717-33.

65. Parak, F., E.W. Knapp, and D. Kucheida, *Protein dynamics. Mossbauer spectroscopy on deoxymyoglobin crystals.* J Mol Biol, 1982. **161**(1): p. 177-94.

66. Rector, K.D., et al., *A dynamical transition in the protein myoglobin observed by infrared vibrational echo experiments.* Journal of Physical Chemistry A, 1999. **103**(14): p. 2381-2387.